Advancements in primary fixation modeling of cementless total knee replacement

From experiment to computational model

Thomas Gersie

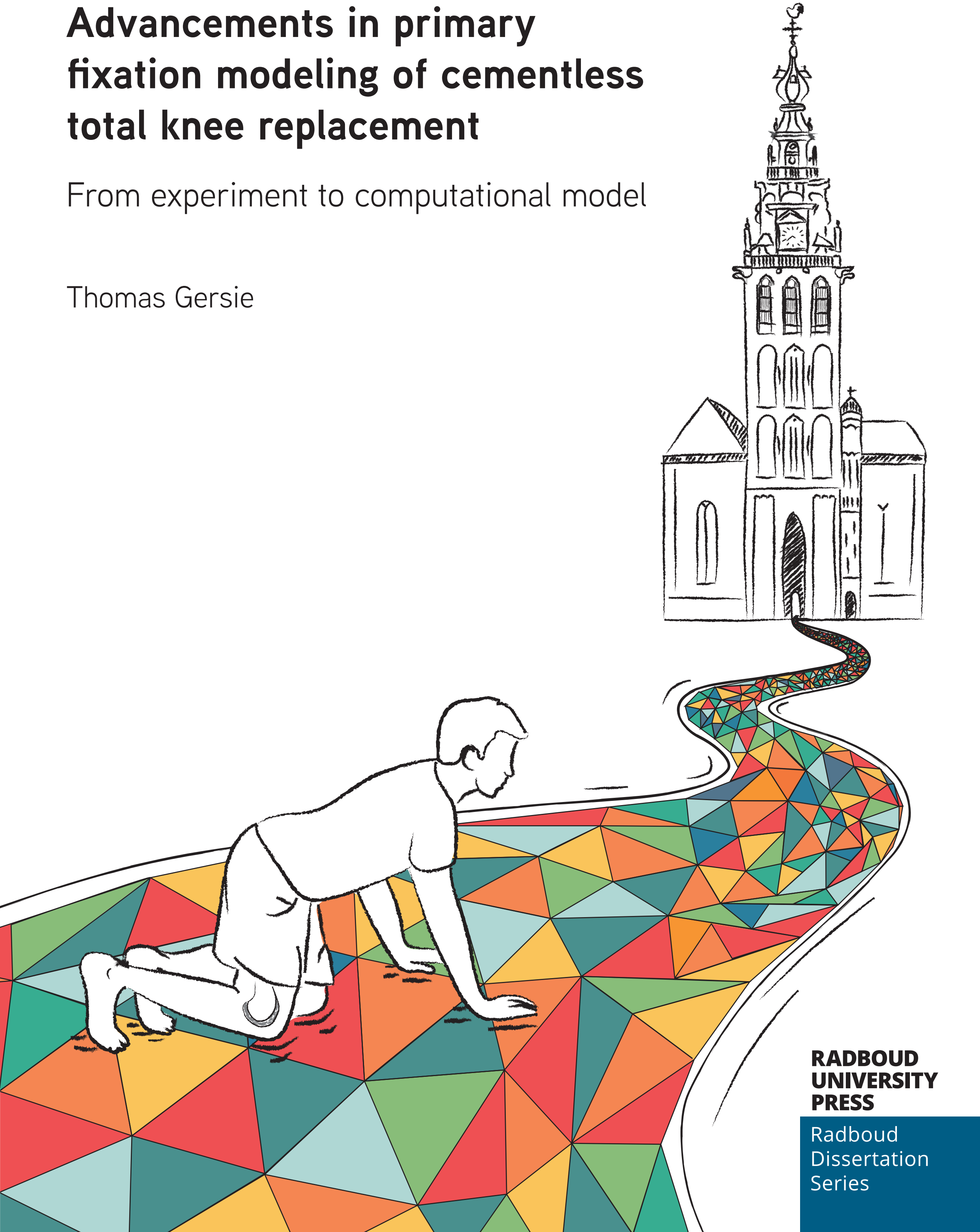

RADBOUD UNIVERSITY PRESS

Radboud Dissertation Series

Advancements in primary fixation modeling of cementless total knee replacement

From experiment to computational model

Thomas Gersie

This publication has been made possible by the PPP allowance made available by Health~Holland, Top Sector Life Sciences & Health, to simulate public-private partnerships, and DePuy Synthes (Leeds, UK).

Advancements in primary fixation modeling of cementless total knee replacement - From experiment to computational model
Thomas Gersie

Radboud Dissertation Series
ISSN: 2950-2772 (Online); 2950-2780 (Print)

Published by RADBOUD UNIVERSITY PRESS
Postbus 9100, 6500 HA Nijmegen, The Netherlands
www.radbouduniversitypress.nl

Design: Proefschrift AIO | Annelies Lips
Cover: Proefschrift AIO | Guntra Laivacuma
Printing: DPN Rikken/Pumbo

ISBN: 9789465152745
DOI: 10.54195/9789465152745
Free download at: https://doi.org/10.54195/9789465152745

RADBOUD
UNIVERSITY
PRESS

Advancements in primary fixation modeling of cementless total knee replacement

From experiment to computational model

Proefschrift ter verkrijging van de graad van doctor
aan de Radboud Universiteit Nijmegen
op gezag van de rector magnificus prof. dr. J.M. Sanders,
volgens besluit van het college voor promoties
in het openbaar te verdedigen op

maandag 25 augustus 2025
om 12.30 uur precies

door

Thomas Sebastiaan Gersie
geboren op 12 oktober 1996
te Nijmegen

Promotoren:
Prof. dr. ir. N.J.J. Verdonschot
Dr. ir. D.W. Janssen

Copromotor:
Dr. ir. T. Bitter

Manuscriptcommissie:
Prof. dr. B.A.C. Loomans
Prof. dr. P.J. Laz (University of Denver, Verenigde Staten)
Dr. ir. B. van Rietbergen (Technische Universiteit Eindhoven)

Advancements in primary fixation modeling of cementless total knee replacement

From experiment to computational model

Dissertation to obtain the degree of doctor
from Radboud University Nijmegen
on the authority of the Rector Magnificus prof. dr. J.M. Sanders,
according to the decision of the Doctorate Board
to be defended in public on

Monday, August 25, 2025
at 12.30 pm

by

Thomas Sebastiaan Gersie
born on October 12, 1996
in Nijmegen (the Netherlands)

Supervisors:
Prof. dr. N.J.J. Verdonschot
Dr. D.W. Janssen

Co-supervisor:
Dr. T. Bitter

Manuscript Committee:
Prof. dr. B.A.C. Loomans
Prof. dr. P.J. Laz (University of Denver, United States)
Dr. B. van Rietbergen (Eindhoven University of Technology)

Table of contents

Chapter 1

General introduction and thesis outline

1.1 Osteoarthritis

Osteoarthritis (OA) is a degenerative joint disease characterized by the breakdown of the cartilage and structural changes in the underlying bone. Factors that influence the development of OA include aging, obesity and injury to a joint [1]. Cartilage degeneration causes pain, stiffness, swelling and reduced mobility in the affected joints, and therefore has a big impact on the quality of life [2]. Knee OA is one of the most common forms of OA, representing 80% of the cases (Figure 1-1) [3]. In 2019, there were around 365 million people worldwide suffering from knee OA [4]. With a growing and aging population, along with rising obesity rates, the global prevalence of knee OA is expected to keep increasing. It is expected that by 2050, approximately 640 million people will have knee OA, which places a considerable economic burden on the healthcare systems and society in general [4].

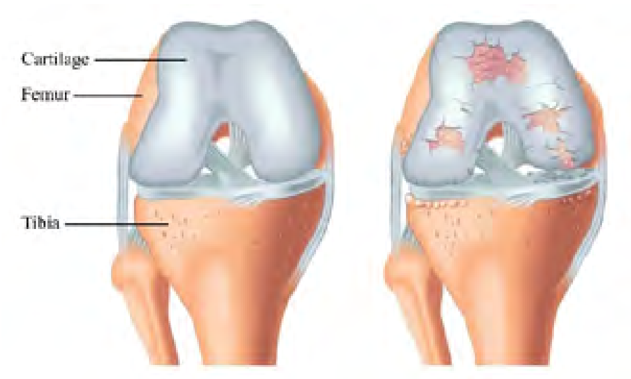

Figure 1-1: A healthy knee (left) in flexion and a knee with advanced osteoarthritis in flexion (right). In the healthy knee, the cartilage forms a smooth layer over the bone, while in the osteoarthritic knee, the cartilage is damaged, exposing the bone. Additionally, the bone is affected by the formation of bone spurs, or osteophytes. Figure adapted from [5].

1.2 Total knee arthroplasty

Total knee arthroplasty (TKA) is one of the most common orthopedic procedures for treating advanced OA of the knee, providing pain relief and restoring joint function [6]. During TKA, the damaged articular surfaces of the distal femur (thigh bone) and proximal tibia (shin bone) are replaced with prosthetic components, which include a metal femoral component, a metal tibial tray, and a polyethylene tibial insert that serves as a bearing surface (Figure 1-2). Two fixation techniques are used in TKA: cemented and cementless fixation. Cemented fixation involves fixating the prosthetic components to the bone with bone cement, ensuring immediate stability. In contrast, cementless fixation relies on bone ingrowth into the implant's porous surface, a process known as osseointegration, to achieve long-term stability. Cementless fixation is often preferred for specific patient groups, particularly younger and more physically active individuals. Over the past decade, its use has increased considerably as studies have shown comparable long-term outcomes to cemented TKA [7]. TKA is performed approximately one million times annually in the European Union (EU), and as the prevalence of knee OA continues to rise, the demand for knee replacements is expected to increase [8]. By 2050, the number of TKAs in the EU is projected to grow by 40%, with the highest increase observed in patients under 50 years old [9-11]. Although TKA generally has high success rates and favorable clinical outcomes, it does not always last a lifetime [12, 13]. Some reconstructions require revision after 15 to 30 years, posing a particular challenge for younger patients who are more active, place greater mechanical demands on the implant, and have longer life expectancies. Registry data indicate that younger patients face a higher risk of revision surgery, which is a complex and demanding procedure with significantly worse outcomes and lower survival rates compared to the primary operation [12, 13]. The most common cause of TKA failure, though second to infection in some countries, is loss of fixation at the implant-bone interface, a phenomenon known as aseptic loosening [12, 13].

This type of failure is primarily mechanical and influenced by patient-related factors, surgical technique, and implant design. In cementless TKA, early failure can occur due to inadequate primary fixation, which may ultimately prevent successful bone ingrowth into the implant surface.

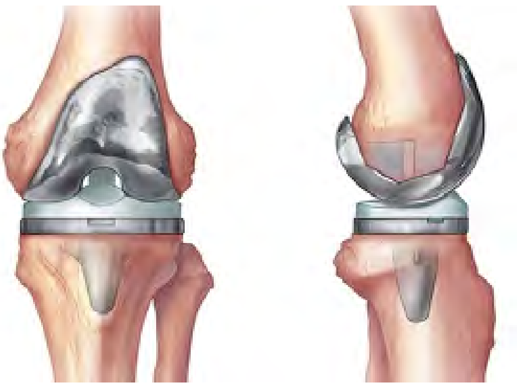

Figure 1-2: A front and side view of a knee joint after receiving a cementless total knee replacement. The femoral component and tibial tray are secured through the press-fit of the implant system, while a plastic insert serves as a bearing surface between the two components. Figure adapted from [14].

1.3 Primary fixation

In cementless TKA, fixation relies on the press-fit forces generated during surgery. To achieve this, the orthopedic surgeon cuts the femur and tibia slightly larger than the internal dimensions of the implant (Figure 1-3). During implantation, the prosthetic components are impacted onto the prepared bone using hammers and impactors. The size difference between the implant and the bone cuts, known as the interference fit, ensures a press-fit connection between the implant and the bone. The compressive forces at the implant-bone interface, along with the implant's rough surface texture, provide a stable primary fixation, which is crucial for long-term bone ingrowth (Figure 1-3). Primary stability is influenced by multiple factors, including patient-specific aspects, surgical technique and implant characteristics. To prevent early failures in TKA, it is essential to understand the underlying mechanical processes, which involve bone-implant mechanics. From a contact mechanics perspective, friction plays a key role in cementless TKA fixation, as it dictates the mechanical interaction between the implant and bone. During implantation, mechanical friction between the implant and bone causes bone damage and the removal of bone tissue, a process known as bone abrasion. This results in localized bone damage and the formation of debris, which can alter the interface properties and potentially compromise implant stability. Experimental studies have reported bone debris accumulation along the bone-implant interface, particularly in the posterior condyles, as well as residual bone particles adhering to the inner surface of removed implants [15]. In addition to contact mechanics, the mechanical properties of bone are fundamental to primary fixation. These properties directly affect the compressive forces at the bone-implant interface and ultimately determine the long-term success of cementless fixation. Understanding bone's mechanical response is essential for optimizing both surgical techniques and implant designs.

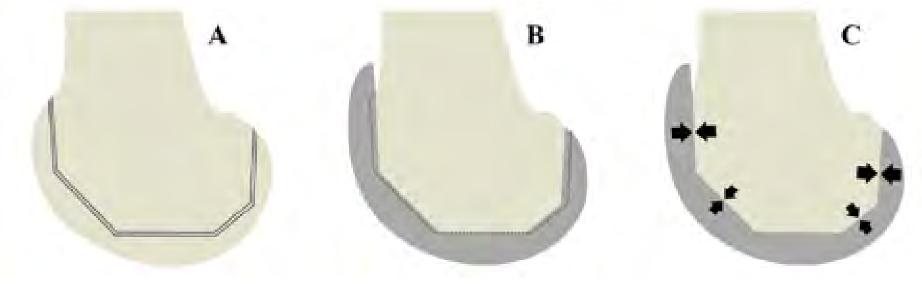

Figure 1-3: A) Side view of an intact distal femur, showing the planned cutting lines for preparing the bone to receive the femoral implant. **B)** The femur is cut slightly larger than the internal dimensions of the femoral implant (indicated by the dashed line), creating a tight press-fit that provides primary stability. **C)** This size difference, known as the interference fit, generates compressive stresses at the bone-implant interface once the implant is impacted onto the bone.

1.4 Influence of bone biomechanics on primary stability

From an engineering perspective, bone displays a complex constitutive behavior that includes elastic, plastic, and viscoelastic properties, all of which contribute to its ability to absorb and distribute mechanical loads. The overall mechanical response of bone is largely influenced by the distinct properties of its two types: cortical bone, which forms the dense outer layer and is stiffer and stronger, and trabecular bone, which is more porous and located in the inner regions. While trabecular bone is less stiff, its porous structure allows it to undergo larger deformations, enabling greater energy absorption [16]. The difference in bone stiffness, often quantified by its elastic modulus, between cortical and trabecular bone can be partly attributed to variations in bone mineral density (BMD) [17]. It is commonly known that higher BMD is associated with increased stiffness [18, 19]. Experimental studies have shown that femurs with higher BMD exhibit greater implant primary stability compared to those with lower BMD [20]. This is likely due to the more compliant response of lower BMD bone, which can compromise initial fixation stability.

Beyond elasticity, bone also undergoes plastic deformation under high loading conditions. Studies have shown that plastic damage occurs in bone after the implantation of press-fit knee implants, but the precise role of plasticity in relation to implant fixation is still not fully understood. While increasing the interference fit has been shown to improve fixation strength, beyond a certain point, further increases in the interference fit do not lead to corresponding improvement [21]. This is likely due to the creation of excessive stresses during implantation, which cause bone damage and limit further stability [22]. This highlights the importance of considering bone plasticity when evaluating implant fixation strength.

Additionally, bone exhibits viscoelastic behavior, meaning its mechanical response is time-dependent and includes phenomena such as creep and stress relaxation. Creep describes the gradual deformation of bone under a constant load, while stress relaxation refers to a decrease in stress over time under constant displacement. In the context of cementless TKA, stress relaxation may reduce the press-fit forces at the implant-bone interface after implantation, affecting primary fixation. Experimental studies have demonstrated the relevance of bone viscoelasticity [21, 23, 24]. One study on cementless femoral components observed a 17–37% reduction in implant surface strains within the first 24 hours post-implantation, indirectly indicating bone relaxation [23]. Cadaveric studies furthermore have shown that pull-out forces of press-fit pegs decrease substantially within 30 minutes of implantation, and fixation strength of press-fit hip stems is significantly reduced after 24 hours [21, 24].

While it is evident that bone biomechanics influence primary stability, quantifying these effects remains a challenge. Since direct investigation of primary fixation in patients is not feasible, preclinical testing provides a valuable alternative.

1.5 Preclinical testing of primary fixation

Preclinical experimental studies and computational modeling are essential for evaluating biomechanical interactions of press-fit designs of implants before they are used in patients. Various methods have been developed to assess primary stability, including a pull-off test, which offers a quick and straightforward measure of initial fixation strength [25]. While this test provides valuable insights, its direct correlation with long-term osseointegration and clinical success remains uncertain. What is well established is that micromotions at the bone-implant interface play a critical role in the bone ingrowth process. Animal studies have shown that osseointegration occurs when micromotions remain below 40 µm, whereas excessive micromotions above 150 µm lead to the formation of a soft tissue layer, ultimately resulting in failed fixation [26]. To assess these micromotions, both physical testing and computational modeling techniques have been employed [27-29]. Among these, finite element (FE) analysis offers a distinct advantage by enabling the simulation of complex loading conditions and quantifying micromotions that are difficult or impossible to measure experimentally, especially those occurring between specific measurement locations or in regions that are hidden from direct observation, such as the internal face of the femoral component [30].

1.6 Finite element analysis

FE analysis is a powerful computational tool used to simulate the mechanical behavior of structures under various loading conditions. In orthopedics, FE modeling has become indispensable for evaluating the performance of new implant designs, predicting failure mechanisms, and optimizing surgical techniques. By discretizing complex geometries into smaller elements, FE models can calculate stresses, strains, and deformations in both bone and implant materials under physiological loads. The mechanical properties of bone are defined in material models derived from experimental testing, which help explain its constitutive behavior [18]. In the context of cementless TKA, FE simulations have been used extensively to investigate primary fixation of implants (Figure 1-4) [15, 31-33]. Despite the widespread use of FE models in TKA research, most still rely on elastic representations of bone, which fail to accurately capture the stress and strain distributions occurring when bone stresses exceed the yield limit [31, 34-36]. As previously mentioned, observations in clinical practice confirm that plastic deformation occurs during implantation, yet this important aspect is often overlooked in FE models of TKA [37]. Some studies have incorporated plasticity models, such as the von Mises yield criterion, to simulate bone's post-yield behavior [15, 38]. However, these models still tend to underestimate micromotions and overestimate fixation strength when compared to experimental data (Figure 1-5). A potential explanation for this discrepancy could be the exclusion of time-dependent bone properties, such as stress relaxation, in the material model, as well as the neglect of bone abrasion effects during implantation.

Figure 1-4: Finite element model of a femur with a femoral component, used to study primary fixation. The smaller elements on both the bone and the implant represent the mesh used for detailed analysis of micromotions and implant-bone interaction during the early fixation phase.

These omissions lead to an inaccurate representation of bone-implant interactions, which likely contribute to discrepancies between experimental and computational micromotions. By incorporating bone stress relaxation and abrasion into FE models, a more realistic depiction of implant fixation can be achieved. This would enhance the accuracy of predictions related to primary stability of TKA components, ultimately benefiting both implant design and surgical techniques.

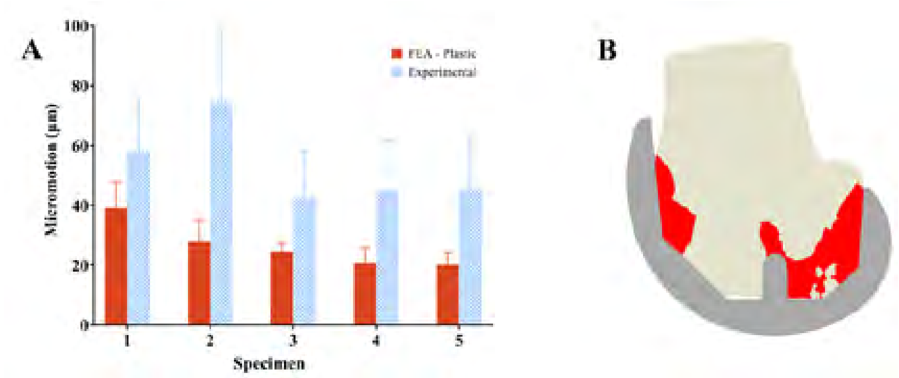

Figure 1-5: A) Comparison of experimental and computational (FEA) micromotions in femoral TKA. Despite implementing a (plastic) damage model, the simulation underestimated the experimental micromotions. **B)** A cross-section of the femur, taken through the lateral condyle in the coronal plane and directed toward the femoral center, illustrates the extent of bone plasticity, after femoral component implantation, highlighted in red. Figures adapted from Berahmani et al. (2017) [15].

1.7 Thesis outline

This thesis addresses the central question of whether incorporating viscoelastic bone behavior and bone abrasion, in addition to elastic-plastic bone properties, results in more realistic simulations that more accurately predict the primary fixation of cementless total knee implants. By improving the accuracy of FE models with these additions, the aim is to enhance implant design and surgical techniques, ultimately contributing to better clinical outcomes. To answer this question, a constitutive material model was developed to describe the viscoelastic behavior of human trabecular bone, chosen because most cortical bone is removed during the surgical procedure, leaving the implants in primary contact with trabecular bone. This model was validated using femoral TKA reconstructions, in which varying levels of bone abrasion were simulated. Finally, the impact of bone stress relaxation and abrasion on the primary fixation of femoral TKA components was analyzed.

In **Chapter 2**, an experimental method was developed using bovine bone cores to construct a material model that describes the nonlinear viscoelastic behavior of trabecular bone through uniaxial stress relaxation experiments. This method also incorporated the effect of bone density and stress relaxation duration on the material model. Using the experimental approach and testing duration from the previous chapter, **Chapter 3** investigates the viscoelastic properties of human cadaveric material from the distal femur and proximal tibia. Uniaxial stress relaxation experiments were conducted, and the results were used to develop a material model that accurately describes the nonlinear viscoelastic behavior, while also determining the influence of bone density on the model. Additionally, this new material model was applied in FE simulations to replicate the stress relaxation experiments on human trabecular bone. The focus then shifted to femoral TKA reconstructions, where **Chapter 4** examines the impact of the bone material model on press-fit force generation and primary fixation, with a particular focus on the relationship to bone density of the distal femur. For this purpose, a pull-off experiment was simulated in femoral TKA reconstructions, using models that simulated elastic, plastic, or plastic-viscoelastic responses, based on the previously developed material models. However, the plastic-viscoelastic material model had not yet been validated in a TKA reconstruction. Therefore, in **Chapter 5**, bone relaxation was incorporated in the simulation of fixation strength for femoral TKA components, and these simulations were compared with experimental measurements. Experimental prosthetic strain measurements and a physical pull-off test were performed and replicated using FE analysis. This study also examined the effect of bone abrasion on fixation strength. Since primary fixation is typically assessed by measuring or simulating micromotions at the implant-bone interface, **Chapter 6** investigates whether incorporating bone relaxation and abrasion improved the accuracy of micromotion predictions at the bone-implant interface of an uncemented femoral knee implant, making them more representative of experimental measurements. To achieve this, experimental measurements of micromotions were compared with cadaver-specific FE models, which were assigned elastic, plastic, or plastic-viscoelastic bone material properties with varying levels of virtual bone abrasion. **Chapter 7** summarizes the findings of this thesis, discusses its limitations, and outlines the implications of the results, along with potential directions for future research.

References

1. Disease, G.B.D., I. Injury, and C. Prevalence, Global, regional, and national incidence, prevalence, and years lived with disability for 310 diseases and injuries, 1990-2015: a systematic analysis for the Global Burden of Disease Study 2015. Lancet, 2016. 388(10053): p. 1545-1602 DOI: 10.1016/S0140-6736(16)31678-6.
2. Hunter, D.J. and S. Bierma-Zeinstra, Osteoarthritis. Lancet, 2019. 393(10182): p. 1745-1759 DOI: 10.1016/S0140-6736(19)30417-9.
3. Long, H., et al., Prevalence Trends of Site-Specific Osteoarthritis From 1990 to 2019: Findings From the Global Burden of Disease Study 2019. Arthritis Rheumatol, 2022. 74(7): p. 1172-1183 DOI: 10.1002/art.42089.
4. Collaborators, G.B.D.O., Global, regional, and national burden of osteoarthritis, 1990-2020 and projections to 2050: a systematic analysis for the Global Burden of Disease Study 2021. Lancet Rheumatol, 2023. 5(9): p. e508-e522 DOI: 10.1016/S2665-9913(23)00163-7.
5. Figure 1-1. https://www.knieschmerzen-wien.at/osteoarthritis-knee-en.html.
6. Bellemans, J., Ries, M.D., Victor, J.M.K., Total Knee Arthroplasty: A Guide to Get Better Performance. 2005, Springer S.
7. Agarwal, A.R., et al., Trend of using cementless total knee arthroplasty: a nationwide analysis from 2015 to 2021. Arthroplasty, 2024. 6(1): p. 24 DOI: 10.1186/s42836-024-00241-7.
8. OECD/European Union, Health at a Glance: Europe 2016: State of Health in the EU Cycle. OECD Publishing, 2016 DOI: https://doi.org/10.1787/9789264265592-en.
9. Culliford, D., et al., Future projections of total hip and knee arthroplasty in the UK: results from the UK Clinical Practice Research Datalink. Osteoarthritis Cartilage, 2015. 23(4): p. 594-600 DOI: 10.1016/j.joca.2014.12.022.
10. Klug, A., et al., The projected volume of primary and revision total knee arthroplasty will place an immense burden on future health care systems over the next 30 years. Knee Surg Sports Traumatol Arthrosc, 2021. 29(10): p. 3287-3298 DOI: 10.1007/s00167-020-06154-7.
11. Nemes, S., et al., Historical view and future demand for knee arthroplasty in Sweden. Acta Orthop, 2015. 86(4): p. 426-31 DOI: 10.3109/17453674.2015.1034608.
12. Australian Orthopaedic Association National Joint Replacement Registry (AOANJRR) Hip, Knee & Shoulder Arthroplasty: 2023 Annual Report. AOA, Adelaide, 2023.
13. National Joint Registry for England, W., Northern Ireland and the and Isle of Man, 20th Annual Report 2023. 1821, Hertfordshire, 2023.
14. Figure 1-2. https://www.mayoclinic.org/tests-procedures/knee-replacement/about/pac-20385276.
15. Berahmani, S., D. Janssen, and N. Verdonschot, Experimental and computational analysis of micromotions of an uncemented femoral knee implant using elastic and plastic bone material models. J Biomech, 2017. 61: p. 137-143 DOI: 10.1016/j.jbiomech.2017.07.023.
16. Rho, J.Y., R.B. Ashman, and C.H. Turner, Young's modulus of trabecular and cortical bone material: ultrasonic and microtensile measurements. J Biomech, 1993. 26(2): p. 111-9 DOI: 10.1016/0021-9290(93)90042-d.
17. Keyak, J.H., et al., Prediction of femoral fracture load using automated finite element modeling. J Biomech, 1998. 31(2): p. 125-33 DOI: 10.1016/s0021-9290(97)00123-1.
18. Keyak, J.H., et al., Predicting proximal femoral strength using structural engineering models. Clin Orthop Relat Res, 2005(437): p. 219-28 DOI: 10.1097/01.blo.0000164400.37905.22.

19. Helgason, B., et al., Mathematical relationships between bone density and mechanical properties: a literature review. Clinical biomechanics, 2008. 23(2): p. 135-146.
20. Berahmani, S., et al., Evaluation of interference fit and bone damage of an uncemented femoral knee implant. Clin Biomech (Bristol), 2018. 51: p. 1-9 DOI: 10.1016/j.clinbiomech.2017.10.022.
21. Berahmani, S., et al., An experimental study to investigate biomechanical aspects of the initial stability of press-fit implants. J Mech Behav Biomed Mater, 2015. 42: p. 177-85 DOI: 10.1016/j.jmbbm.2014.11.014.
22. Gebert, A., et al., Influence of press-fit parameters on the primary stability of uncemented femoral resurfacing implants. Med Eng Phys, 2009. 31(1): p. 160-4 DOI: 10.1016/j.medengphy.2008.04.007.
23. Burgers, T., et al., Time-dependent fixation and implantation forces for a femoral knee component--an in vitro study. Med Eng Phys, 2010. 32(9): p. 968-73 DOI: 10.1016/j.medengphy.2010.06.011.
24. Norman, T.L., et al., Cortical bone viscoelasticity and fixation strength of press-fit femoral stems: an in-vitro model. J Biomech Eng, 2006. 128(1): p. 13-7 DOI: 10.1115/1.2133766.
25. Berahmani, S., et al., Experimental pre-clinical assessment of the primary stability of two cementless femoral knee components. J Mech Behav Biomed Mater, 2017. 75: p. 322-329 DOI: 10.1016/j.jmbbm.2017.07.043.
26. Jasty, M., et al., In vivo skeletal responses to porous-surfaced implants subjected to small induced motions. J Bone Joint Surg Am, 1997. 79(5): p. 707-14 DOI: 10.2106/00004623-199705000-00010.
27. Abdul-Kadir, M.R., et al., Finite element modelling of primary hip stem stability: the effect of interference fit. J Biomech, 2008. 41(3): p. 587-94 DOI: 10.1016/j.jbiomech.2007.10.009.
28. Chong, D.Y., U.N. Hansen, and A.A. Amis, Analysis of bone-prosthesis interface micromotion for cementless tibial prosthesis fixation and the influence of loading conditions. J Biomech, 2010. 43(6): p. 1074-80 DOI: 10.1016/j.jbiomech.2009.12.006.
29. Conlisk, N., et al., The influence of stem length and fixation on initial femoral component stability in revision total knee replacement. Bone Joint Res, 2012. 1(11): p. 281-8 DOI: 10.1302/2046-3758.111.2000107.
30. Yang, H., et al., Validation and sensitivity of model-predicted proximal tibial displacement and tray micromotion in cementless total knee arthroplasty under physiological loading conditions. J Mech Behav Biomed Mater, 2020. 109: p. 103793 DOI: 10.1016/j.jmbbm.2020.103793.
31. Taylor, M., D.S. Barrett, and D. Deffenbaugh, Influence of loading and activity on the primary stability of cementless tibial trays. J Orthop Res, 2012. 30(9): p. 1362-8 DOI: 10.1002/jor.22056.
32. Quevedo Gonzalez, F.J., et al., An Anterior Spike Decreases Bone-Implant Micromotion in Cementless Tibial Baseplates for Total Knee Arthroplasty: A Biomechanical Study. J Arthroplasty, 2024. 39(5): p. 1323-1327 DOI: 10.1016/j.arth.2023.11.020.
33. Post, C.E., et al., A FE study on the effect of interference fit and coefficient of friction on the micromotions and interface gaps of a cementless PEEK femoral component. J Biomech, 2022. 137: p. 111057 DOI: 10.1016/j.jbiomech.2022.111057.
34. Tarala, M., et al., Experimental versus computational analysis of micromotions at the implant-bone interface. Proc Inst Mech Eng H, 2011. 225(1): p. 8-15 DOI: 10.1243/09544119JEIM825.
35. van der Ploeg, B., et al., Toward a more realistic prediction of peri-prosthetic micromotions. J Orthop Res, 2012. 30(7): p. 1147-54 DOI: 10.1002/jor.22041.

36. Viceconti, M., et al., Large-sliding contact elements accurately predict levels of bone-implant micromotion relevant to osseointegration. J Biomech, 2000. 33(12): p. 1611-8 DOI: 10.1016/s0021-9290(00)00140-8.
37. Rapagna, S., et al., Quantification of human bone microarchitecture damage in press-fit femoral knee implantation using HR-pQCT and digital volume correlation. J Mech Behav Biomed Mater, 2019. 97: p. 278-287 DOI: 10.1016/j.jmbbm.2019.04.054.
38. Kelly, N., et al., An investigation of the inelastic behaviour of trabecular bone during the press-fit implantation of a tibial component in total knee arthroplasty. Med Eng Phys, 2013. 35(11): p. 1599-606 DOI: 10.1016/j.medengphy.2013.05.007.

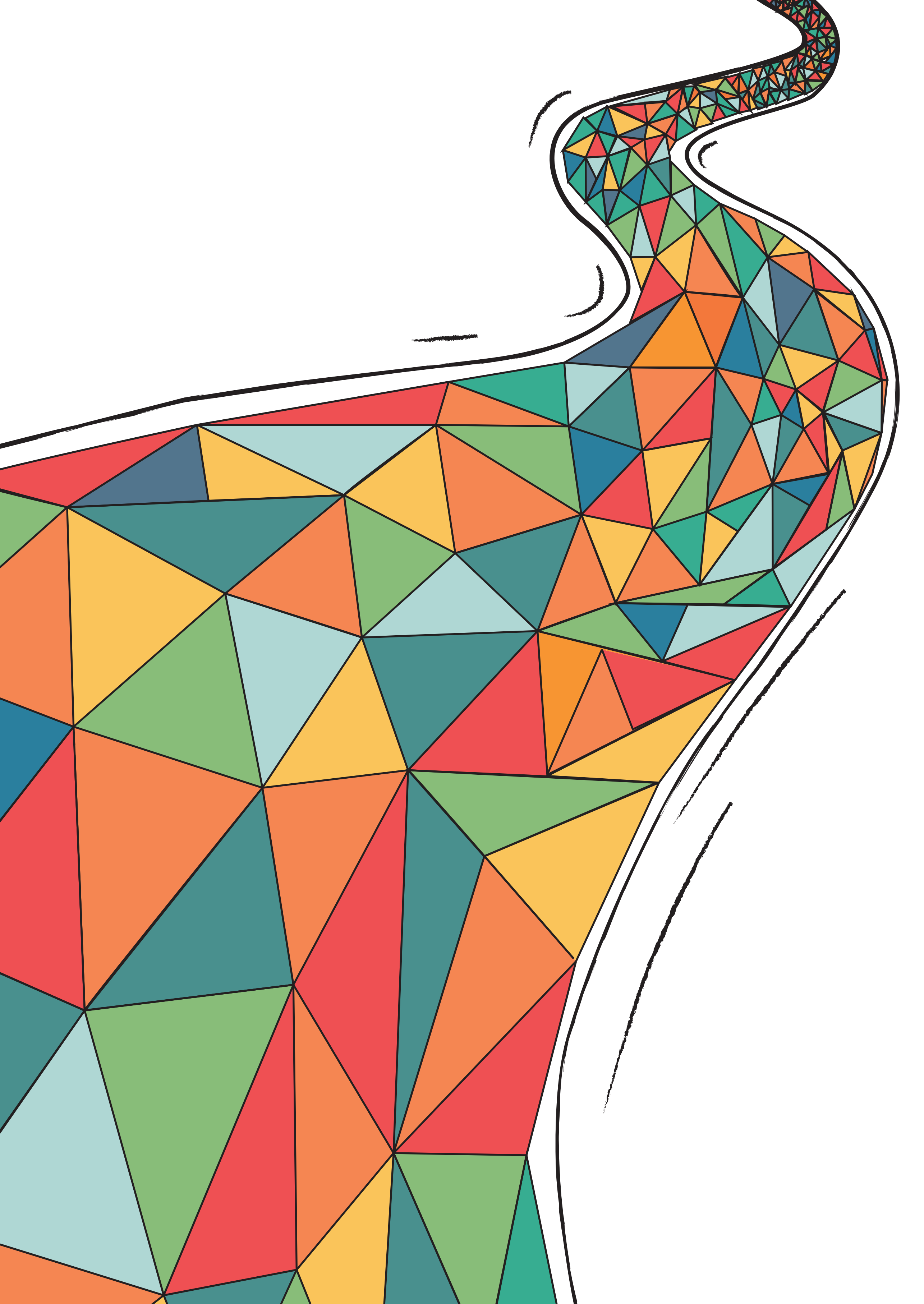

Chapter 2

Quantification of long-term nonlinear stress relaxation of bovine trabecular bone

Thomas Gersie, Thom Bitter, David Wolfson, Robert Freeman, Nico Verdonschot, Dennis Janssen

Published in Journal of the Mechanical Behavior of Biomedical materials:
https://doi.org/10.1016/j.jmbbm.2024.106434

Abstract

The reliability of computational models in orthopedic biomechanics depends often on the accuracy of the bone material properties. It is widely recognized that the mechanical response of trabecular bone is time-dependent, yet it is often ignored for the sake of simplicity. Previous investigations into the viscoelastic properties of trabecular bone have not explored the relationship between nonlinear stress relaxation and bone mineral density. The inclusion of this behavior could enhance the accuracy of simulations of orthopedic interventions, such as primary fixation of implants. Although methods to quantify the viscoelastic behavior are known, the time period during which the viscoelastic properties should be investigated to obtain reliable predictions is currently unclear. Therefore, this study aimed to: 1) Investigate the duration of stress relaxation in bovine trabecular bone; 2) construct a material model that describes the nonlinear viscoelastic behavior of uniaxial stress relaxation experiments on trabecular bone; and 3) implement bone density into this model. Uniaxial compressive stress relaxation experiments were performed with cylindrical bovine femoral trabecular bone samples (n=16) with constant strain held for 24 hours. Additionally, multiple stress relaxation experiments with four ascending strain levels with a holding time of 30 minutes, based on the results of the 24-hour experiment, were executed on 18 bovine bone cores. The bone specimens used in this study had a mean diameter of 12.80 mm and a mean height of 28.70 mm. A Schapery and a superposition model were used to capture the nonlinear stress relaxation behavior in terms of applied strain level and bone mineral density. While most stress relaxation happened in the first 10 minutes (up to 53%) after initial compression, the stress relaxation continued even after 24 hours. Up to 69% of stress relaxation was observed at 24 hours. Extrapolating the results of 30 minutes of experimental data to 24 hours provided a good fit for accuracy with much improved experimental efficiency. The Schapery and superposition model were both capable of fitting the repeated stress relaxation in a sample-by-sample approach. However, since bone mineral density did not influence the time-dependent behavior, only the superposition model could be used for a group-based model fit. Although the sample-by-sample approach was more accurate for an individual specimen, the group based approach is considered a useful model for general application.

2.1 Introduction

The reliability of computational models of bone biomechanics in orthopedic applications, such as total joint reconstructions or bone fracture repair, depends on the accuracy of the bone material properties. Trabecular bone is generally modelled as a linear time-independent elastic material in which the Young's modulus is related to the density of the bone [1-3]. Although it is widely recognized that the mechanical response of trabecular bone is time-dependent, it is often ignored for the sake of simplicity [4, 5]. However, in some cases, such as in the analysis of primary stability of press-fit implants, the viscoelastic behavior may have a significant effect on the biomechanics.

The viscoelastic response of trabecular bone has been experimentally investigated either using relaxation tests in which the time-dependent change in stress under an applied constant strain is measured over time [4-8], or in creep tests in which the change in strain under an applied constant load is measured over time [9-12]. It has previously been shown that the linear time-dependent relaxation modulus is correlated to the density of bone, thus playing a prominent role in predicting viscoelasticity [10]. However, the magnitude of the time-dependent response is affected by the applied stress/strain level [8, 11, 13], making it incorrect to be modelled using linear viscoelasticity. Hence, a nonlinear viscoelastic material model that takes bone density into account should be constructed.

The time period during which the viscoelastic properties are being investigated are important to obtain a reliable indication of the extent of stress relaxation or creep. In previous research the holding time of the constant strain/stress was as short as 100 seconds, while others showed a decreasing stress even after 1000 seconds [4, 14]. Thus, there is no consensus of the required experimental time based on current literature, while the duration of the stress relaxation behavior of bone may be of significant importance. Accordingly, the effect of duration on stress relaxation should be investigated.

From the above, it is clear that the relationship between bone density and the nonlinear stress relaxation of the trabecular bone at different strain levels should be quantified. Therefore, the objectives of this study were to: 1) Investigate the duration of stress relaxation in bovine trabecular bone; 2) construct a material model that describes the nonlinear viscoelastic behavior of uniaxial stress relaxation experiments on bovine trabecular bone; and 3) implement the bone density into this model.

2.2 Materials and methods

To accomplish the three aforementioned objectives, two separate experiments were conducted. Firstly, a 24-hour stress relaxation experimented was performed to examine the duration of stress relaxation in trabecular bone. Secondly, repeated stress relaxation experiments were used to establish a viscoelastic material model that incorporates the dependence on BMD. Subsequently, the fit accuracy and experimental testing time was optimized using the 24-hour experimental data. Additionally, the two nonlinear models were fitted on the data of the repeated stress relaxation experiments.

2.2.1 Sample preparation

Six distal bovine femora (male, age under 30 months) were obtained from a local abattoir and stored individually at -16°C in plastic bags prior to usage. Most of the cortical bone was removed using an oscillating saw (Conmed, USA), whereafter cylindrical bone cores were extracted from the trochlear region and from the anterior and posterior condyles using a diamond core drill bit (Articomed, Poland) (Figure 2-1). The drill bit had an inner diameter of 12.85 mm and a length of 70 mm. A low-speed rotating saw (Conmed, USA) was used to create parallel sections and to remove remaining cortical bone at the articulating surface, thereby creating a cylindrical sample only consisting of trabecular bone. Coring and cutting was performed on frozen femurs in air. In total 34 samples were harvested with a diameter of 12.80 ± 0.05 mm and a mean height of 28.70 ± 0.70 mm, which were of similar size as in previous studies [8, 10]. Bone cylinders were wrapped in saline-soaked gauze and stored in separate plastic airtight containers at -16°C. Before testing each end of the thawed cylindrical sample was fixed using bone cement (polymethyl-methacrylate, Candulor, Switzerland) in aluminum endcaps to minimize end-artefacts during compression testing [15]. To determine the average strain for each specific bone sample, the effective length (25.50 ± 0.56 mm) was calculated as the length of the sample between the endcaps plus half the length of the sample embedded within the endcaps [15]. A height-to-width ratio of 2.0 was chosen to avoid buckling of the samples during compression [16]. An example of a bone specimen embedded in the endcaps can be seen in Figure 2-2.

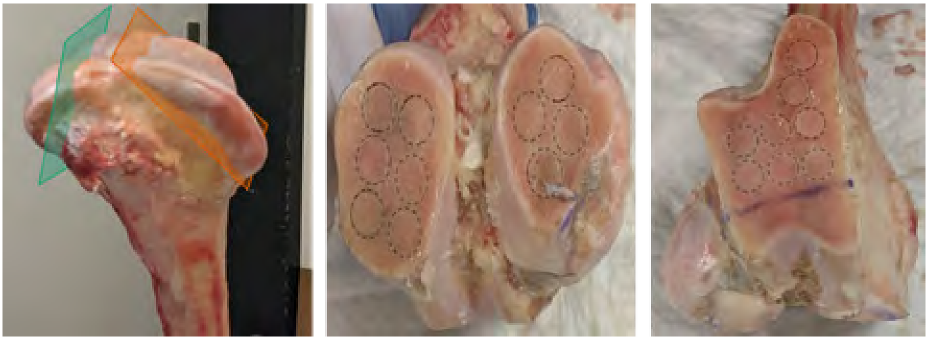

Figure 2-1: Overview of coring and cutting locations. On the left picture, the cutting planes on the distal femur are shown. The green plane shows the cut through the cortex of the condyles and the orange plane shows the trochlear cut. In the middle image, the drilling holes and thereby specimen locations in the condyles. On the right, the specimens locations in the trochlea of this particular bovine femur are displayed.

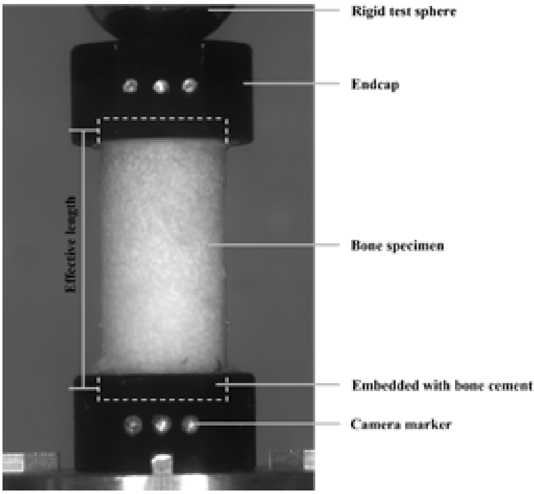

Figure 2-2: Picture of bone specimen embedded in endcaps with bone cement made by a camera system to measure actual displacement of the bone specimen using the camera markers on the endcaps. The effective length is defined as the length of the sample between the endcaps plus half the length of the sample embedded within the endcaps. On top of the upper endcap, a rigid test sphere was placed to accommodate for slight angular variations of the sample and endcap.

2.2.2 CT imaging

Before extraction of the bone samples, computed tomography (CT) images were made of each drilled distal femur with a voxel size of 0.5 x 0.47 x 0.47 mm (Canon medical systems, Japan – 80 kV 250 mA) along with a solid calibration phantom (Image Analysis, USA) [17]. In-house developed software was used to convert

Hounsfield Units to calibrated BMD values [18]. A cylindrical model was aligned with the (drilled) specimen in the CT scan after which an average BMD was calculated for each specimen. All cylinders were then sorted based on their average BMD value.

2.2.3 Stress relaxation experiments

After being embedded in the endcaps, the samples were placed in the testing environment, which consisted of a water basin filled with physiological saline, supplemented with 1% penicillin/streptomycin (Capricorn scientific, Germany), with a temperature of 37.0 ± 0.5 °C. After 30 minutes in the basin, each sample was preconditioned by applying ten cycles of 0.1% strain and was allowed to recover for 30 minutes, which is similar to previous studies [9]. Stress relaxation experiments were conducted using an MTS machine (MTS Systems Corporation, USA) with a measuring frequency of 10 Hz (24-hours of stress relaxation) and 100 Hz (repeated stress relaxation experiments). The sample was compressed using a rigid test sphere on top of the upper endcap (Figure 2-2). Static strains of 0.2, 0.4, 0.6, and 0.8 % were applied to measure the viscoelastic response to stay below the yield strain of 0.8% of bovine trabecular bone [19]. The strains were applied and removed at a strain rate of 0.01 s^{-1}. A 500 N loadcell (type AT101 – 0.5/5) was used when applying 0.2% strain. At higher strain levels, a 15 kN (type 2816) loadcell was used. An overview of the stress relaxation experiments is displayed in Figure 2-3.

A digital camera (Pixelink, Canada) was used to optically measure the axial displacement applied to the bone samples. Markers on the endcaps (Figure 2-2) were used to calculate the actual strains the samples were subjected to. Images were calibrated using a reference object in the field of view. Prior testing showed the accuracy of our system to be 2 µm. Images of the uniaxial compression test were continuously captured (2 images/second for the first 30 seconds, then 1 image each 30 seconds) and deformations of the samples were calculated with a custom-written Matlab script (Matlab R2021b, USA).

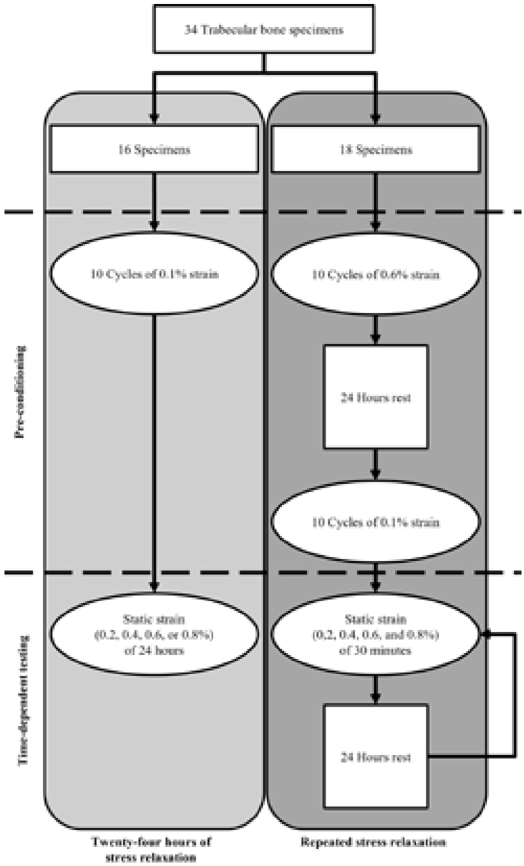

Figure 2-3: Overview of executed stress relaxation experiments.

2.2.3.1 Twenty-four hours stress relaxation

To determine if the strain level influenced the duration of stress relaxation of trabecular bone, four specimens per strain level were selected to ensure homogeneous distribution of the BMD. Therefore, 16 samples were used in total. Each sample was subjected to a single static strain level for 24 hours to measure the duration of the stress relaxation response.

2.2.3.2 Repeated stress relaxation

The remaining 18 samples were used for the repeated stress relaxation and were pre-conditioned at 0.6% strain for ten cycles and were then allowed to recover for 24 hours. This strain level was chosen because no plastic deformation was observed during the twenty-four hours stress relaxation. By increasing the strain level, our goal was to enhance repeatability, which is even more important in the repeated stress relaxation experiments. Repeated stress relaxation experiments were conducted on the samples to examine the influence of applied strain level on the time-dependent response, without interference of the specific properties of that individual sample. These samples were compressed on four consecutive days at increasing static strains from 0.2 to 0.8%, with 0.2% increments. Prior to the static strain, the samples were subjected to ten cycles of 0.1% strain as described previously and were allowed to recover for 30 minutes. After each experiment the sample was allowed to recover in saline at 5 °C for 24 hours, as it has been demonstrated that bone fully recovers within this timeframe [6]. The holding time of the constant strain was determined after analysis of the 24-hour experiments with the aim to determine a feasible testing time which included most of the stress relaxation behavior.

2.2.4 Experimental testing time

To optimize fit accuracy and experimental testing time, the data of the 24-hour experiment were analyzed in the following manner. First, the stress relaxation modulus was calculated using the actual strain data, obtained by the camera. Thereafter, the first 10, 30, 60, and 120 minutes of data per experiment were used to create a power law representation (Equation 2-1) of the relaxation modulus (E(t)). Using the power law representation each data set was extrapolated to 24 hours.

$$E(t) = E_1 + E_2 t^n \qquad (2\text{-}1)$$

Where E_1, E_2 and n are constants. Fitting was carried out in Matlab using the curve fitting toolbox, by minimizing the error using nonlinear least squares (Matlab R2021b, Mathworks, USA). The mean percentual error was calculated to determine which experimental time showed the optimal trade-off between fit accuracy and testing time. This experimental time was then used as the holding time of the constant strain as explained in 2.2.3.2.

2.2.5 Nonlinear viscoelastic models

To capture the effect of applied strain level on the time-dependent mechanical properties, two nonlinear viscoelastic models were considered in this study. In previous studies, these models were successful in describing nonlinear stress relaxation in dentin and ligaments [20, 21]. The material models were fitted to the repeated stress relaxation experiments after extrapolation to 24 hours. It was assumed that the strain rate of 0.01 s^{-1} was sufficiently fast to act as instantaneous for the strains examined in this study. As a result, the initial ramp to the maximum force before the stress relaxation was considered as a step and excluded from the fitting process [12]. Fitting was carried out using the same procedure as described previously in section 2.2.4.

2.2.5.1 Simplified Schapery method (SSM)

The original Schapery model was simplified by considering a given strain, ε_0, as a step function, setting h_1 and α_ε to unity, and where the transient modulus is in the form of a power law ($C * t^n$) [21, 22]:

$$\sigma(\varepsilon_0, t) = h_e(\varepsilon_0)E_e\varepsilon_0 + h_2\varepsilon_0 C t^n \tag{2-2}$$

in which, $E_e\varepsilon_0$ and E_0Ct^n refer to equilibrium and transient stress levels, respectively. Constants C, E_e and n can be determined based on the experimental relaxation results. In addition, h_e and h_2 reflect the nonlinearity in elastic properties and the rate of relaxation, respectively, which are both functions of strain [21]. Moreover, it is hypothesized that both the linear and nonlinear parameters are correlated to the BMD.

2.2.5.2 Modified superposition method (MSM)

Findley took another approach by suggesting a single power law in the form of [23]:

$$\sigma(\varepsilon_0, t) = \varepsilon_0 Z(\varepsilon_0) t^{M(\varepsilon_0)} \tag{2-3}$$

Where $Z(\varepsilon_0)$ and $M(\varepsilon_0)$ are functions of strain and could be obtained from isochronal stress-strain data, and from stress relaxation rate-strain data, respectively. It is assumed that both Z and M are also functions of the BMD, representing the initial stress relaxation modulus and the rate of relaxation respectively. Different than in the SSM formulation, the exponent (M) in the MSM is not a constant value and is dependent on the strain.

2.3 Results

The first part of this section focuses on presenting the results from the 24-hour experiment, which aimed to examine the stress relaxation duration in bovine trabecular bone while also optimizing fit accuracy and experimental testing time. Subsequently, two nonlinear viscoelastic models were used to capture the stress relaxation of trabecular bone, utilizing the experimental data obtained from the repeated stress relaxation experiments. Both a sample-by-sample approach and a group-based approach were employed, and the model fits were compared to each other. Furthermore, the influence of BMD on the stress relaxation is shown.

2.3.1 Duration of stress relaxation

In total 16 samples were subjected to 24 hours of constant strain, varying from 0.14 to 0.75% actual strain measured optically, whereas the target was 0.2 to 0.8% strain. The range of BMD of the bone samples was 229.3 – 562.3 mg cm^{-3}. All samples showed a typical stress relaxation response, which can be seen in Figure 2-4 using the load, normalized to full scale. After 24 hours, stress relaxation ranging from 41.0% to 68.7% was observed. Both applied strain level and BMD did not show any significant effect on the level of stress relaxation. Large proportions of stress relaxation occurred in the first 10 minutes in which the maximal peak force (the maximally measured load directly after the strain is applied) decreased by 25.6 to 52.9% (Figure 2-5).

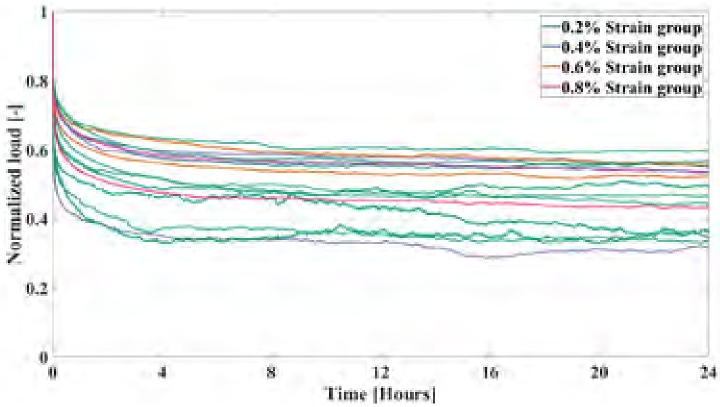

Figure 2-4: Experimental stress relaxation recovery after 24 hours of constant strain for all applied strain levels. The optically measured strain level was used to assign the samples to the different strain groups.

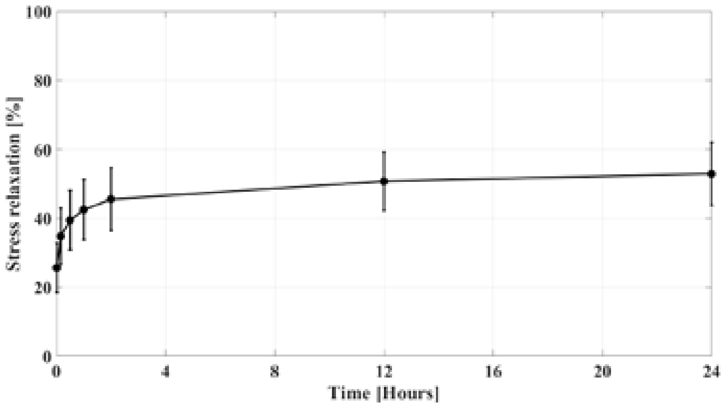

Figure 2-5: The mean percentage of stress relaxation and the standard deviation for different amounts of experimental time, without strain level taken into account.

2.3.1.1 *Experimental testing time*

The experimental data of the 16 samples from the 24-hour stress relaxation experiments were used to optimize the fit accuracy and experimental testing time. First, the stress relaxation modulus was calculated from the actual strain, measured using the camera system and the experimental load. 10 Minutes to 2 hours of experimental data were extrapolated with a first order power law (extrapolated fit or EF) and compared to a power law fit of the original 24-hour data (original fit or OF). These calculations were conducted for each sample, and the results for one sample are displayed in Figure 2-6.

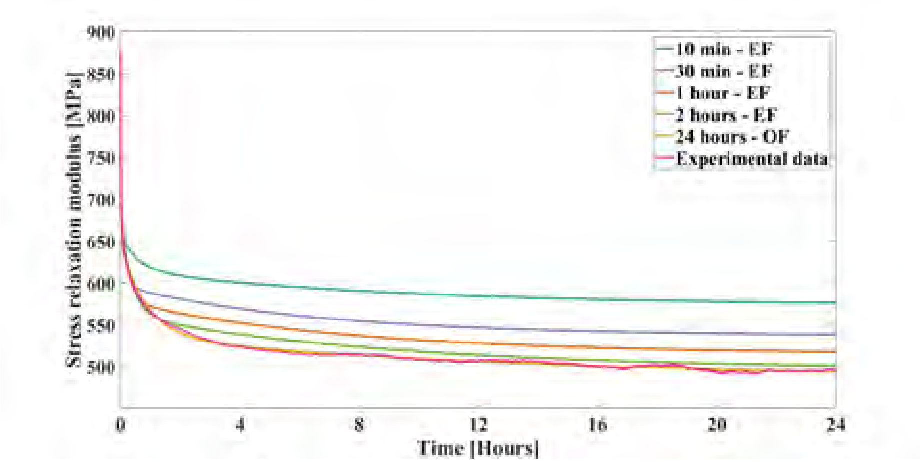

Figure 2-6: Typical behavior when comparing extrapolated fits and the 24-hour experimental data/fit. The sample displayed here underwent 0.49% strain and has a BMD of 335.1 mg cm^{-3}.

The mean accumulated percentual error was then compared between the different extrapolated fits and the original fit. The extrapolated fit from 10 minutes experimental data showed the highest percentual error of 18.5% and 2 hours the lowest mean error of 5.4% (Figure 2-7).

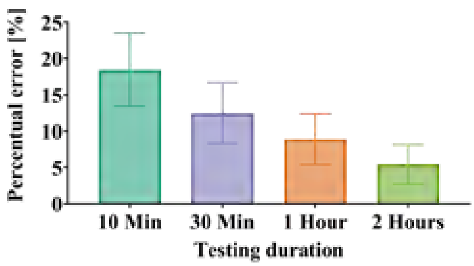

Figure 2-7: Mean accumulated percentual errors and standard deviation when comparing the fits on the experimental data of different durations extrapolated to 24 hours to the original 24-hour fit on the experimental data.

A holding time of 30 minutes showed an acceptable compromise between fit accuracy and experimental testing time. Therefore, the subsequent repeated stress relaxation experiments were executed with a constant displacement for 30 minutes.

2.3.2 Repeated stress relaxation

Although the intention was to impose strains ranging from 0.2% to 0.8%, in reality, the strains, optically measured, were for the 4 levels: 0.19 ± 0.02%; 0.34 ± 0.05%; 0.49 ± 0.06%; 0.62 ± 0.09%. The BMD range of the samples was 210.4 to 503.9 mg cm^{-3}. The experimental data were extrapolated using a first order power law to 24 hours.

2.3.2.1 Influence of BMD on viscoelasticity

To quantify the influence of the bone mineral density on the viscoelastic properties, first it was verified if the bone mineral density actually influenced the time-dependent properties. For the different strain levels, the spearman correlation between bone mineral density and the stress relaxation rates (the slope of the log-log stress relaxation (stress vs. time)) was calculated. A very weak negative correlation (-0.322; p = 0.007) was found between bone density and the stress relaxation rate, which is the slope of the log-log time-stress curve (Figure 2-8).

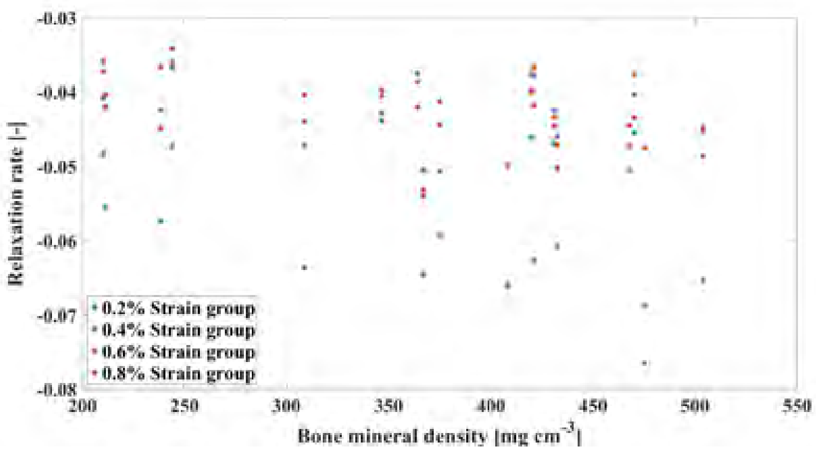

Figure 2-8: The BMD versus the stress relaxation rate for all the 18 samples per strain level. The optically measured strain level was used to assign the samples to the different strain groups.

2.3.3 Quantification of nonlinear viscoelastic parameters

2.3.3.1 Sample-by-sample model fit

The Schapery method and the Modified Superposition method were used to determine the nonlinear viscoelastic parameters for each sample individually. This is shown for a single sample in Figure 2-9.

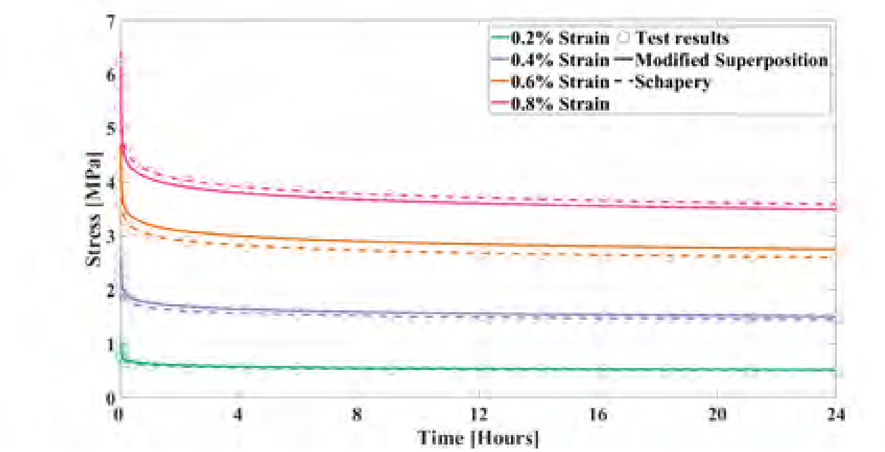

Figure 2-9: An example of sample-based fitting on the experimental results of the repeated stress relaxation experiments of a sample with a BMD of 432.4 mg cm^{-3} using the Modified Superposition (MSM) and Simplified Schapery (SSM) models.

To determine the accuracy of both models to the experimental data, the initial stress relaxation modulus (the initial modulus calculated using the maximal stress and the actual applied strain), and the stress relaxation rate (the slope of the log-log time-stress curve), were compared for the different models at each strain level (Figure 2-10).

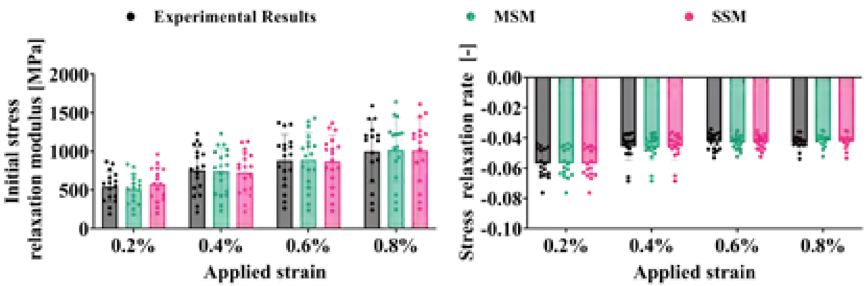

Figure 2-10: On the left side, the initial stress relaxation modulus is displayed for the experimental results, the MSM and the SSM models. On the right side, the stress relaxation rate is shown for the experimental results, the MSM and the SSM models. MSM and SSM models were calculated based on four strain levels per sample.

Both the MSM and the SSM models show a good resemblance with the experimental results for the initial modulus and the relaxation rate. The initial stress relaxation modulus demonstrated a high variety between samples, while this was limited for the stress relaxation rate.

2.3.3.2 Group-based model fit

In the previous approach, a sample-by-sample approach was used to fit the two models. To obtain a more global overview of the viscoelastic behavior and the effect of bone density and strain level, a group-based model fit, using the BMD values and the actual applied strain levels of all samples simultaneously, was performed. However, given the weak correlation between the BMD and the stress relaxation rate (2.3.2.1), it was assumed that the BMD and the stress relaxation rate were not correlated, meaning the BMD did not influence the time-dependent properties. As earlier mentioned, the effect of BMD on the time-independent properties is already established [24, 25]. Since the time-dependent and the time-independent properties cannot be separated in the SSM model, only the MSM model was used in these further analyses.

In the MSM (Equation 2-3), the M parameter accounts for the time-independent properties and was correlated to both BMD and the initial strain, while the Z parameter, accounting for the time-dependent properties, was assumed to only be dependent on the strain level, resulting in Equation 2-4. The numerical values of the nonlinear viscoelastic parameters are presented in Table 2-1.

$$\sigma(\phi,\varepsilon,t) = (A\varepsilon + (B * \phi^{C} + D)) * \varepsilon t^{E\varepsilon^{F}+G} \tag{2-4}$$

Table 2-1: Parameters for the stress function $\sigma(\phi,\varepsilon,t)$ displayed in Equation 2-4.

Nonlinear viscoelastic parameters		
A = 4.34 x 10^{4}	D = 670	G = -3.86 x 10^{2}
B = -5.14 x 10^{10}	E = -3.63 x 10^{-6}	
C = -3.61	F = -1.35	

The material model based on the group-based model fit led to a reduced accuracy of the prediction of the experimental results, in comparison to the method used in of 2.3.3.1.

In Figure 2-11, an example of an accurate fit and a poor fit using the group-based MSM model can be observed. For both samples, it is shown that the actual shape of the MSM and the experimental results for the corresponding strain did match, while the absolute values of stress did not. As previously explained, the A-term of the MSM relates to the initial modulus and therefore corresponds to the absolute values (and the starting point of the stress relaxation curve). Moreover, a large difference in fit accuracy can be observed between the two samples depicted in Figure 2-11.

The initial moduli and stress relaxation rates are displayed per strain level in Figure 2-12. The highlighted icons resemble the samples in Figure 2-11.

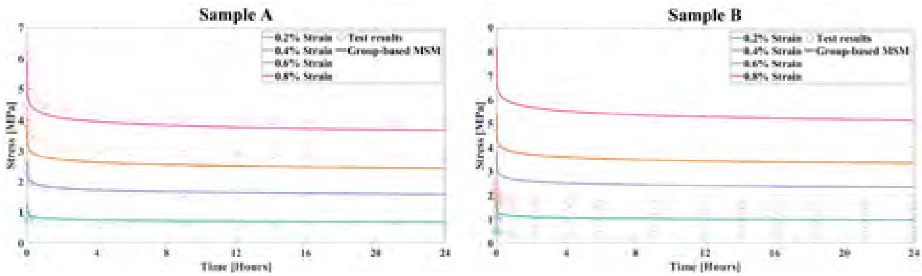

Figure 2-11: Time versus stress for the four strain levels for two samples with a density of: **A)** 375.3 mg cm^{-3}; **B)** 470.5 mg cm^{-3} using the group-based MSM model.

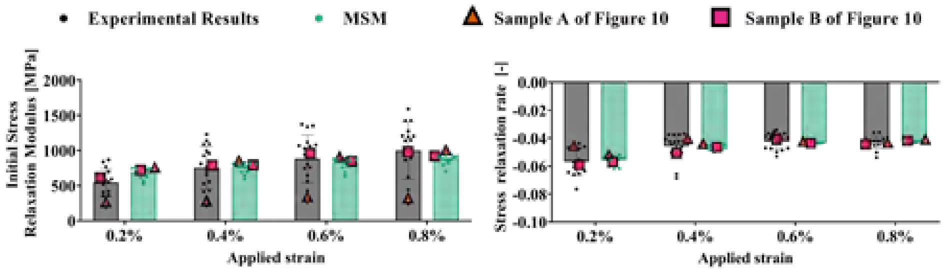

Figure 2-12: Left: The initial stress relaxation modulus is displayed for the experimental results and the BMD-dependent MSM per strain level. Right: Stress relaxation rate is shown for the experimental results and calculated from the BMD-dependent MSM material model per strain level. The highlighted samples show the samples which are displayed in Figure 2-11.

2.4 Discussion

The aim of this study was threefold: 1) To investigate the duration of stress relaxation in bovine trabecular bone; 2) to construct a material model that describes the nonlinear viscoelastic behavior of uniaxial stress relaxation experiments on bovine trabecular bone; and 3) to implement bone density into this model.

In line with these objectives, it was demonstrated that the majority of stress relaxation of the trabecular bone occurs during the first ten minutes, but it did not level off completely after 24 hours of constant strain. Moreover, a material model for the nonlinear stress relaxation of bovine trabecular bone was developed using two different models. Both nonlinear material models showed accurate predictions of the nonlinear viscoelastic behavior when examining a single sample. However, this accuracy was significantly decreased when a group-based model was constructed using the multiple superposition model. The time-dependent behavior did not show a correlation with BMD, but, as expected, was found to be nonlinearly influenced by the applied strain [8, 11, 13].

In contrast with other studies, we found that even after 24 hours of constant strain the stress relaxation did not level off completely: After 10 minutes an average stress relaxation of 35% was observed, which increased to 53% after 24 hours [8, 10, 12]. However, in the previously mentioned studies typically a holding time of up to 10 minutes (600 seconds) was used, which means on average 18% of the total stress relaxation that would occur in 24 hours was missed. However, an experimental time of 24 hours may not be feasible when examining large numbers of specimens. Our study demonstrated that extrapolating data from a testing period of 30 minutes to 24 hours provides a good compromise between accuracy and testing time, but when a higher accuracy is desired, longer testing is advisable. However, increasing the testing period from 30 minutes to 1 hour only results in a slight decrease in the percentual error, from 12.5% to 8.9%.

While the testing time in our study was different from other studies, the stress relaxation could be compared during the first 100 seconds of testing. Deligianni et al. found on average 20% stress relaxation in comparison to the observed 27% after 100 seconds in the current study [6]. Quaglini et al. observed only 10% of stress relaxation in same time period [8]. However, they defatted the specimens from the bone marrow, which is known to have a significant effect on the viscoelastic behavior [26].

Our experiments showed that as the strain increased, the rate of stress relaxation decreased in a non-linear fashion, indicating less stress relaxation is occurring. This finding is consistent with previous research [8]. However, the exact reason for this behavior is unknown. Possibly, marrow is pushed out of the samples at higher strain values, which may affect the viscoelastic response [26]. Alternatively, it can be hypothesized that due to higher compression the pore size decreases, which limits the outflow of water and decreases the viscoelastic behavior.

For the second objective, a simplified Schapery model and a multiple superposition model were used for a specimen-specific fit (which excluded the influence of BMD on the viscoelastic behavior) of the uniaxial stress relaxation experiments. These models have previously successfully been used to describe stress relaxation of other tissues, such as ligaments and dentin [20, 21]. In this study, both models captured the nonlinear stress relaxation of trabecular bone with great accuracy.

Most studies into the viscoelastic properties of trabecular bone and other biological tissues exclusively use the aforementioned specimen-specific approach, which hinders the prediction of the time-dependent response in a population [8, 12, 20, 21]. This study also implemented a group-based fitting approach, incorporating both the applied strain and the BMD as input factors. However, when all samples were considered and BMD was taken into account, the accuracy of the models decreased significantly.

Surprisingly, BMD did not influence the time-dependent behavior, which contrasts with the findings of Manda et al. [10, 12]. However, these results support the idea that bone viscoelasticity is solely influenced by collagen [27]. In this study, the collagen content of the bone specimens was not determined to verify comparable levels of collagen among the samples, despite variations in BMD.

Since the BMD exclusively influenced the time-independent mechanical behavior investigated in this study, rather than the stress relaxation, it is crucial to distinguish between the elastic and viscoelastic properties in the material models. However, the SSM model is unable to separate elastic and viscoelastic properties and thereby was not suitable for fitting the group-based model. The MSM model is separable and therefore, the experimental results were fitted with an adapted version of this model (Equation 2-4). The MSM model demonstrated a high variation in the accuracy of predicted stress relaxation between different samples (Figure 2-11). The model showed less variability in the initial stress relaxation modulus (term Z in Equation 2-3) than what was found in the experimental results for all strain levels. Therefore, the MSM model is capable of predicting the stress relaxation behavior of bone with an average initial modulus at each strain level, while for samples with an initial modulus which deviates greatly from the average modulus, the accuracy of the predictive capabilities of the MSM decreases vastly. The large variability in initial stress relaxation modulus observed in the experiments could be caused by the method to calculate this modulus. In this study, the measured stiffness or initial stress relaxation modulus was determined by calculating the initial apparent modulus (at t=0.001s) for each strain, which is the tangent of two data points.

However, traditionally the apparent modulus is calculated over a larger range of strain levels (e.g., 0.2% - 0.7% strain), which provides a higher accuracy of the tangent modulus.

In this study bovine tissue was used as an alternative material for human trabecular bone. Considering that the strength and stiffness of bovine trabecular bone are comparable to that of human trabecular bone, it can be hypothesized that their viscoelastic properties are also similar [28, 29]. Consequently, this study holds the potential to be employed in simulations of various orthopedic applications, providing a reliable first estimate of the viscoelastic response. In the event that varying levels of stress relaxation are observed between bovine and human trabecular bone in the future, the multiple stress relaxation protocol developed in this work establishes a solid foundation for experiments at investigating the time-dependent behavior of human trabecular bone. Due to the limited sample size the anatomical location of the samples was not taken into account. As the anatomical location does have an effect on the stiffness of the trabecular bone, future research should include its effect on the viscoelastic behavior [24].

Despite the limitations, the newly developed material model is useful for implementing in simulations of many orthopedic applications, since samples close to the average relaxation modulus of the experimental results could be predicted accurately, which is displayed in Figure 2-11A and Figure 2-12. The sample of Figure 2-11B showed an experimentally measured initial modulus on the lower end, which led to a significant difference in the calculated modulus using the MSM, which can be seen in Figure 2-12. Furthermore, the experimentally measured stress relaxation does correspond with the determined stress relaxation rate by the MSM.

This study provides valuable insights into the stress relaxation of trabecular bone under constant loading for up to 24 hours. While longer testing may not always be practical, we recommend holding the constant strain for a minimum of 30 minutes and extrapolating the data to 24 hours. When incorporating the time-dependent response of bone in finite element models, it is important to simulate this 24-hour period, considering the large amount of stress relaxation that still occurs on the longer term. The significant level of stress relaxation observed in trabecular bone highlights the importance of incorporating viscoelastic behavior in orthopedic simulations, such as those related to implant fixation, to ensure more accurate results.

References

1. Pankaj, P., Patient-specific modelling of bone and bone-implant systems: the challenges. Int J Numer Method Biomed Eng, 2013. 29(2): p. 233-49 DOI: 10.1002/cnm.2536.
2. Taylor, M., D.S. Barrett, and D. Deffenbaugh, Influence of loading and activity on the primary stability of cementless tibial trays. J Orthop Res, 2012. 30(9): p. 1362-8 DOI: 10.1002/jor.22056.
3. van der Ploeg, B., et al., Toward a more realistic prediction of peri-prosthetic micromotions. J Orthop Res, 2012. 30(7): p. 1147-54 DOI: 10.1002/jor.22041.
4. Schoenfeld, C.M., E.P. Lautenschlager, and P.R. Meyer, Jr., Mechanical properties of human cancellous bone in the femoral head. Med Biol Eng, 1974. 12(3): p. 313-7 DOI: 10.1007/BF02477797.
5. Zilch, H., et al., Material properties of femoral cancellous bone in axial loading. Part II: Time dependent properties. Arch Orthop Trauma Surg (1978), 1980. 97(4): p. 257-62 DOI: 10.1007/BF00380706.
6. Deligianni, D.D., A. Maris, and Y.F. Missirlis, Stress relaxation behaviour of trabecular bone specimens. J Biomech, 1994. 27(12): p. 1469-76 DOI: 10.1016/0021-9290(94)90196-1.
7. Bredbenner, T.L. and D.T. Davy, The effect of damage on the viscoelastic behavior of human vertebral trabecular bone. J Biomech Eng, 2006. 128(4): p. 473-80 DOI: 10.1115/1.2205370.
8. Quaglini, V., V. La Russa, and S. Corneo, Nonlinear stress relaxation of trabecular bone. Mechanics Research Communications, 2009. 36(3): p. 275-283 DOI: 10.1016/j.mechrescom.2008.10.012.
9. Bowman, S.M., et al., Compressive creep behavior of bovine trabecular bone. J Biomech, 1994. 27(3): p. 301-10 DOI: 10.1016/0021-9290(94)90006-x.
10. Manda, K., et al., Linear viscoelasticity - bone volume fraction relationships of bovine trabecular bone. Biomech Model Mechanobiol, 2016. 15(6): p. 1631-1640 DOI: 10.1007/s10237-016-0787-0.
11. Yamamoto, E., et al., Development of residual strains in human vertebral trabecular bone after prolonged static and cyclic loading at low load levels. J Biomech, 2006. 39(10): p. 1812-8 DOI: 10.1016/j.jbiomech.2005.05.017.
12. Manda, K., et al., Nonlinear viscoelastic characterization of bovine trabecular bone. Biomech Model Mechanobiol, 2017. 16(1): p. 173-189 DOI: 10.1007/s10237-016-0809-y.
13. Bowman, S.M., et al., Creep contributes to the fatigue behavior of bovine trabecular bone. J Biomech Eng, 1998. 120(5): p. 647-54 DOI: 10.1115/1.2834757.
14. Burgers, T.A., et al., Post-yield relaxation behavior of bovine cancellous bone. J Biomech, 2009. 42(16): p. 2728-33 DOI: 10.1016/j.jbiomech.2009.08.005.
15. Keaveny, T.M., et al., Systematic and random errors in compression testing of trabecular bone. J Orthop Res, 1997. 15(1): p. 101-10 DOI: 10.1002/jor.1100150115.
16. Zhao, S., et al., Standardizing compression testing for measuring the stiffness of human bone. Bone Joint Res, 2018. 7(8): p. 524-538 DOI: 10.1302/2046-3758.78.BJR-2018-0025.R1.
17. Eggermont, F., et al., Calibration with or without phantom for fracture risk prediction in cancer patients with femoral bone metastases using CT-based finite element models. PLoS One, 2019. 14(7): p. e0220564 DOI: 10.1371/journal.pone.0220564.
18. Derikx, L.C., et al., Implementation of asymmetric yielding in case-specific finite element models improves the prediction of femoral fractures. Comput Methods Biomech Biomed Engin, 2011. 14(2): p. 183-93 DOI: 10.1080/10255842.2010.542463.

19. Kopperdahl, D.L. and T.M. Keaveny, Yield strain behavior of trabecular bone. J Biomech, 1998. 31(7): p. 601-8 DOI: 10.1016/s0021-9290(98)00057-8.

20. Emamian, A., et al., Nonlinear viscoelastic properties of human dentin under uniaxial tension. Dent Mater, 2021. 37(2): p. e59-e68 DOI: 10.1016/j.dental.2020.10.025.

21. Provenzano, P.P., et al., Application of nonlinear viscoelastic models to describe ligament behavior. Biomech Model Mechanobiol, 2002. 1(1): p. 45-57 DOI: 10.1007/s10237-002-0004-1.

22. Schapery, R.A., On Characterization of Nonlinear Viscoelastic Materials. Polymer Engineering and Science, 1969. 9(4): p. 295-+ DOI: DOI 10.1002/pen.760090410.

23. Findley, W.N., Creep And Relaxation Of Nonlinear Viscoelastic Materials. 1976.

24. Morgan, E.F., H.H. Bayraktar, and T.M. Keaveny, Trabecular bone modulus-density relationships depend on anatomic site. J Biomech, 2003. 36(7): p. 897-904 DOI: 10.1016/s0021-9290(03)00071-x.

25. Keyak, J.H., et al., Predicting proximal femoral strength using structural engineering models. Clin Orthop Relat Res, 2005(437): p. 219-28 DOI: 10.1097/01.blo.0000164400.37905.22.

26. Linde, F., Elastic and viscoelastic properties of trabecular bone by a compression testing approach. Dan Med Bull, 1994. 41(2): p. 119-38.

27. Bowman, S.M., et al., Results from demineralized bone creep tests suggest that collagen is responsible for the creep behavior of bone. J Biomech Eng, 1999. 121(2): p. 253-8 DOI: 10.1115/1.2835112.

28. Oftadeh, R., et al., Biomechanics and mechanobiology of trabecular bone: a review. J Biomech Eng, 2015. 137(1): p. 0108021-01080215 DOI: 10.1115/1.4029176.

29. Poumarat, G. and P. Squire, Comparison of mechanical properties of human, bovine bone and a new processed bone xenograft. Biomaterials, 1993. 14(5): p. 337-40 DOI: 10.1016/0142-9612(93)90051-3.

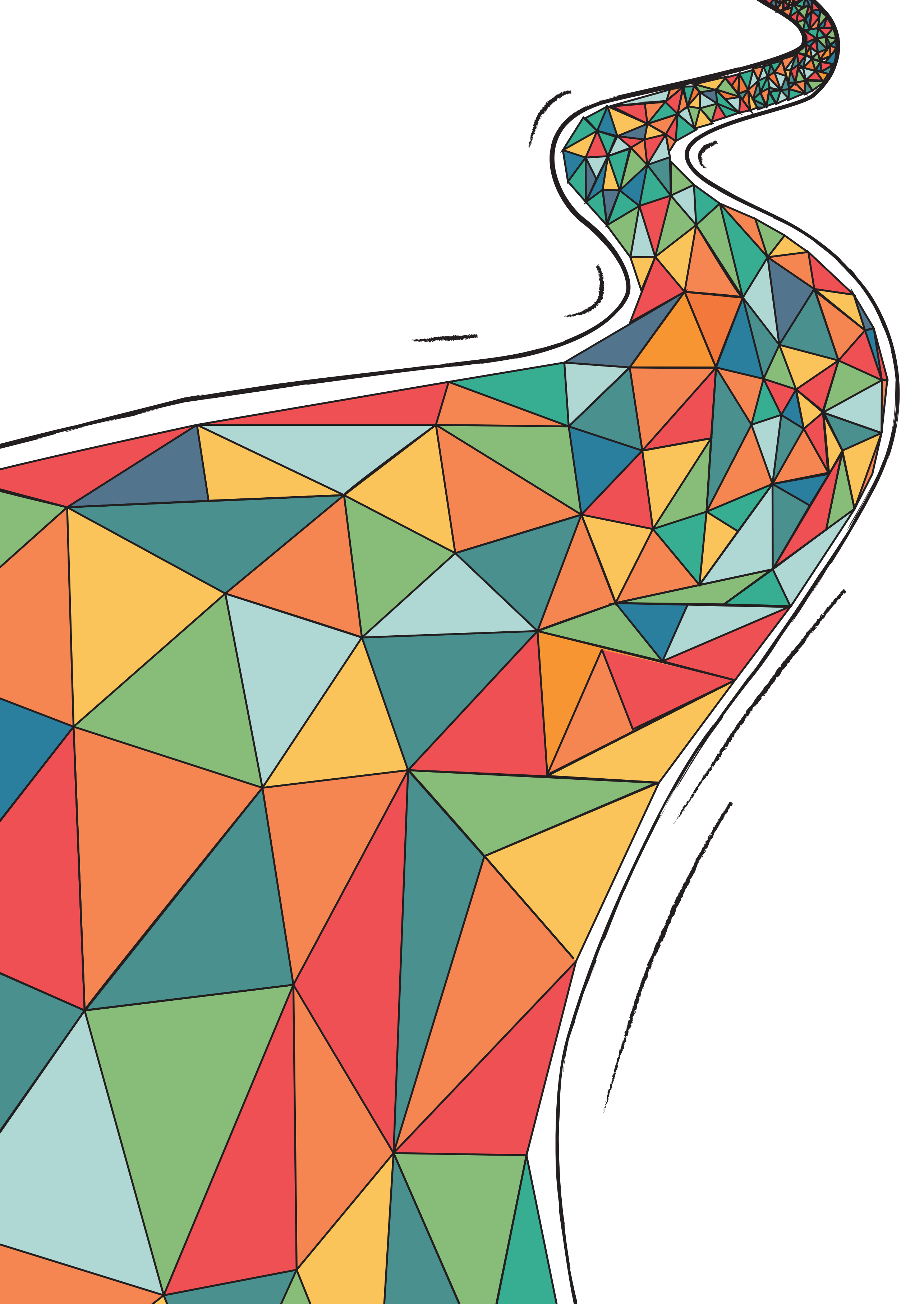

Chapter 3

Characterization of nonlinear stress relaxation of the femoral and tibial trabecular bone for computational modeling

Thomas Gersie, Thom Bitter, David Wolfson, Robert Freeman, Nico Verdonschot, Dennis Janssen

Published in Medical Engineering & Physics: https://doi.org/10.1016/j.medengphy.2025.104324

Abstract

Computational models of orthopedic reconstructions are reliant on bone material properties, but viscoelastic behavior of trabecular bone is often ignored in numerical simulations. The inclusion of stress relaxation could be of importance for the accuracy of models simulating the primary stability of cementless implants. In this study, a material model to describe the nonlinear viscoelastic behavior of human trabecular bone was constructed based on uniaxial stress relaxation experiments. The relationship of bone mineral density (BMD) and stress relaxation was explored, and the material model was implemented in sample-specific finite element (FE) simulations.

Cylindrical trabecular human bone specimens, from the distal femur and proximal tibia, were subjected to stress relaxation tests, undergoing compression with strains from 0.2% to 0.8% for 30 min on four consecutive days. The experimental data were extrapolated to 24 h. Similar levels of stress relaxation were found for femoral and tibial specimens, with an average 54.4% stress relaxation and a maximum level of 81.6%. Using a modified superposition model, the specimen-specific nonlinear stress relaxation behavior was captured. However, when the samples were considered collectively, no correlation was found between applied strain, BMD and the viscoelastic response. Therefore, the average level of stress relaxation in combination with existing BMD-stiffness relationships were implemented in FE simulations for each individual specimen. While the FE models, on average, overestimated the overall stiffness by 64%, they were able to adequately capture the stress relaxation response.

3.1 Introduction

Computational models to study orthopedic issues related to total joint arthroplasty or bone fracture repair rely heavily on bone biomechanics. Accurately determining and representing the bone material properties is important for the reliability of these models and may affect performance predictions for measures such as primary stability of cementless implants. Previous work has shown that linear elastic bone models can result in mechanical behavior that is not representative, and more complex bone material models may provide a better approximation. For instance, using a Von Mises material model that simulates the plastic behavior of bone has been shown to significantly improve the prediction of primary stability of knee implants compared to a linear elastic bone model [1]. An additional property that is generally ignored is viscoelasticity, while the mechanical response of trabecular bone is time-dependent [2–6]. Including viscoelasticity can have a significant effect on the simulating of the primary stability of press-fit implants.

The viscoelastic response of trabecular bone has been investigated through relaxation or creep tests, which measure the time-dependent change in stress or strain under an applied constant strain or load [4, 6–13]. While it has been shown that the linear time-dependent relaxation modulus is correlated to the density of bone, the time-dependent response is not linear and varies with the level of applied stress or strain. Therefore, a linear viscoelastic model may be insufficient to model the bone behavior [9,11,13,14]. Thus, a nonlinear viscoelastic material model that considers bone density as a predictor should be developed to accurately model the viscoelastic behavior of trabecular bone in orthopedic applications.

In our previous study we developed a nonlinear material model for bovine trabecular bone, and we found that BMD did not influence the viscoelastic response [15]. While bovine bone may have different time-independent mechanical properties than human trabecular bone, the actual difference in viscoelastic properties is currently unknown [16]. Similarly, it is currently not known if the relationships with BMD of the viscoelastic response depends on the anatomic location, such as is the case for the relation between BMD and the Young's modulus [17, 18]. Therefore, in this study, the viscoelastic properties of both the distal femur and proximal tibia were studied. In addition, the material model should be useable in a finite element (FE) framework to investigate its effect on the biomechanics of orthopedic applications. As such, the aims of the current study were to: (1) perform uniaxial stress relaxation experiments on human trabecular bone; (2) to construct a material model that accurately describes the nonlinear viscoelastic behavior and determine the effect of bone density on the developed model; and (3) implement this material model in FE simulations of the stress relaxation experiments.

3.2 Materials and methods

This study is divided in three parts: (1) Experimental testing of bone specimens to measure the nonlinear stress relaxation; (2) identification of the model parameters of a nonlinear viscoelastic material model based on the experimental results; (3) finite element simulations of the experimental specimens, based on CT images and the developed material model, with a comparison against the experimental results.

3.2.1 Experimental testing

A schematic overview of the experimental testing can be found in Figure 3-1.

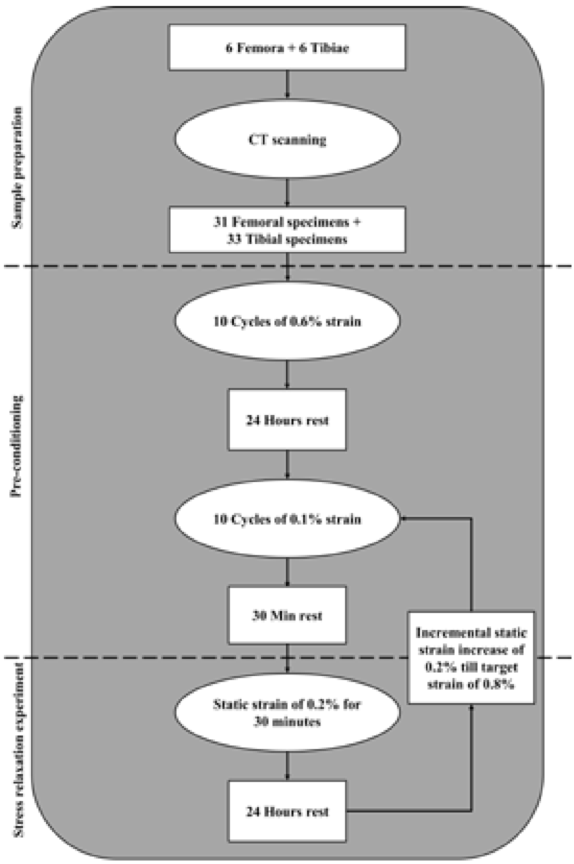

Figure 3-1: Overview of sample preparation, preconditioning and executed stress relaxation experiments.

3.2.1.1 CT imaging

Six fresh-frozen human cadaveric femora and paired tibiae (2 male and 4 female, average 67 (SD: 15) years of age) were received from the Anatomy Department of the Radboud University Medical Center. Computed tomography (CT) images were made of each distal femur and proximal tibia with a voxel size of 0.25 × 0.20 × 0.20 mm (Toshiba medical systems, Japan – 120 kV 250 mA) along with a solid calibration phantom (Image Analysis, USA) [19]. CT scanning was conducted after the bone cores were drilled, with the cored regions remaining intact within the bone, allowing for precise alignment of the 3D specimen meshes in the CT scans. In-house developed software was used to convert Hounsfield Units to calibrated BMD values [20]. A cylindrical model was aligned with the (drilled) specimen in the CT scan, after which the average BMD was calculated for each specimen.

3.2.1.2 Sample preparation

Thirty cylindrical trabecular bone samples were taken from the distal femora and thirty-three bone specimens from the proximal site of the paired tibiae. Specimens were cored from load-bearing regions, with tibial samples taken parallel to the long axis and distributed across the anterior, posterior, medial, and lateral regions of the tibial plateau (Figure 3-2). Femoral samples were cored from the anterior and posterior condyles, with fewer specimens retrieved from the posterior regions due to spatial constraints. The articulating surface and cortical bone were removed using a low-speed rotating saw (Conmed, USA), resulting in samples consisting only of trabecular bone. The bone specimens were drilled to identical dimensions, with a diameter of 9.55 ± 0.05 mm and a mean height of 21.5 ± 0.51 mm, ensuring a consistent height-to-width ratio of 2.0 to avoid buckling of the samples during compression [21]. The bone specimens were wrapped in saline-soaked gauze and stored individually in airtight containers at -16 °C until use. Before experimental testing, each end of the cylindrical sample was fixated in an aluminum endcap, with visual markers, using bone cement (poly methyl-methacrylate, Candulor, Switzerland) to minimize end-artifacts during compression testing [22]. A minimal amount of bone cement was applied to ensure fixation of the bone core in the endcaps, while minimizing the influence of the cement on the observed stress relaxation. A 3D-printed aligner tool was used to ensure proper alignment of the bone specimen within the endcaps. To determine the actual strain on the bone specimen, the effective length (18.9 ± 0.51 mm) was calculated as the length of the sample between the endcaps plus half of the length embedded within the endcaps (Figure 3-3) [22].

Figure 3-2: Anatomical locations of cylindrical trabecular bone specimens harvested from the distal femur (left) and proximal tibia plateau (right). Dashed circles indicate the coring sites, distributed across anterior, posterior, medial, and lateral regions to ensure representative sampling of load-bearing areas.

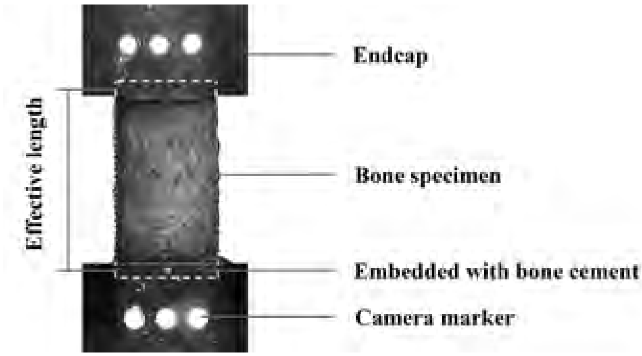

Figure 3-3: Picture of a femoral bone specimen embedded in endcaps with bone cement made by a camera system to measure actual displacement of the bone specimen using the camera markers on the endcaps. The effective length is defined as the length of the sample between the endcaps plus half the length of the sample embedded within the endcaps.

3.2.1.3 Stress relaxation experiments

Prior to testing the embedded bone specimens were immersed in a water basin containing a physiological saline solution, supplemented with 1% penicillin/streptomycin (Capricorn scientific, Germany), at a temperature of 37.0 ± 0.5 °C for 30 min. Stress relaxation experiments were conducted using a custom-built MTS system (MTS Systems Cor poration, USA) equipped with a 15 kN load cell (type 2816, Interface, USA). A measuring frequency of 10 Hz was used. The samples were preconditioned at 0.6% strain for ten cycles to reduce experimental variability and were then allowed to recover for 24 hours, fully submerged in an airtight container filled with saline at 5 °C. The next day, the samples underwent a cyclic strain with an amplitude of 0.1% strain and were allowed to recover for 30 min prior to testing [10]. Then, the specimens were loaded at a strain rate of 0.01 s^{-1} to 0.2% strain, which was held constant for 30 min, which was the optimal holding time determined in our previous study [15]. The specimens were then allowed to recover for another 24 hours under the same conditions as the first recovery period, as it has been demonstrated that bone fully recovers within this timeframe [7]. After recovery, specimens were tested at the next strain level. In total, the samples were compressed on four consecutive days at static axial strains of 0.2, 0.4, 0.6 and 0.8%. These strain levels were chosen to remain below the yield strain of 0.84% of human trabecular bone [23]. Repeated stress relaxation experiments were conducted to examine the influence of applied strain level on the time-dependent response, without interference of the specific properties of that individual sample.

A digital camera (Pixelink, Canada) was used to optically measure (accuracy: 2 µm) the axial and lateral displacement applied to the bone samples, using markers on the endcaps (Figure 3-3) to calculate the (actual) strain that was achieved during testing. Images of the uniaxial compression test were continuously captured (2 images/second for the first 30 s, then 1 image each 30 seconds) and deformations of the samples were calculated based on a custom-written MATLAB script (MATLAB R2023a, USA).

3.2.2 Determination of nonlinear viscoelastic model parameters

The experimental data were extrapolated to 24 hours using a first-order power law, since our previous study indicated that stress relaxation in trabecular bone did not level off within 30 min (the experimental time in this study) [15]. Further explanation regarding the first-order power law and its application can be found in Gersie et al. [15]. In our previous study, a modified superposition model (MSM) effectively captured the effect of applied strain level on the time-dependent mechanical properties of bovine trabecular bone. Therefore, following the extension of the data, an MSM was fitted to the experimental data of the human specimens. The model parameters were quantified for each specific sample (referred to as sample-specific) and collectively for all specimens (group-based). The sample-specific approach is able to identify the strain dependency, whereas the group-based approach incorporates both the strain dependency and the effect of BMD on stress relaxation. Fitting was conducted in MATLAB (MATLAB R2023a, MathWorks, USA) using the curve fitting toolbox, by minimizing the error using nonlinear least squares.

3.2.2.1 *Modified superposition model (MSM)*

Findley suggested a single power law to describe the viscoelasticity of materials in the form of [24]:

$$\sigma(\varepsilon_0, t) = \varepsilon_0 Z(\varepsilon_0) t^{M(\varepsilon_0)} \tag{3-1}$$

In which $\sigma(\varepsilon_0, t)$ is the stress, ε_0 is the applied strain, and *t* is the time. $Z(\varepsilon_0)$ and $M(\varepsilon_0)$ are functions of strain in the form of:

$$Z(\varepsilon_0) = A\varepsilon_0 + B \tag{3-2}$$

$$M(\varepsilon_0) = C{\varepsilon_0}^{D+F} \tag{3-3}$$

Whereby, A to F represent material constants. The choice for the power law in Equation 3-3 was based on the experimental data of our previous study on bovine femoral trabecular bone [15]. The $Z(\varepsilon_0)$ represents the initial relaxation modulus. The parameters of Equation 3-2 were derived from isochronal stress-strain data constructed from the stress relaxation data of each individual specimen. Moreover, Equation 3-3, denoting the stress relaxation rate, $M(\varepsilon_0)$, was fitted to stress relaxation rate-strain data of each bone core, which was calculated as the tangent of the log-log plot of the stress-time curve for each strain level. In the group-based method, the relationship between the initial relaxation moduli and stress relaxation rates, determined in the sample-specific approach, with both applied strain and BMD was examined.

3.2.3 Numerical simulation

The established material model of Equation 3-1 with strain and BMD dependency was implemented in FE software (Marc-Mentat 2023.1, Hexagon, USA) using an in-house developed Fortran subroutine. The material model was verified by simulating the stress-relaxation experiments for all specimens. The outcomes of the numerical simulations were compared to stress-time curves of the experiments.

The FE simulation was divided into two distinct phases. In the first phase, the sample-specific actual strains, measured on the endcaps using DIC, were applied to the surface nodes of the bone core that were in contact with the upper endcap during the experiments. In the second phase, this displacement was held constant during which the stress relaxation that occurred in 24 hours was simulated. Throughout both phases, the bone cylinder was constrained in all directions at the nodes of the bone surfaces, which were within the lower endcap in the experiments, thereby replicating the experimental setup.

3D meshes of the cylindrical trabecular bone specimens were created with sample-specific geometries, using linear four-noded tetrahedral elements (element size: 0.5 mm). Since the CT scanning was conducted after drilling the specimens but before their removal from the bone, the 3D mesh of each bone cylinder was manually aligned with the CT scan by matching its outer surfaces with the drill cuts. This ensured proper positioning within the calibrated CT images for assigning element-specific BMD values. A Poisson's ratio of 0.3 was assigned to all elements.

In case no correlation was found between the stress relaxation and both the strain and BMD, the element-specific BMD values were converted to Young's moduli using previously determined relationships [25]:

$$E(BMD) = 1.49 * 10^4(8.87 * 10^{-4}BMD + 6.33 * 10^{-2})^{1.86} \quad (3\text{-}4)$$

The average level of stress relaxation of 24 hours (μSR), determined from the stress relaxation experiments of all specimens, was then modelled as described by Equation 3-5 using a custom subroutine.

$$\sigma_{phase2} = \sigma_{phase1} - \mu SR * \sigma_{phase1} \quad (3\text{-}5)$$

In this case, the stress relaxation was simulated in an isotropic manner, resulting in uniform relaxation levels in all directions.

3.2.4 Statistical analysis

All statistical analyses were performed using GraphPad Prism 9.5.0 (GraphPad Software, USA). A p-level of 0.05 was defined as statistically significant. A Kruskal-Wallis test was performed to examine the differences between the amount of stress relaxation for each strain level for both the femoral and tibial specimens. Subsequently, a Dunn's test was used for the post hoc analysis to examine which groups differed significantly. Moreover, the average stress relaxation, for each strain level, of the femoral and tibial specimens was compared using a Mann-Whitney test. To examine the correlation between the applied strain or BMD and the stress relaxation rate, a Spearman's correlation coefficient was calculated.

3.3 Results

In this section, first the experimental testing and quantification of the nonlinear viscoelastic parameters are shown, after which the implementation in FE simulations is presented.

3.3.1 Experimental testing

The strains measured optically were slightly below the target strains for both the femoral specimens as the tibial specimens (Table 3-1). The BMD range of the femoral samples was 95.2 to 288.5 mg cm^{-3}, and 64.6 to 319.3 mg cm^{-3} for the tibial samples.

Table 3-1: The optically measured strains using the endcap markers for the four target strain groups for specimens originating from the distal femur and proximal tibia.

Target strain	Femoral specimens	Tibial specimens
0.2%	0.18 ± 0.02%	0.18 ± 0.05%
0.4%	0.34 ± 0.06%	0.34 ± 0.06%
0.6%	0.50 ± 0.08%	0.48 ± 0.11%
0.8%	0.67 ± 0.11%	0.64 ± 0.11%

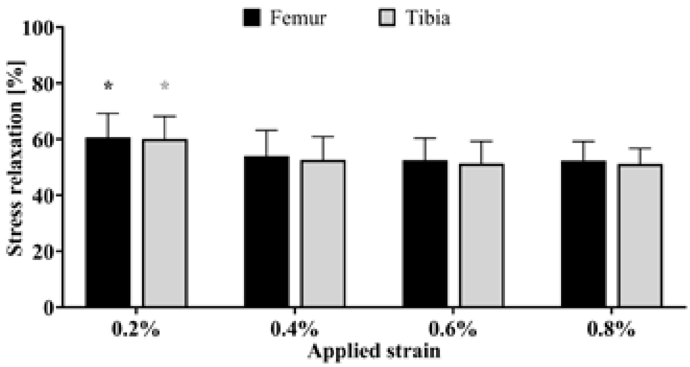

Figure 3-4: Average amount of stress relaxation for each strain level for trabecular bone specimens originating from the distal femur and proximal tibia in 24 hours. Significantly higher levels of stress relaxation were found when testing at 0.2% strain compared to higher strain levels, which is indicated by the asterisk symbol.

The extrapolated experimental data are shown in Figure 3-4. An average stress relaxation of 54.9% and 53.8% was observed in femoral and tibial specimens, respectively. No significant difference in the average level of stress relaxation was found at each strain level between the femoral and tibial samples Thus, similar levels of stress relaxation after 24 hours were observed for specimens harvested from the distal femur and from the proximal tibia. Specimens from both the femur and tibia showed higher levels of stress relaxation at a strain level of 0.2% compared to when tested at higher strain levels, which was statistically significant.

3.3.2 Quantification of nonlinear viscoelastic parameters

The repeated stress relaxation experiments were used to construct a modified superposition model to predict the nonlinear stress behavior of the trabecular bone. The model fitting was performed for each specific sample and collectively for all specimens.

3.3.2.1 Sample-specific approach

The MSM was used to determine the nonlinear viscoelastic parameters for each sample individually. The sample-specific approach only takes applied strain level into account, while ignoring the samples characteristics, such as BMD. The typical stress relaxation response and the predictions by the MSM are shown in Figure 3-5 for a femoral specimen. The predictions using the MSM showed a mean accumulated percentual error for the femur and tibia of respectively: 7.2 ± 5.3% and 7.5 ± 5.7%.

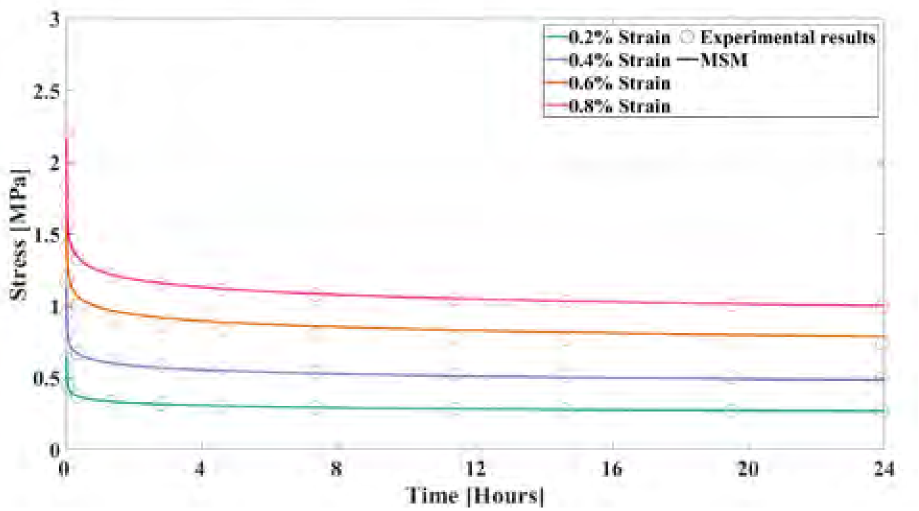

Figure 3-5: An example of sample-based fitting on the extrapolated experimental results of the repeated stress relaxation experiments of a femoral sample with a BMD of 171.1 mg cm^{-3} using the Modified Superposition model (MSM).

3.3.2.2 *Group-based approach*

To obtain a more global overview of the viscoelastic behavior and the effect of bone density and strain level, a group-based model fit, using the BMD values and the actual applied strain levels of all samples simultaneously, was performed. Since specimens from the femur and tibia showed similar amounts of stress relaxation, the samples were combined in this approach.

3.3.2.2.1 Strain and BMD dependency of the model parameters

To construct a nonlinear viscoelastic material model, the correlation between the applied strain, the BMD and the stress relaxation rate was determined. The stress relaxation rate was calculated as the tangent of the log-log plot of the time-stress curve. Figure 3-6A shows the weak ($r = 0.2320$, $p = 0.0003$) correlation between the applied strain and the relaxation rate. No significant correlation was found between the BMD and the stress relaxation rate (Figure 3-6B). These findings indicate no accurate material model could be constructed with input parameters that depended on the applied strain level or the BMD using the group-based approach. Therefore, the average level of stress relaxation of stress relaxation was used in the FEA.

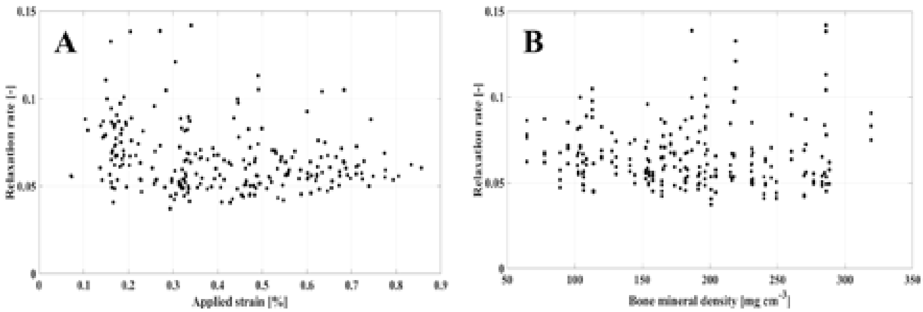

Figure 3-6: The relaxation rate versus the applied strain **(A)** or BMD **(B)** to display the effect of these parameters on the amount of stress relaxation.

3.3.2.2.2 Average levels of stress relaxation

Since the stress relaxation rate was independent of applied strain and BMD, the mean level of stress relaxation observed from the stress relaxation experiments was used in the FE simulations. The stress was normalized to full scale to be applicable for each individual specimen (Figure 3-7). The average amount of stress relaxation was 54.4%, while a minimal and maximal value of 38.1 and 81.6%, respectively, were observed.

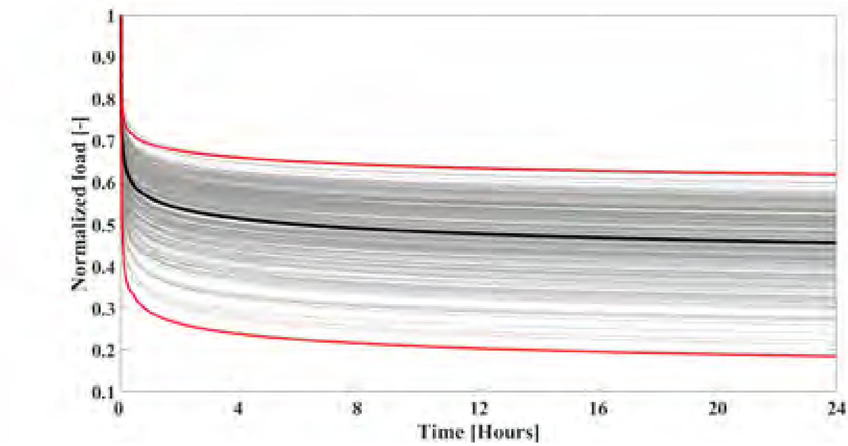

Figure 3-7: Stress relaxation curves of all executed experiments after normalization over the initial value of axial load. The black line indicates the average level of stress relaxation, while the red lines show the minimal and maximal stress relaxation curves.

3.3.2.3 FE implementation

Stress relaxation of 54.4% in 24 hours was successfully implemented in the FE framework, which is visualized in Figure 3-8. Since previously determined BMD-stiffness relations were used (Equation 3-4), an overestimation of the stiffness relative to the experimental measurements was observed. Therefore, rather than an intrasample comparison to verify the simulated level of stress relaxation, the average stress over time in the experiments and the simulations was compared (Figure 3-9). The stress for each sample-specific FE model was determined by summing the equivalent reaction forces at the nodes constrained at the bottom of the bone core. This constraint simulated the bottom endcap used in the experiments. Utilizing these reaction forces guaranteed consistent stress measurements in the bone core for both the experiment and the simulation. While the FE models on average overestimated the stresses by 63.9% as a result of the stiffness overestimation, the simulations were able to capture the variability observed in the experiments (Figure 3-9).

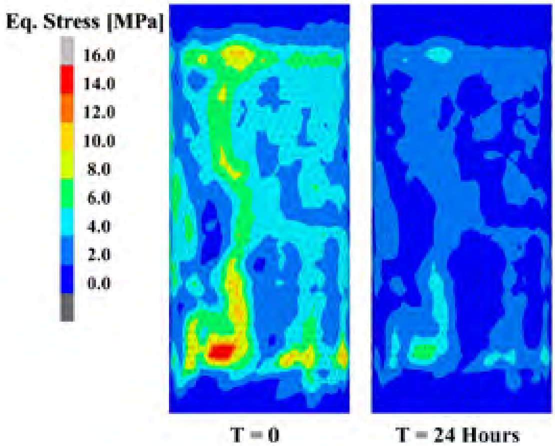

Figure 3-8: Equivalent stress (von Mises stress) map of the simulation of a bone specimen with a BMD of 249.3 mg cm^{-3} and with 0.6% strain applied at T = 0 (start point of stress relaxation) and after simulation of 24 hours.

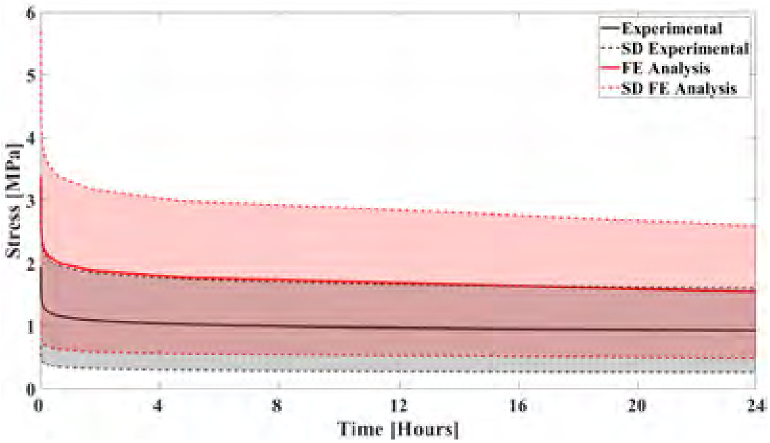

Figure 3-9: Average stress relaxation curves from the stress relaxation experiments and FE simulations with the standard deviation.

3.4 Discussion

The aim of this study was threefold: 1) perform uniaxial stress relaxation experiments on human trabecular bone; (2) to construct a material model that accurately describes the nonlinear viscoelastic behavior and determine the effect of bone density on the developed model; and (3) implement this material model in FE simulations of the stress relaxation experiments.

The experimental results indicated that femoral and tibial trabecular bone have a similar stress relaxation response. On average 54.4% stress relaxation was observed in 24 hours, with a maximum of 81.6%. A modified superposition model was able to accurately capture the sample-specific nonlinear stress relaxation of the human femoral and tibial trabecular bone. However, when defining a material model based on the data of all samples, no correlation was found between the applied strain level nor the bone mineral density and the viscoelastic response. Therefore, the average level of stress relaxation of all executed stress relaxation experiments was used to define the material model, which was subsequently implemented in FE simulations of each specimen.

The nonlinear viscoelastic parameters were first quantified using a sample-specific approach, in which BMD was excluded as a parameter in the equation. The stress relaxation decreased as the applied strain increased, showing the clear correlation between the two factors. This correlation was also found in similar studies and our previous study on bovine bone [9,15]. The precise cause of this behavior remains uncertain. It has been speculated that at higher strain values displacement of marrow within the samples occurs, potentially impacting the viscoelastic response [26]. Another hypothesis is that increased compression may lead to a reduction in pore size, thereby restricting water outflow and limiting the viscoelastic behavior.

While most studies only quantify the sample-specific nonlinear viscoelastic parameters in this study, a group-based approach was implemented as well [9,12]. In this approach all stress relaxation experiments were used to determine a correlation between the viscoelastic response, the applied strain, and the bone density. In contrast with the sample-specific approach, no relation was found between the applied strain level and the stress relaxation rate. Bone density also did not show a relation with the viscoelastic parameters, which was in agreement with what was observed in bovine trabecular bone [15]. It has been suggested that bone viscoelasticity is solely influenced by collagen [27]. Unfortunately, in the current study, the collagen content was not examined, so we were unable to verify this suggestion. Moreover, in the collective analysis performed here, the individual characteristics of the specimens, except the BMD, are ignored, while it is known that other microarchitectural indices may play a role in the viscoelastic behavior [11].

Since no correlation was found between the applied strain, BMD, and stress relaxation using the group-based approach, the average stress relaxation (54.4%) was applied in the FE models of the sample-specific trabecular bone cores.

Additionally, previously established relations between BMD and stiffness were used to calculate the initial stress relaxation modulus in the simulations [25]. The stress relaxation behavior was successfully implemented in the FE framework using a user subroutine, resulting in 54.4% stress relaxation after 24 hours. However, the use of the BMD-stiffness relationship led to a 63.9% overestimation of stresses in the simulations, likely due to a mismatch between the literature-derived elastic modulus and the actual stiffness of the specimens. Despite this, the FE simulations accurately captured the experimental stress relaxation behavior, as indicated by the parallel nature of the FE and experimental curves over time. This suggests that the stress-relaxation model is robust, effectively capturing bone's time-dependent behavior. Moreover, the FE simulation was able to capture the variability that was observed in the experimental results.

An additional limitation of the simulations was that the stress relaxation response was applied in an isotropic manner, with the same amount of stress relaxation applied in all directions. It is possible that the level of stress relaxation varies in different directions, due to the microstructure of trabecular bone [28]. To investigate whether the relaxation behavior actually is direction dependent, experiments should be conducted on trabecular bone in multiple loading directions to be able to capture the possible anisotropic viscoelasticity, bearing in mind the anatomical location and orientation of the specimens, which may prove to be challenging.

The workflow that was developed here to simulate long-term stress relaxation of the trabecular bone can be applied in several types of analyses, such as the prediction of the initial stability of press-fit implants in which it could have a significant effect, demonstrating the importance of this study. To achieve insights into the implications of stress relaxation levels, one could not only implement the average amount of stress relaxation of the population, but also the maximal level (almost 82% of relaxation) could be used in analysis to showcase the worst-case scenario. In the future the developed workflow and its potential effect on the primary fixation of cementless implants should be validated in experiments, for instance by monitoring stress relaxation using strain gauges. Finite element simulations can be used to more accurately study the interface micromotions between implant and bone as an actual measure of primary fixation.

This study offers valuable insights into the stress relaxation characteristics of human trabecular bone when subjected to a constant loading over a period of 24 hours. It was found that applied strain and BMD did not influence the viscoelastic behavior. Subsequently, the average stress relaxation was successfully implemented in sample-specific FE simulations. The substantial level of stress relaxation observed in the human trabecular bone emphasizes the significance of incorporating viscoelastic behavior in orthopedic simulations, particularly those pertaining to implant fixation, to ensure more realistic results.

References

1. Berahmani, S., D. Janssen, and N. Verdonschot, Experimental and computational analysis of micromotions of an uncemented femoral knee implant using elastic and plastic bone material models. J Biomech, 2017. 61: p. 137-143 DOI: 10.1016/j.jbiomech.2017.07.023.
2. Pankaj, P., Patient-specific modelling of bone and bone-implant systems: the challenges. International Journal for Numerical Methods in Biomedical Engineering, 2013. 29(2): p. 233-249 DOI: 10.1002/cnm.2536.
3. Taylor, M., D.S. Barrett, and D. Deffenbaugh, Influence of loading and activity on the primary stability of cementless tibial trays. J Orthop Res, 2012. 30(9): p. 1362-8 DOI: 10.1002/jor.22056.
4. Schoenfeld, C.M., E.P. Lautenschlager, and P.R. Meyer, Jr., Mechanical properties of human cancellous bone in the femoral head. Med Biol Eng, 1974. 12(3): p. 313-7 DOI: 10.1007/BF02477797.
5. van der Ploeg, B., et al., Toward a more realistic prediction of peri-prosthetic micromotions. Journal of Orthopaedic Research, 2012. 30(7): p. 1147-1154 DOI: 10.1002/jor.22041.
6. Zilch, H., et al., Material Properties of Femoral Cancellous Bone in Axial Loading .2. Time-Dependent Properties. Archives of Orthopaedic and Trauma Surgery, 1980. 97(4): p. 257-262 DOI: Doi 10.1007/Bf00380706.
7. Deligianni, D.D., A. Maris, and Y.F. Missirlis, Stress-Relaxation Behavior of Trabecular Bone Specimens. Journal of Biomechanics, 1994. 27(12): p. 1469-1476 DOI: Doi 10.1016/0021-9290(94)90196-1.
8. Bredbenner, T.L. and D.T. Davy, The effect of damage on the viscoelastic behavior of human vertebral trabecular bone. Journal of Biomechanical Engineering-Transactions of the Asme, 2006. 128(4): p. 473-480 DOI: 10.1115/1.2205370.
9. Quaglini, V., V. La Russa, and S. Corneo, Nonlinear stress relaxation of trabecular bone. Mechanics Research Communications, 2009. 36(3): p. 275-283 DOI: 10.1016/j.mechrescom.2008.10.012.
10. Bowman, S.M., et al., Compressive Creep-Behavior of Bovine Trabecular Bone. Journal of Biomechanics, 1994. 27(3): p. 301-& DOI: Doi 10.1016/0021-9290(94)90006-X.
11. Manda, K., et al., Linear viscoelasticity - bone volume fraction relationships of bovine trabecular bone. Biomechanics and Modeling in Mechanobiology, 2016. 15(6): p. 1631-1640 DOI: 10.1007/s10237-016-0787-0.
12. Manda, K., et al., Nonlinear viscoelastic characterization of bovine trabecular bone (vol 16, pg 173, 2017). Biomechanics and Modeling in Mechanobiology, 2017. 16(1): p. 191-195 DOI: 10.1007/s10237-016-0819-9.
13. Yamamoto, E., et al., Development of residual strains in human vertebral trabecular bone after prolonged static and cyclic loading at low load levels. Journal of Biomechanics, 2006. 39(10): p. 1812-1818 DOI: 10.1016/j.jbiomech.2005.05.017.
14. Bowman, S.M., et al., Creep contributes to the fatigue behavior of bovine trabecular bone. Journal of Biomechanical Engineering-Transactions of the Asme, 1998. 120(5): p. 647-654 DOI: Doi 10.1115/1.2834757.
15. Gersie, T., et al., Quantification of long-term nonlinear stress relaxation of bovine trabecular bone. J Mech Behav Biomed Mater, 2024. 152: p. 106434 DOI: 10.1016/j.jmbbm.2024.106434.
16. Keaveny, T.M., et al., Biomechanics of trabecular bone. Annu Rev Biomed Eng, 2001. 3: p. 307-33 DOI: 10.1146/annurev.bioeng.3.1.307.

17. Morgan, E.F., H.H. Bayraktar, and T.M. Keaveny, Trabecular bone modulus-density relationships depend on anatomic site. J Biomech, 2003. 36(7): p. 897-904 DOI: 10.1016/s0021-9290(03)00071-x.
18. Goldstein, S.A., The mechanical properties of trabecular bone: dependence on anatomic location and function. J Biomech, 1987. 20(11-12): p. 1055-61 DOI: 10.1016/0021-9290(87)90023-6.
19. Eggermont, F., et al., Calibration with or without phantom for fracture risk prediction in cancer patients with femoral bone metastases using CT-based finite element models. PLoS One, 2019. 14(7): p. e0220564 DOI: 10.1371/journal.pone.0220564.
20. Derikx, L.C., et al., Implementation of asymmetric yielding in case-specific finite element models improves the prediction of femoral fractures. Comput Methods Biomech Biomed Engin, 2011. 14(2): p. 183-93 DOI: 10.1080/10255842.2010.542463.
21. Zhao, S., et al., Standardizing compression testing for measuring the stiffness of human bone. Bone Joint Res, 2018. 7(8): p. 524-538 DOI: 10.1302/2046-3758.78.BJR-2018-0025.R1.
22. Keaveny, T.M., et al., Systematic and random errors in compression testing of trabecular bone. J Orthop Res, 1997. 15(1): p. 101-10 DOI: 10.1002/jor.1100150115.
23. Kopperdahl, D.L. and T.M. Keaveny, Yield strain behavior of trabecular bone. J Biomech, 1998. 31(7): p. 601-8 DOI: 10.1016/s0021-9290(98)00057-8.
24. Findley, W.N., Creep And Relaxation Of Nonlinear Viscoelastic Materials. 1976.
25. Keyak, J.H., et al., Predicting proximal femoral strength using structural engineering models. Clin Orthop Relat Res, 2005(437): p. 219-28 DOI: 10.1097/01.blo.0000164400.37905.22.
26. Linde, F., Elastic and viscoelastic properties of trabecular bone by a compression testing approach. Dan Med Bull, 1994. 41(2): p. 119-38.
27. Bowman, S.M., et al., Results from demineralized bone creep tests suggest that collagen is responsible for the creep behavior of bone. J Biomech Eng, 1999. 121(2): p. 253-8 DOI: 10.1115/1.2835112.
28. Ciarelli, M.J., et al., Evaluation of orthogonal mechanical properties and density of human trabecular bone from the major metaphyseal regions with materials testing and computed tomography. J Orthop Res, 1991. 9(5): p. 674-82 DOI: 10.1002/jor.1100090507.

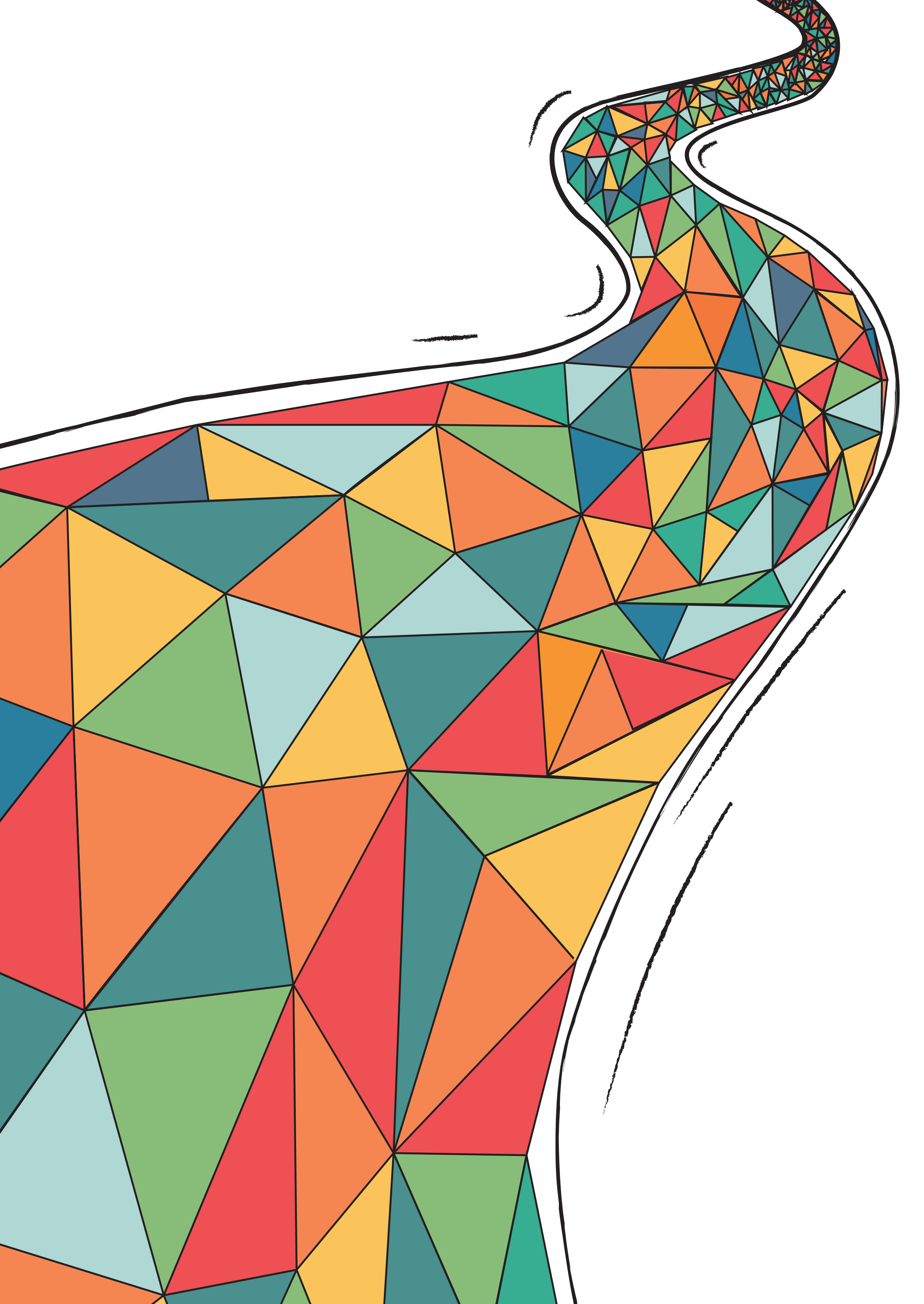

Chapter 4

The effect of bone relaxation on the simulated pull-off force of a cementless femoral knee implant

Thomas Gersie, Thom Bitter, Robert Freeman, Nico Verdonschot, Dennis Janssen

Published in Journal of Biomechanics:
https://doi.org/10.1016/j.jbiomech.2025.112528

Abstract

Aseptic loosening is the primary cause of revision in cementless total knee arthroplasty (TKA), emphasizing the importance of strong initial stability for long-term implant success. Pre-clinical evaluations are crucial for understanding implant fixation mechanics and improving implant designs. Finite element (FE) models often use linear elastic bone material models, which do not accurately reflect bone's mechanical behavior. Incorporating a von Mises yield model to simulate bone's plastic behavior improved predictions of primary stability but tends to overestimate fixation, potentially due to neglecting bone viscoelasticity. Stress relaxation in bone can affect primary stability by reducing press-fit forces on implants. This study aimed to include bone relaxation into FE models of femoral TKA reconstructions to investigate the impact of bone material models on primary fixation. Simulated pull-off tests were conducted using three material models: elastic, plastic, and plastic-viscoelastic. Six femoral reconstructions, previously used in another study, were included. The average pull-off force decreased (about 79%) from 31 kN with the elastic model to 6.3 kN when bone plasticity was included. Introducing stress relaxation showed a minimal effect, leading to an additional reduction in pull-off force of 0.8%. A significant positive correlation was found between bone mineral density and pull-off force across the three material models. Additionally, elastic strain energy within the femur correlated strongly with pull-off force, suggesting higher strain energy increases pull-off force. This study is the first to integrate plastic and viscoelastic bone behavior in FE simulations, offering insights into cementless implant fixation within context of realistic bone mechanics.

4.1 Introduction

Total knee arthroplasty (TKA) is one of the most common orthopedic interventions, offering pain relief and restoration of function in patients suffering from osteoarthritis in the knee joint [1]. With an increasing number of TKA operations, also the number of revision surgeries increases, with an elevated risk particularly for younger patients [2]. The most common reason for revision in cementless TKA is aseptic loosening [3, 4]. A good primary stability is therefore essential for long-term fixation. The primary stability depends on the compressive forces between the bone and implant resulting from the press-fit implant design.

Pre-clinical testing is essential to better understand fixation mechanics, and to inform the design process of implant systems. Various experimental and numerical testing methods have been developed to evaluate the primary fixation of cementless knee implants [5-7]. Computational models based on Finite Element Analysis (FEA) allow for the investigation of the initial stability in a relatively fast and cost-effective manner. However, FEA-based models often use a linear elastic bone material model [8-11], resulting in a response that is not representative for the stresses and large deformations occurring in the bone at the contact interface. Applying an elastic material model typically results in bone stresses that exceed the yield limit, causing an overestimation of the primary stability of the implant. Incorporating a Von Mises yield model that simulates plastic bone behavior significantly improves the prediction of the primary stability of knee implants [12]. However, even the plastic bone material model overestimates the fixation compared to experimental measurements. One potential explanation for this discrepancy is the absence of viscoelasticity in the bone material model.

Previous studies investigating viscoelastic behavior of bone in bone-implant constructs have shown that stress relaxation may affect the primary stability by reducing the press-fit forces acting on the implant [13-16]. A cadaveric study with human femurs showed that the pull-out force of press-fit pegs decreased already 30 minutes after implantation [13]. Another study demonstrated that the fixation strength of press-fit hip stems significantly reduced after 24 hours [15].

We previously quantified the stress relaxation that occurs within 24 hours in trabecular bone specimens of cadaveric femurs and tibias. No correlation between the applied strain or bone mineral density (BMD) and the level of relaxation was found. Therefore, the observed average relaxation level (54%) in the experiments was integrated with previously determined BMD-stiffness relationships and effectively applied in FEA models replicating the relaxation experiments [17]. To further improve the bone response at the implant-bone interface, the bone relaxation needs to be combined with plasticity to account for large permanent deformations.

The aim of the current study is therefore to investigate the effect of bone material models on the press-fit force generation and primary fixation and how this is related to BMD of the distal femur. For this purpose, a pull-off experiment was simulated in femoral TKA reconstructions, in models that simulated either an elastic, plastic, or plastic-viscoelastic bone response, based on previously developed material models.

4.2 Methods

The models in this study were based on a previous experimental study [18] in which six cadaveric femurs (two pairs and two single bones; 82, 89, 50 and 83 years old, respectively) were implanted with uncemented SIGMA® cruciate retaining femoral knee implants (DePuy Synthes Joint Reconstructions, UK). Based on clinical pre-planning, five size 5 implants and one size 3 implant were used. The bone specimens were CT- and micro-CT scanned after cutting but prior to implantation, to extract material properties and detailed bone geometries, respectively. After implantation, the implant position relative to the bone was determined using optical scans (TRIOS Color-P13, 3Shape, Denmark). CAD files were supplied by the manufacturer (DePuy Synthes Joint Reconstruction, USA). All simulations were performed using Marc/ Mentat 2023.1 (MSC software, USA). An average edge length of 1 mm was selected based on a previous mesh convergence study [19]. This edge length has also been used in similar computational studies examining bone strains and implant stability following TKA [20, 21]. Linear four-noded tetrahedral elements were used for the bone and implants. More details can be found in Berahmani et al. [12].

4.2.1 Material behavior

Isotropic elastic material properties were assigned to the implants (Young's modulus: 210 GPa, Poisson ratio: 0.3). Bone properties were assigned using in-house software converting Hounsfield units to ρQCT values based on calibrated CT scans [22]. The ash density of each element was then computed using the following relationship: ρ_{ash} = 0.0633 + 0.887ρ_{QCT} [23]. Elements with a lower ρ_{ash} than 250 mg cm^{-3} were considered as trabecular bone, based on previous literature [24]. Element-specific calcium values were related to Young's modulus using existing bone density-stiffness relationships (see Table S1 [23]). Three bone material models were used: elastic, plastic, and plastic-viscoelastic. First, an isotropic elastic material model was used. Then, plastic models were generated by introducing a non-linear isotropic post-yield material model, using a Von Mises yield criterion. The yield stress was based on the ash density for both trabecular and cortical bone [23]. Finally, viscoelastic bone behavior was incorporated based on our previous study on femoral and tibial trabecular bone [17]. The average level of stress relaxation (54%) was used, given the absence of a correlation between applied strain or BMD and relaxation level. Stress relaxation was simulated using a subroutine by incrementally introducing a creep strain, based on the elastic strain post-implantation and the target level of stress relaxation (54%). As creep strain increases, the elastic strain must decrease to keep the total strain constant, since the bone is constrained by the implant. Because the elastic strain is directly proportional to stress, this reduction in elastic strain results in a corresponding decrease in stress. Viscoelastic response was limited to trabecular bone elements, while cortical bone elements remained unchanged. In elements where the ρ_{ash} was below 600 mg cm^{-3}, stress relaxation occurred, marking a higher threshold compared to that for the mechanical properties. This heightened threshold was based on observations in our CT-scans, where elements with a ρ_{ash} lower than 600 mg cm^{-3} showed structural trabecular bone characteristics, but were assigned with mechanical properties of cortical bone due to their values. The stress relaxation was incorporated in a specific stress relaxation phase (see 4.2.2). Table 4-1 shows the mechanical property relationships used for each material model.

Table 4-1: The mechanical property relationships per bone material model for the trabecular and cortical bone. The plastic behavior for each model was represented by an initial perfectly plastic phase at stress S until the plastic strain was ε_{AB}, followed by a strain softening phase with plastic modulus E_p until the stress was σ_{min} and then an indefinite perfectly plastic phase. In the plastic-viscoelastic model, the stress at the end of the stress relaxation phase (Phase 2) is calculated as the stress at the end of the virtual implantation (Phase 1) after 54% of stress relaxation.

Relationship	Type of Bone	Bone material model
$E = 14900\rho_{ash}^{1.86}$	Trabecular and cortical	Elastic, Plastic, Plastic-Viscoelastic
$S = 102\rho_{ash}^{1.86}$	Trabecular and cortical	Plastic, Plastic-Viscoelastic
$\varepsilon_{AB} = 0.00189 + 0.0241\rho_{ash}$	Trabecular	Plastic, Plastic-Viscoelastic
$\varepsilon_{AB} = 0.00184 - 0.0100\rho_{ash}$	Cortical	Plastic, Plastic-Viscoelastic
$\varepsilon_{AB} = 0.00189 + 0.0241\rho_{ash}$	Trabecular	Plastic, Plastic-Viscoelastic
$E_p = -2080\rho_{ash}^{1.45}$	Trabecular	Plastic, Plastic-Viscoelastic
$E_p = -1000$	Cortical	Plastic, Plastic-Viscoelastic
$\sigma_{min} = 43.1\rho_{ash}^{1.81}$	Trabecular and cortical	Plastic, Plastic-Viscoelastic
$\sigma_{Phase\ 2} = \sigma_{Phase\ 1} - 0.54\sigma_{Phase\ 1}$	Trabecular	Plastic-Viscoelastic

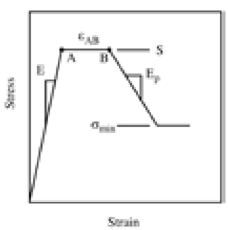

4.2.2 Boundary conditions and contact definition

The simulations were divided into distinct phases, visualized in Figure 4-1. First, the femoral component was virtually implanted. During implantation, the surface nodes of the bone that initially penetrated the implant (Figure 4-2A) were compressed by implementing a negative interference fit that was gradually reduced to zero. During this process, contact pressures would build up at the interface. A frictional touching contact algorithm based on a coulomb bilinear (displacement) friction model was assigned to the implant-bone interface. A coefficient of friction of 0.95 was used, provided by the manufacturer for the POROCOAT® surface coating (DePuy Synthes Joint Reconstruction, UK). In this phase the implant was fixated distally in all directions (Figure 4-2B). The femur was fixated proximally in all directions during all phases.

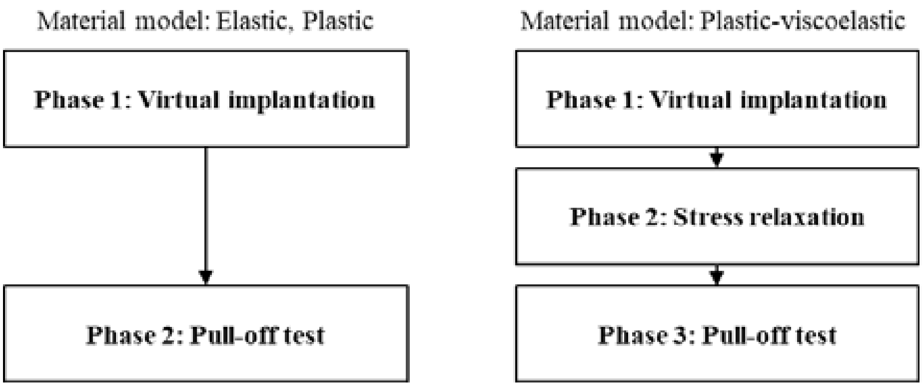

Figure 4-1: Flowchart of different simulation phases for the models with elastic or plastic bone material models and the models with plastic-viscoelastic bone mechanical properties.

In simulations with only elastic bone behavior, the initial penetration of the bone elements would result in elastic contact stresses at the interface. In simulations with a Von Mises material model, plastic deformations were allowed to occur in the bone during (and after) the implantation phase. In simulations with plastic-viscoelastic bone behavior, the implantation phase was followed by a second phase in which the trabecular bone elements were subjected to stress relaxation [17]. The elastic-plastic stress at the end of phase 1, caused by the implantation, was gradually decreased by 54%, replicating the average experimental bone relaxation. In the final phase, the implant was pulled off the bone in a virtual pull-off test. In this phase, the implant was displaced at the medial and lateral condyles in the axial direction to simulate a pull-off test (Figure 4-2B). The implant was displaced 3 mm in 0.1 mm increments to ensure full release of the implant-bone interface. The maximum sum of the nodal reaction forces was taken as the pull-off force.

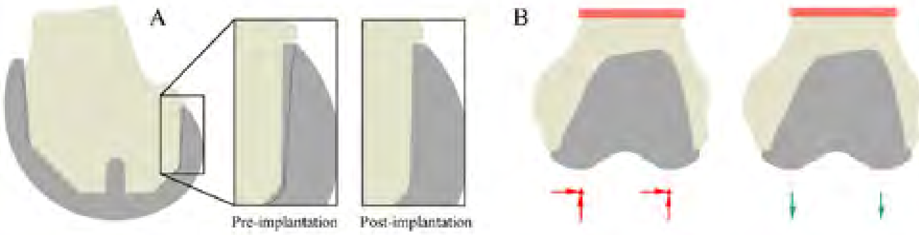

Figure 4-2: A) The bone elements that penetrate the implant are shown on both the anterior and posterior side. The femur is cut through the lateral condyle in the coronal plane and the cross section displays the perspective towards the center of the femur. In the implantation phase, these elements are gradually compressed until the bone nodes that initially penetrated touch the implant surface. After the virtual implantation, the surface nodes are touching the implant surface. **B)** In the left picture, the boundary condition to fixate the femur proximally in all directions during all stages of the simulation is shown by the red bar. The implant was during the implantation also fixated distally on both condyles using three nodes on both condyles. On the right picture: The pull-off experiment is simulated by pulling the implant off the bone at the medial and lateral condyles along the axial direction of the femur while the proximal femur was still constrained.

4.2.3 Data analysis

To investigate the influence of BMD, the mean BMD was calculated as the average BMD in three regions of interest (ROI – anterior flange, medial and lateral posterior condyle (Figure 4-3)). These regions were selected as they correspond with the locations where press-fit forces exerted on the bone, which is predominantly in the anteroposterior direction. These ROIs were defined from the contact interface to a depth of 5 mm, with the width matching the implant size.

The same ROIs were used to determine the average equivalent von Mises stress for each femoral reconstruction, as plastic bone deformation has been shown to be localized near the implant-bone interface [25]. Conversely, the elastic strain energy was calculated over all bone elements located between the anterior flange and the posterior condyles (Figure 4-3). Elastic strain energy was calculated as a measure for fixation energy accumulated in the bone due to the press-fit condition.

Statistical analyses were performed using GraphPad Prism 10.1.2 (GraphPad Software, USA) with a level of significance set to 0.05. Since the pull-off results for the bone material models were normally distributed (Shapiro-Wilk test), pairwise comparisons of the pull-off forces were analyzed using the Repeated Measures one-way ANOVA. A Sidak's test was used for the post-hoc analysis to examine which groups differed significantly. The Pearson correlation coefficient was calculated to determine the relationship between BMD and pull-off force. The Spearman correlation coefficient was used to determine the relationship between the strain energy and the pull-off force.

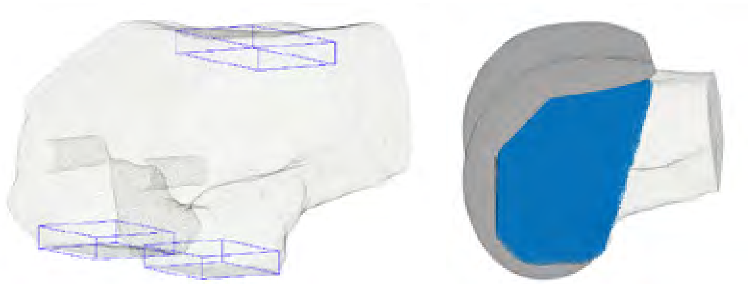

Figure 4-3: Left: The three regions of interest (anterior flange, medial posterior condyle, and lateral posterior condyle) to determine the average BMD and equivalent von Mises stress. The ROI was defined from the bone-implant interface to a depth of 5 mm in the femur. Right: The region of the bone, highlighted in blue, over which the strain energy is determined, is situated between the anterior and posterior surfaces of the implant.

4.3 Results

The BMD range of the femurs was 120.4 – 318.2 mg cm^{-3}. During the implantation phase, bone stresses increased up to 1012 MPa for the elastic bone material model. On average, in the three ROIs, the von Mises stress was 22.2 ± 7.2 MPa for the elastic model (Figure 4-4). When plasticity was included, the bone stresses were reduced by 65%, with an average von Mises stress of 7.8 ± 3.9 MPa, with maximal stresses in the bone of around 80 MPa. After the relaxation phase, the average von Mises stress was further reduced by 22% to 6.1 ± 3.5 MPa. With the inclusion of plasticity, plastic strains extended deeply in the bone (Figure 4-4).

The large stresses in the elastic material model led to significant strains in the femoral component (up to 8,368 με), which were reduced by including plasticity (max. 4,840 με) and further reduced when including viscoelastic bone behavior (max. 4,257 με) (Figure 4-5). The highest equivalent strains were found at the anterior and posterior chamfers.

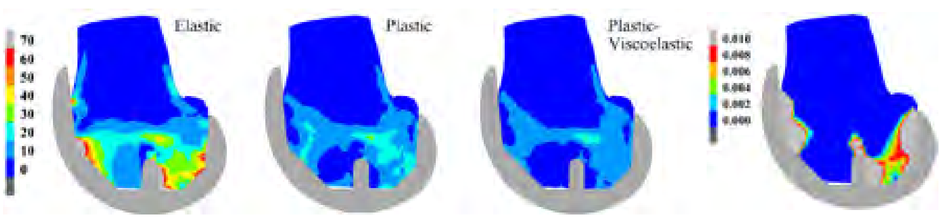

Figure 4-4: The left images display the equivalent von Mises stresses (in MPa) at a cross-section through the lateral condyle after virtual implantation for the three bone material models. In the right image, the equivalent plastic strain is shown for both the plastic and plastic-viscoelastic material models after the implantation. Areas where the plastic strain exceeds 1% are highlighted in light gray.

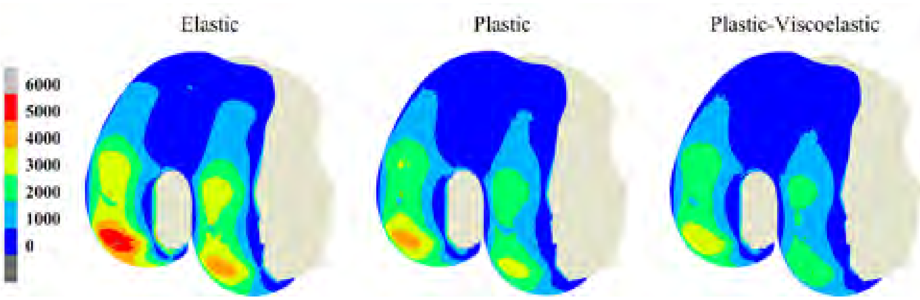

Figure 4-5: The equivalent total strain (με) on the outer surface of the femoral component after implantation (and after stress relaxation for the plastic-viscoelastic material model) for the different bone material models. The strain has decreased due to the stress relaxation of the trabecular bone in the second phase.

4.3.1 Pull-off

Implantation caused an imprint of the implant into the bone in models that included plasticity (Figure 4-6). A typical pull-off force graph for the three material models is shown in Figure 4-7, in which the maximal force was identified as the pull-off force. On average, the pull-off force for the elastic models was 30,594 N. When incorporating plasticity, the pull-off force decreased by 79% (average force 6,318 N). When bone stress relaxation was simulated, the pull-off forces decreased on average by another 0.8% (average force 6,297 N) (Figure 4-7). Significant differences were found between the elastic and plastic model ($p<0.05$) and between the elastic and plastic-viscoelastic bone material model ($p<0.05$).

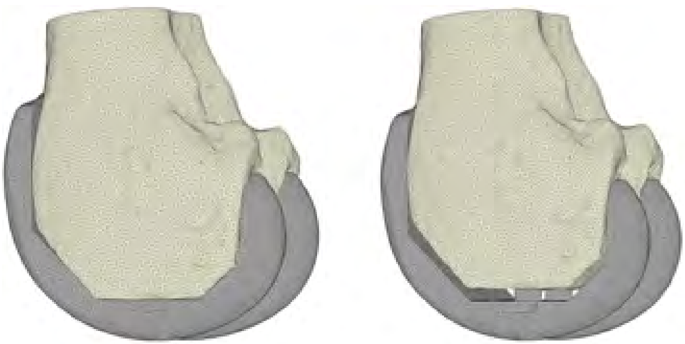

Figure 4-6: The simulated pull-off experiment by displacing the implant from the medial and lateral condyle by 3 mm. In this particular case, plasticity was considered, which enables the visualizing of the imprint of the implant in the posterior condyles.

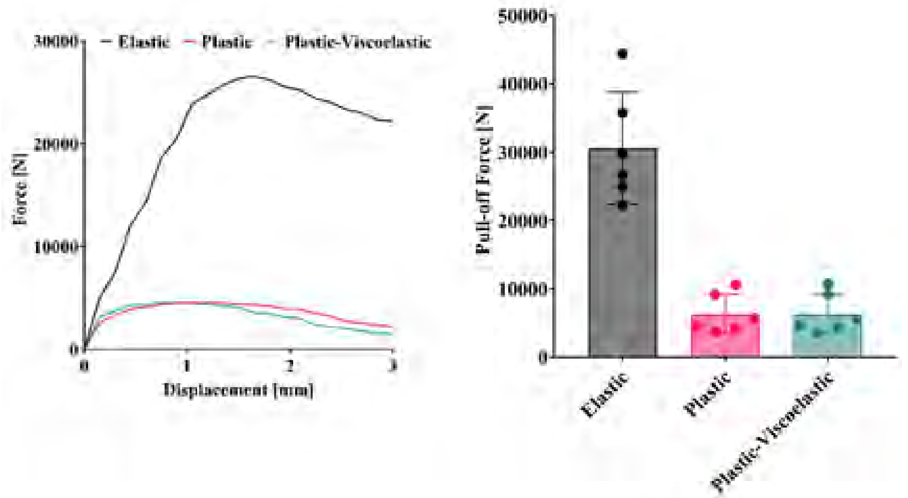

Figure 4-7: Left: A typical example of the force-displacement relationship for the three different bone material models. The pull-off force is determined as the maximal value for each material model. Right: The effect of bone material model on the pull-off force for a femoral component. The pull-off forces, when an elastic material mode is considered, are up to five times higher in comparison to when a plastic and plastic-viscoelastic model are considered. The addition of stress relaxation to the plastic bone material model has a minor effect on the simulated pull-off force.

A higher BMD led to an increased pull-off force, highlighted by the strong positive correlation between BMD and pull-off force for elastic ($r=0.87$, $p<0.05$), plastic ($r=0.91$, $p<0.05$), and plastic-viscoelastic material models ($r=0.90$, $p<0.05$) (Figure 4-8).

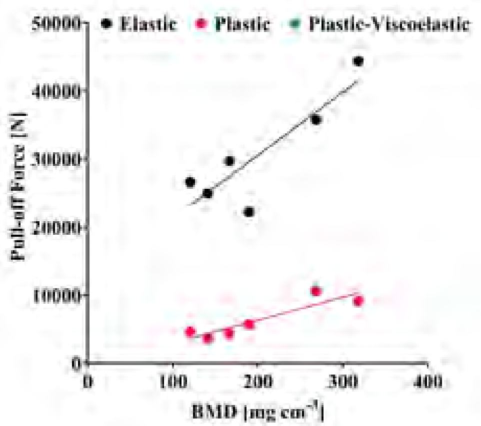

Figure 4-8: The pull-off force versus the BMD for the elastic, plastic, and plastic-viscoelastic bone material model. The BMD was determined by averaging the BMD in three different regions of interest (anterior, posterior condyle, anterior condyle). The trendlines, representing linear regression analysis, highlight the relationship between pull-off force and BMD for each material model.

The elastic strain energy in the femur was strongly associated with the pull-off force (r = 0.82, p<0.05), with a larger elastic strain energy corresponding to an increased pull-off force (Figure 4-9).

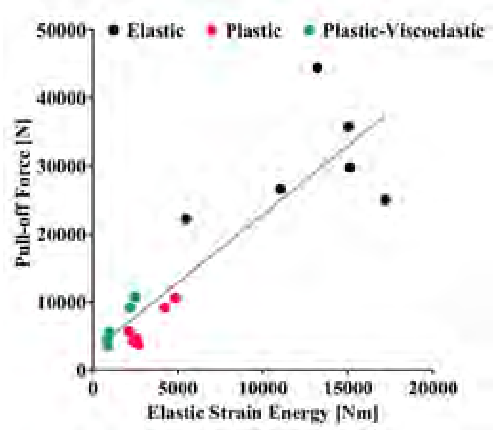

Figure 4-9: The pull-off force versus sum of the elastic strain energy for the elastic, plastic, and plastic-viscoelastic bone material model. The purple line, representing linear regression analysis, highlights the strong positive relation between the two.

4.4 Discussion

This is the first study that attempts to incorporate both plastic as viscoelastic bone material behavior in FE analysis of the primary fixation of press-fit implants. The goal of this study was to investigate the effect of bone relaxation on the press-fit behavior of the implant and the pull-off force in simulations of a cementless femoral knee component. Including plasticity resulted in pull-off forces that were nearly five times lower compared to when the bone was modeled as linear elastic. Incorporating stress relaxation had a minimal effect, leading to an additional reduction in the average pull-off force of just 0.8%.

The effect of viscoelastic behavior on implant fixation has previously only been reported in an FEA study on the fixation of a press-fit hip stem. In that study, the simulated push-out force of the femoral stem was compared between an elastic and viscoelastic bone material model for cortical bone [26]. The reduction in push-out load ranged from 2.6% to 82.6%, indicating significantly more variation compared to our study. Comparisons between that study and the current findings are complicated by the differences in the applied material model, the shape of the implant, and the amount of implant-bone contact. Full bone-stem contact over the total length of the implant was assumed in the stem study, while in our study contact was based on micro-CT and optical scans to replicate the actual contact surface and gaps between the implant and bone.

Although we could not compare our results with previous FEA simulations of femoral component fixation, based on the reduced bone stresses, we expected a larger effect of introducing bone viscoelasticity on the pull-off force. Our results indicate a strong relation between elastic strain energy and pull-off strength. However, even though the elastic strain energy was reduced by roughly 50%, this did not lead to a lower pull-off force for the viscoelastic models compared to the plastic models. Both these material models exhibited extensive areas of shearing deformation of the bone at the contact interface during implant pull-off, while this was not the case for the elastic models. This difference in bone response may indicate a more complex interplay of friction and bone stresses in case of loss of structural integrity of the bone, leading to a similar failure mechanism (and therefore force magnitude) for the plastic and viscoelastic bone models. An experimental study on press-fit pegs previously already demonstrated that the fixation strength of rough-surfaced pegs was less sensitive to bone relaxation than that of smooth-surfaced pegs [13]. The coefficient of friction used in this study was determined based on testing against Sawbones® bone analogue. However, bone is a fatty tissue, which may alter the frictional properties when testing in cadaveric bones. This indicates testing of the fixation strength of femoral TKA components may be heavily dependent on accurate material properties, frictional properties and correct bone and implant geometries.

While a pull-off test provides an indirect insight into the quality of the fixation of a femoral component, it is not representative of a clinical failure scenario. Primary fixation is generally evaluated by measuring or simulating micromotions at the implant-bone interface, as a proxy for osseointegration and bone ingrowth. Although the current study did not find a large effect of including viscoelastic behavior on the fixation strength, it is unclear how a reduction of the bone stresses (or elastic strain energy, as reported here) will influence interface micromotions. This will require further investigation, for instance in a model such as presented by Berahmani et al. [12].

A limited number of studies have incorporated a non-linear plastic model in the FE analysis of press-fit analysis [14, 16, 27]. Berahmani et al. showed that the addition of a plastic model significantly improved the prediction of micromotions at the bone-implant interface of an uncemented femoral knee implant in comparison with a linear elastic model [12]. The current study also indicates that using a plastic model relative to a linear elastic model is more representative of the bone biomechanics when examining pull-off forces. However, further experimental validation is required to demonstrate the validity of the approach that was taken in our study.

While this study reproduced the interference fit that is typically designed into press-fit implant systems, other FEA studies often simulate an interference fit that is significantly smaller than clinically employed. For example, Schultz et al. and Rothstock et al. used 0.01 to 0.50 mm and 0.08 to 0.32 mm, respectively, while implant systems generally have a designed press-fit of 1.00 – 2.00 mm. In the current study, optical scans were used to determine the position of the implant on the bone. In combination with the virtual implantation procedure, this resulted in an average interference fit close to the nominal value of 1.5 mm, which was provided by the manufacturer (DePuy Synthes Joint Reconstruction, USA). Since we used the actual interference fit, excessive stresses were observed when using an elastic bone material model. Therefore, it is of paramount importance to include plastic bone behavior when using realistic interference fit values in the study of the fixation of orthopedic implants, or, for instance, when evaluating new implant designs in the early pre-clinical stage.

The viscoelastic material law used here was derived from stress relaxation experiments with trabecular tibial and femoral bone [17]. In that study, no correlation was observed between BMD or applied strain and the degree of stress relaxation. Consequently, in this study, the stress relaxation was kept constant at 54% in the trabecular bone. The average Von Mises stress decreased on average by 22%, which was less than the applied relaxation. This is due to the complex interactions between trabecular bone, the cortex, and the implant, resulting in a less straightforward response. Previous studies have demonstrated that the surface strains of the implant can serve as an indirect measure of stress relaxation [28, 29]. We therefore plan on validating the stress relaxation in 24-hour strain gauge measurements at the articulating surface of the femoral component after implantation and will compare these to FE models (Figure 4-5).

The pull-off force showed notable variations for each bone material model, with two specimens particularly displaying a substantially larger pull-off force. These specimens concerned a femur pair from a single donor, characterized by a higher BMD compared to the other four specimens (300 mg cm^{-3} vs. 120-200 mg cm^{-3}). We found a significant positive correlation between BMD and pull-off force in both the plastic and plastic-viscoelastic bone models. These positive correlations align with experimental studies, which have demonstrated that higher BMD correlates with increased pull-off and roll-off forces, resulting in improved fixation [13, 30].

Research on the fixation of pegs in the femur indicated that a greater interference fit results in improved fixation and higher pull-off forces. However, there appears to be a limit beyond which an increased interference fit causes more bone damage, and limits further increase of the pull-off force [13, 31]. In the current study, however, the impact of interference fit on the pull-off force was not examined.

In our simulations, stress relaxation was not applied to the cortical bone. To our knowledge, no study has investigated the level of stress relaxation in human cortical bone over an extended period. Considering that the implant primarily is in contact with trabecular bone at the contact interface, it is likely that including the viscoelastic behavior of cortical bone would only have a negligible effect on the fixation strength. The division of cortical bone elements was based on our calibrated CT-images. However, this threshold (600 mg cm^{-3}) may vary when using different bones, so it will need to be recalibrated accordingly.

This study has certain limitations. For example, only one type of implant was studied, with a limited sample size (N=6), and with implantations performed by a single surgeon. Additionally, this study used a softening von Mises yield criterion, which is known to cause the yielding zone to extend deeply into the bone (Figure 4-4). In reality, however, the damage is more localized near the bone-implant interface [25]. Therefore, other plasticity models may be more suitable, such as an isotropic crushable foam model [32]. Moreover, the level of bone stress relaxation was based on experiments with trabecular bone cores up to 0.8% strain [17]. In the current study, plasticity was modeled with strains well beyond this range. Literature lacks consensus on stress relaxation beyond the yield strain; a study on bovine cancellous bone reported increased relaxation, while human cortical bone showed constant relaxation after yielding [33, 34]. Stress relaxation experiments beyond the yield strain could provide deeper insights into the material behavior of human trabecular bone. The level of stress relaxation has only been measured in compression in our previous study, aligning with the current study where the strain field is predominantly compressive [17]. However, in other studies, the strain field may not be compression-dominated. Since no previous research has quantified the stress relaxation response in tension or shear, it would be valuable to determine stress relaxation levels for these strain states where relevant. Despite these limitations, we believe the current study provides insights into the simulation of fixation of orthopedic implants, emphasizing the advantages of incorporating bone plasticity and viscoelasticity into the modeling.

In future work, we will conduct axial pull-off experiments 24 hours after implanting a different type of femoral component in cadaveric femurs. Subsequent pull-off simulations involving these reconstructions will be developed to compare the experimental pull-off force with the computational values.

The integration of bone stress relaxation into plastic bone material models and asssessing the effect on initial stability is not explored previously. It was found that higher BMD generally resulted in higher storage of elastic strain for all three material models and that these trends were statistically significant. A higher elastic energy accumulated within the bone due to the implant's press-fit resulted in higher pull-off forces. This study furthermore shows that the inclusion of plastic bone behavior results in more representative bone behavior and allows for the use of realistic interference fits. This study offers a valuable approach for investigating FE simulations of primary fixation of cementless implants within the context of realistic bone biomechanics. We intend to investigate the effect of viscoelastic bone behavior on implant-bone interface micromotions, which will provide a different measure for primary stability, more focused on implant osseointegration.

References

1. Bellemans, J., Ries, M.D., Victor, J.M.K., Total Knee Arthroplasty: A Guide to Get Better Performance. 2005, Springer S.
2. Aggarwal, V.K., et al., Revision total knee arthroplasty in the young patient: is there trouble on the horizon? J Bone Joint Surg Am, 2014. 96(7): p. 536-42 DOI: 10.2106/JBJS.M.00131.
3. Australian Orthopaedic Association National Joint Replacement Registry (AOANJRR) Hip, Knee & Shoulder Arthroplasty: 2023 Annual Report. AOA, Adelaide, 2023.
4. National Joint Registry for England, W., Northern Ireland and the and Isle of Man, 20th Annual Report 2023. 1821, Hertfordshire, 2023.
5. Abdul-Kadir, M.R., et al., Finite element modelling of primary hip stem stability: the effect of interference fit. J Biomech, 2008. 41(3): p. 587-94 DOI: 10.1016/j.jbiomech.2007.10.009.
6. Chong, D.Y., U.N. Hansen, and A.A. Amis, Analysis of bone-prosthesis interface micromotion for cementless tibial prosthesis fixation and the influence of loading conditions. J Biomech, 2010. 43(6): p. 1074-80 DOI: 10.1016/j.jbiomech.2009.12.006.
7. Conlisk, N., et al., The influence of stem length and fixation on initial femoral component stability in revision total knee replacement. Bone Joint Res, 2012. 1(11): p. 281-8 DOI: 10.1302/2046-3758.111.2000107.
8. Tarala, M., et al., Experimental versus computational analysis of micromotions at the implant-bone interface. Proc Inst Mech Eng H, 2011. 225(1): p. 8-15 DOI: 10.1243/09544119JEIM825.
9. Taylor, M., D.S. Barrett, and D. Deffenbaugh, Influence of loading and activity on the primary stability of cementless tibial trays. J Orthop Res, 2012. 30(9): p. 1362-8 DOI: 10.1002/jor.22056.
10. van der Ploeg, B., et al., Toward a more realistic prediction of peri-prosthetic micromotions. J Orthop Res, 2012. 30(7): p. 1147-54 DOI: 10.1002/jor.22041.
11. Viceconti, M., et al., Large-sliding contact elements accurately predict levels of bone-implant micromotion relevant to osseointegration. J Biomech, 2000. 33(12): p. 1611-8 DOI: 10.1016/s0021-9290(00)00140-8.
12. Berahmani, S., D. Janssen, and N. Verdonschot, Experimental and computational analysis of micromotions of an uncemented femoral knee implant using elastic and plastic bone material models. J Biomech, 2017. 61: p. 137-143 DOI: 10.1016/j.jbiomech.2017.07.023.
13. Berahmani, S., et al., An experimental study to investigate biomechanical aspects of the initial stability of press-fit implants. J Mech Behav Biomed Mater, 2015. 42: p. 177-85 DOI: 10.1016/j.jmbbm.2014.11.014.
14. Kelly, N., et al., An investigation of the inelastic behaviour of trabecular bone during the press-fit implantation of a tibial component in total knee arthroplasty. Med Eng Phys, 2013. 35(11): p. 1599-606 DOI: 10.1016/j.medengphy.2013.05.007.
15. Norman, T.L., et al., Cortical bone viscoelasticity and fixation strength of press-fit femoral stems: an in-vitro model. J Biomech Eng, 2006. 128(1): p. 13-7 DOI: 10.1115/1.2133766.
16. Rothstock, S., et al., Primary stability of uncemented femoral resurfacing implants for varying interface parameters and material formulations during walking and stair climbing. J Biomech, 2010. 43(3): p. 521-6 DOI: 10.1016/j.jbiomech.2009.09.052.
17. Gersie, T., et al., Characterization of nonlinear stress relaxation of the femoral and tibial trabecular bone for computational modeling. Med Eng Phys, 2025. 138: p. 104324 DOI: 10.1016/j.medengphy.2025.104324.

18. Berahmani, S., et al., Evaluation of interference fit and bone damage of an uncemented femoral knee implant. Clin Biomech (Bristol, Avon), 2018. 51: p. 1-9 DOI: 10.1016/j.clinbiomech.2017.10.022.
19. Berahmani, S., et al., FE analysis of the effects of simplifications in experimental testing on micromotions of uncemented femoral knee implants. J Orthop Res, 2016. 34(5): p. 812-9 DOI: 10.1002/jor.23074.
20. Clary, C.W., et al., The influence of total knee arthroplasty geometry on mid-flexion stability: an experimental and finite element study. J Biomech, 2013. 46(7): p. 1351-7 DOI: 10.1016/j.jbiomech.2013.01.025.
21. Yang, H., et al., Impact of surgical alignment, tray material, PCL condition, and patient anatomy on tibial strains after TKA. Med Eng Phys, 2021. 88: p. 69-77 DOI: 10.1016/j.medengphy.2021.01.001.
22. Derikx, L.C., et al., Implementation of asymmetric yielding in case-specific finite element models improves the prediction of femoral fractures. Comput Methods Biomech Biomed Engin, 2011. 14(2): p. 183-93 DOI: 10.1080/10255842.2010.542463.
23. Keyak, J.H., et al., Predicting proximal femoral strength using structural engineering models. Clin Orthop Relat Res, 2005(437): p. 219-28 DOI: 10.1097/01.blo.0000164400.37905.22.
24. Keyak, J.H., et al., Prediction of femoral fracture load using automated finite element modeling. J Biomech, 1998. 31(2): p. 125-33 DOI: 10.1016/s0021-9290(97)00123-1.
25. Rapagna, S., et al., Quantification of human bone microarchitecture damage in press-fit femoral knee implantation using HR-pQCT and digital volume correlation. J Mech Behav Biomed Mater, 2019. 97: p. 278-287 DOI: 10.1016/j.jmbbm.2019.04.054.
26. Shultz, T.R., et al., Cortical bone viscoelasticity and fixation strength of press-fit femoral stems: finite element model. J Biomech Eng, 2006. 128(1): p. 7-12 DOI: 10.1115/1.2133765.
27. Souffrant, R., et al., Advanced material modelling in numerical simulation of primary acetabular press-fit cup stability. Comput Methods Biomech Biomed Engin, 2012. 15(8): p. 787-93 DOI: 10.1080/10255842.2011.561012.
28. Burgers, T., et al., Time-dependent fixation and implantation forces for a femoral knee component--an in vitro study. Med Eng Phys, 2010. 32(9): p. 968-73 DOI: 10.1016/j.medengphy.2010.06.011.
29. Burgers, T., J. Mason, and H.-L. Ploeg, Initial fixation of a femoral knee component: an in vitro and finite element study. International Journal of Experimental and Computational Biomechanics, 2009. 1 DOI: 10.1504/IJECB.2009.022857.
30. Berahmani, S., et al., The effect of surface morphology on the primary fixation strength of uncemented femoral knee prosthesis: a cadaveric study. J Arthroplasty, 2015. 30(2): p. 300-7 DOI: 10.1016/j.arth.2014.09.030.
31. Gebert, A., et al., Influence of press-fit parameters on the primary stability of uncemented femoral resurfacing implants. Med Eng Phys, 2009. 31(1): p. 160-4 DOI: 10.1016/j.medengphy.2008.04.007.
32. Soltanihafshejani, N., et al., The application of an isotropic crushable foam model to predict the femoral fracture risk. PLoS One, 2023. 18(7): p. e0288776 DOI: 10.1371/journal.pone.0288776.
33. Burgers, T.A., et al., Post-yield relaxation behavior of bovine cancellous bone. J Biomech, 2009. 42(16): p. 2728-33 DOI: 10.1016/j.jbiomech.2009.08.005.
34. Leng, H., X.N. Dong, and X. Wang, Progressive post-yield behavior of human cortical bone in compression for middle-aged and elderly groups. J Biomech, 2009. 42(4): p. 491-7 DOI: 10.1016/j.jbiomech.2008.11.016.

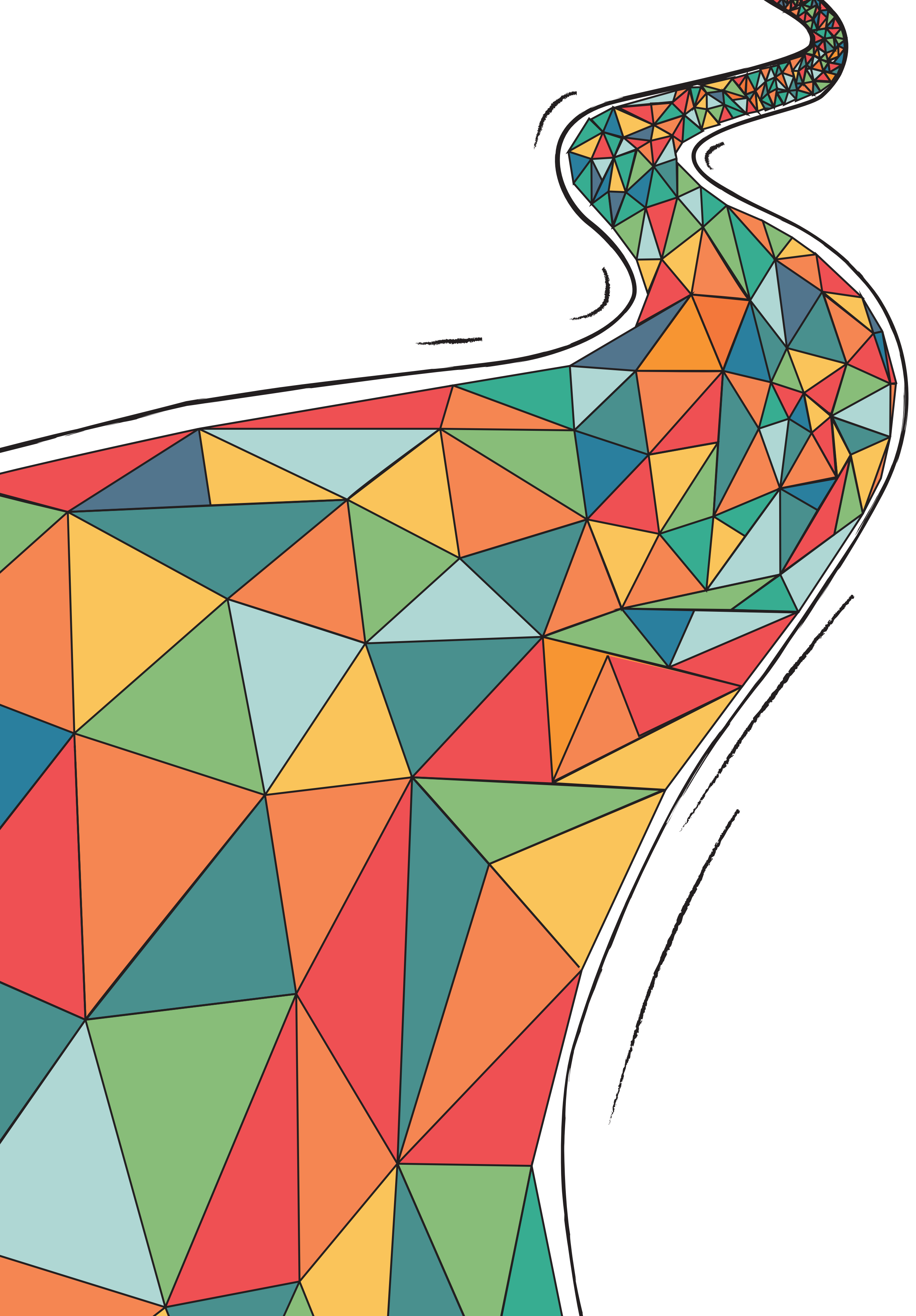

Chapter 5

Bone stress relaxation in press-fit femoral knee implant fixation: A combined experimental and computational analysis

Thomas Gersie, Thom Bitter, Robert Freeman, Nico Verdonschot, Dennis Janssen

Published in Journal of the Mechanical Behavior of Biomedical materials:
https://doi.org/10.1016/j.jmbbm.2025.107067

Abstract

Aseptic loosening is the leading cause of revision in cementless total knee arthroplasty (TKA), emphasizing the need for strong initial stability. Pre-clinical evaluations are essential for understanding implant fixation mechanics. Finite element (FE) models often rely on linear elastic bone material models, which inadequately represent bone behavior. Incorporating bone plasticity enhances predictions of primary stability, but may overestimate fixation by neglecting bone viscoelasticity and abrasion. Stress relaxation reduces press-fit forces, while bone abrasion weakens fixation strength.

This study incorporated bone relaxation and abrasion into FE simulations of femoral TKA fixation and compared results to experimental measurements. Cadaveric femurs were implanted with femoral components, and strain gauges recorded outer surface strain over 24 hours. A pull-off test evaluated fixation strength. FE models, using a plastic-viscoelastic bone material model, simulated these phases with varying levels of bone abrasion.

The computational model without abrasion predicted implant strain 350% higher than experimental measurements. 0.75 mm of virtual abrasion reduced overestimation to 150%. Experimental strain reductions due to bone relaxation varied per reconstruction from 17% to 37%, while computational predictions were on average 41% lower. Substantial variability was observed in both the experimental and simulated pull-off forces. Simulations without abrasion showed 180% to 360% higher pull-off forces than the experiments. Including 0.5 mm of virtual abrasion reduced pull-off forces, aligning them more closely with experimental values, though 0.75 mm led to underestimation in some cases.

These results highlight the need to include bone relaxation and abrasion in simulations to optimize implant designs and surgical outcomes.

5.1 Introduction

Total knee arthroplasty (TKA) is a prevalent orthopedic procedure that provides pain relief and restores function for patients with knee osteoarthritis [1]. However, as the number of TKA surgeries increases, so does the incidence of revision surgeries, with younger patients being at higher risk [2]. In cementless TKA, aseptic loosening is the most frequent cause for revision [3, 4]. Therefore, achieving strong primary stability is essential for long-term fixation. In cementless TKA, primary stability is influenced by factors such as bone quality, the friction coefficient of the implant's inner surface, and the compressive forces between the bone and implant due to the press-fit design of the implant.

Pre-clinical testing of implant fixation is crucial for understanding fixation mechanics and enhancing implant system designs. Both experimental and numerical testing methods have been developed to assess the primary fixation of cementless knee implants [5-7]. Computational models using finite element (FE) analysis enable rapid and cost-effective evaluation of initial stability. However, these models often employ a linear elastic bone material model, which inaccurately represents the stresses and deformations in the bone [8-11]. This approach typically results in bone stresses exceeding the yield limit, leading to an overestimation of the implant's primary stability. Incorporating a Von Mises yield model, which simulates the plastic behavior of bone, has significantly improved the accuracy of primary stability predictions compared to linear elastic models [12]. Nevertheless, this improved model still overestimates fixation when compared to experimental measurements. Possible reasons for this discrepancy are the lack of bone viscoelasticity and the absence of bone abrasion in the models.

It has been shown that the viscoelastic behavior of bone within bone-implant constructs plays a critical role in implant stability, with stress relaxation diminishing the press-fit forces on the implant [13, 14]. A cadaveric study involving human femurs demonstrated that the pull-out force of press-fit implanted pegs decreased within just 30 minutes of implantation [13]. Another study showed a significant reduction in the fixation strength of press-fit hip stems after a 24-hour waiting period [14].

Bone relaxation was incorporated into a plastic bone material model in FE analysis to examine its effect on the pull-off force using six femoral reconstructions [15]. The inclusion of bone plasticity showed a decrease of 79% in pull-off force in comparison to an elastic model, while bone relaxation only had a minor effect on the pull-off force. However, these results were not verified by experiments.

Bone abrasion refers to the damage and removal of bone tissue caused by mechanical friction between the implant and bone during implantation, which can compromise implant stability. In the study by Berahmani et al., bone debris was observed along the edges of the implant-bone interface at the posterior condyles following implantation [12]. Additionally, remnant particles were found at the implant inner surface after implant removal from the bone. These observations suggest that the plasticity model used in that study misrepresented the extent of damage, as bone abrasion was not simulated. This misrepresentation may reduce the effectiveness of implant fixation and lead to increased computational micromotions, highlighting the importance of incorporating bone abrasion into simulations to improve their accuracy.

Therefore, the aim of this study was to incorporate bone relaxation and bone abrasion into the simulation of fixation strength for femoral TKA components and compare these simulations with experimental measurements. To achieve this, experimental prosthetic strain measurements and a physical pull-off test were performed and replicated using FE analysis.

5.2 Methods

In short, femoral knee prosthetic components were implanted into cadaveric femurs, with strain gauges used to measure the outer surface strain of the implants from implantation up to 24 hours post-implantation. These implant strains served as a surrogate measurement for bone relaxation occurring in the femur over the same period. Previous studies have demonstrated that monitoring the implant's outer surface strain is an effective method for indirectly measuring bone relaxation. The press-fit fixation pushes the anterior flange and posterior condyles outward, creating compressive strains on the articular surface [16]. Over time, a reduction in strain has been observed, indicating a decrease in pressure and fixation strength at the bone-implant interface, likely due to stress relaxation of the underlying bone, as noted in prior research [17]. After the 24-hour period, a pull-off experiment was performed. FE models of the reconstructions with the plastic-viscoelastic bone material model were constructed to simulate the implantation, the 24-hours rest period, and the pull-off test. The simulations were conducted with different virtual levels of bone abrasion. Finally, the implant strain after implantation, the reduction in implant surface strain and pull-off force observed in the experiments were compared by those predicted by the computational simulations.

5.2.1 Experimental measurements

5.2.1.1 In vitro implantation

Six fresh-frozen cadaveric femurs (two single bones and two pairs) were obtained from the Anatomy Department of the Radboud University Medical Center. The single femurs were from female donors (both 53 years old, weighing 64 kg and 85 kg), and the paired femurs were from male donors (69 and 79 years old, weighing 62 kg and 71 kg). No information of musculoskeletal or metabolic diseases was known, but CT scans showed no abnormalities. The femurs were thawed at room temperature and cleaned from soft tissue before the bone cutting. The bones were cut with a 3° valgus angle, consistent with normal surgical procedures, and then CT-scanned (Aquilion Precision, Toshiba, Tokio, Japan; tube potential of 120 kV, tube current of 250 mA) with a voxel size of 0.20 x 0.20 x 0.25 mm, along with a hydroxyapatite calibration phantom (Image analysis, Columbia, USA). After CT-scanning, the femurs were wrapped in saline-saturated gauze and stored at -20°C in individual plastic bags.

Four unidirectional strain gauges (CEA-06-250UWA-350, Micro-Measurements, Raileigh, USA) were attached to each implant using a 3D-printed mold. The gauges were positioned at distinct locations on the medial and lateral sides of the anterior and posterior regions and oriented in the circumferential direction (Figure 5-1). These locations, identified in a previous FE study, exhibited high strain magnitude, low gradient, and sensitivity to stress relaxation [15]. The strain gauges were connected to an MTS Flextest 40 controller (MTS systems corporation, Eden Priarie, USA) using a three-wire quarter-bridge circuit, which compensated for temperature-induced resistance changes. Wiring resistance was adjusted in the FlexTest controller for accurate data acquisition.

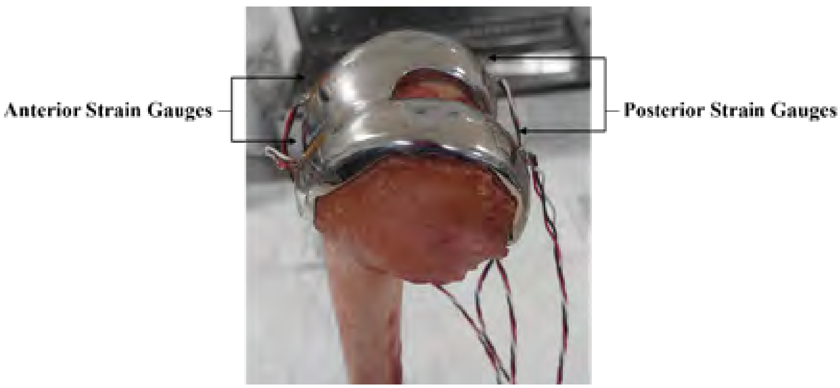

Figure 5-1: Each implant was equipped with four strain gauges to record the outer surface strain over a 24-hour period following implantation.

After thawing, the femurs were implanted with uncemented Attune© cruciate-retaining femoral knee implants (DePuy Synthes Joint Reconstructions, Leeds, UK) by an experienced orthopedic surgeon. Surgical tools, including a hammer (700 grams) were provided by the manufacturer. This procedure was performed within a maximum of one week after CT scanning. Implants of various sizes were used: one size 4, one size 5, three size 7, and one size 8.

Strain gauge signals were recorded continuously from just before the implantation until 24 hours post-implantation at 100 Hz for the first hour, and at 1 Hz for the remainder of the experiment. A 24-hour experimental period was selected based on prior findings that stress relaxation occurs within this timeframe, but it eventually levels off, making it a suitable endpoint for the measurements [16].

After the strain gauge measurements, the constructs were scanned with a 3D-optical scanner (Pop 2, Revopoint 3D Technologies, Shenzhen, China; accuracy 100 µm) to determine the position of the implant with respect to the bone (Figure 5-2).

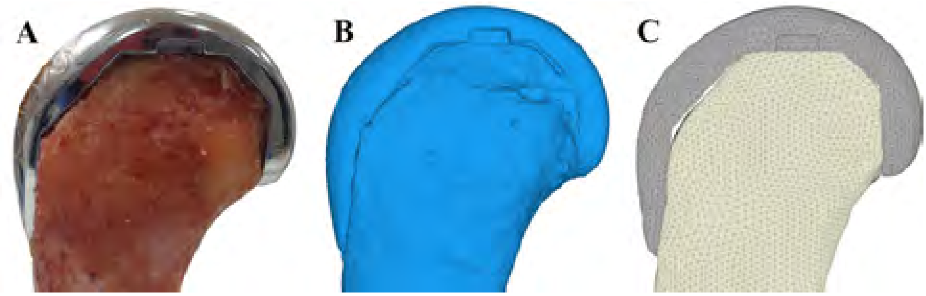

Figure 5-2: After implantation **(A)**, an optical scan of the femoral reconstruction was made **(B)**, which was then used to determine the position of the implant with respect to the bone in the FE software **(C)**.

5.2.1.2 Pull-off test

After optical scanning, the femoral component was aligned perpendicularly to the MTS machine (MTS systems corporation, Eden Prairie, USA) and potted proximally (Figure 5-3). The femoral implant was then pulled-off axially at a speed of 0.5 mm/s. The force was measured using a 15 kN load cell (type 2816, Interface, Scottsdale, USA) at a sampling rate of 100 Hz. Displacement data were sourced from the crosshead of the MTS machine, with no correction for machine compliance, as the primary focus was on the force required to pull the implant from the bone.

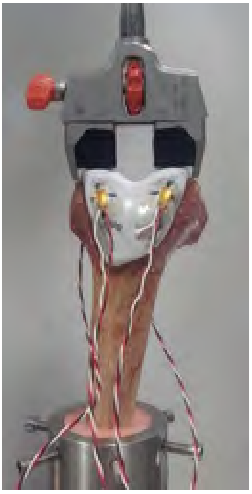

Figure 5-3: Pull-off test setup for the femoral component with the bone fixated proximally with bone cement and the femoral component aligned with the attachment on the MTS. The implant was powder coated to minimize light reflection during the optical scanning.

5.2.2 Finite element model

The femurs, including the 3D geometry of the cut surface, were segmented semi-automatically from CT scans using 3D Slicer (Surgical Planning Laboratory, Cambridge, USA). Optical scans were processed in MATLAB (MathWorks, Natick, USA) to separate and register the surface meshes of the implant and bone. To isolate the bone and implant surface meshes, the angles between adjacent edges at each vertex of the surface scan mesh were calculated. Vertices with high curvatures were removed from the surface mesh, as the implant's edges form sharp features. This approach successfully isolated the implant's edges. The outer surface of the implant was then identified by selecting a single vertex in the implant region, and the algorithm automatically selected and saved all connected vertices, generating a separate surface mesh for the implant. The remaining mesh represented the bone. Finally, the 3D model of the implant, provided by the manufacturer (DePuy Synthes Joint Reconstruction, Warsaw, USA), was registered to the isolated implant surface mesh, aligning it with the surface scan. Simultaneously, the segmented femur from the CT scan was registered to the bone mesh, ensuring proper alignment of the 3D models of both the bone and the implant with the orientation of the implanted experimental specimen (Figure 5-2).

The surface models were then meshed with an average edge length of 1.5 mm (Hypermesh 2022.1, Altair Engineering, Troy, USA). A mesh convergence study was conducted using element sizes of 1.0, 1.5, 2.0, and 2.5 mm with elastic strain energy as output parameter. While the strain energy did not fully converge from 1.5 mm to 1.0 mm, the 1.5 mm mesh provided an optimal balance, with a 5.5 times faster runtime compared to the 1.0 mm mesh (which took approximately 9 hours). The implant mesh was divided into two sections; one for the POROCOAT® surface coating (DePuy Synthes Joint Reconstruction, UK) with a thickness of 0.75 mm, and the other for the implant body. Solid models of the bone, implant, and coating were created using linear four-noded tetrahedral elements. Linear tetrahedral elements were chosen as they perform better in node-to-segment contact analyses as adopted in the current study. Higher-order elements, while more accurate for stress analysis in bulk materials, can lead to over-constraining at the contact interface, which may cause instability and reduce the accuracy of the simulation in those regions.

5.2.2.1 Material behavior

Isotropic linear elastic material properties of cobalt chrome were assigned to the implant elements with a Young's modulus of 210 GPa and a Poisson's ratio of 0.3. The coating layer had a Young's modulus of 20 GPa [17]. Bone properties were assigned based on Hounsfield Units using in-house software [18]. The ash density of each element was computed using the relationship: $\rho_{ash} = 0.0633 + 0.887\rho_{QCT}$ [19]. Elements with a ρ_{ash} lower than 250 mg cm^{-3} were classified as trabecular bone [20]. Element-specific calcium values were correlated to Young's modulus using established bone density-stiffness relationships [19]. Bone was modeled as plastic-viscoelastic. A non-linear isotropic post-yield material response using a von Mises Yield criterion was applied, with the yield stress determined based on ash density for both trabecular and cortical bone [19]. Viscoelastic bone behavior was modeled by incorporating 54% of stress relaxation, based on previous experimental data [16]. Stress relaxation was simulated using a subroutine that incrementally applied a creep strain, based on the elastic strain post-implantation. Given the elastic strain is directly proportional to stress, this reduction in elastic strain leads to a corresponding decrease in stress. Viscoelastic response was applied only to trabecular bone elements, while cortical bone elements remained unchanged. Stress relaxation was applied to elements with a ρ_{ash} below 600 mg cm^{-3}, based on observations from our CT scans, where elements with a ρ_{ash} below 600 mg cm^{-3} exhibited structural trabecular bone characteristics. Stress relaxation was incorporated in a specific stress relaxation phase (see 5.2.2.2). Table 5-1 shows the mechanical property relationships used.

Table 5-1: The mechanical property relationships for the trabecular and cortical bone. The plastic behavior is described by an initial perfectly plastic phase at stress S, until the plastic strain reaches ε_{AB}. This is followed by a strain-softening phase with a plastic modulus of E_p till the stress decreases to σ_{min}, after which the material behaves in a perfectly plastic manner indefinitely.

Relationship	Type of Bone
$E = 14900\rho_{ash}^{1.86}$	Trabecular and cortical
$S = 102\rho_{ash}^{1.86}$	Trabecular and cortical
$\varepsilon_{AB} = 0.00189 + 0.0241\rho_{ash}$	Trabecular
$\varepsilon_{AB} = 0.00184 - 0.0100\rho_{ash}$	Cortical
$\varepsilon_{AB} = 0.00189 + 0.0241\rho_{ash}$	Trabecular
$E_p = -2080\rho_{ash}^{1.45}$	Trabecular
$E_p = -1000$	Cortical
$\sigma_{min} = 43.1\rho_{ash}^{1.81}$	Trabecular and cortical

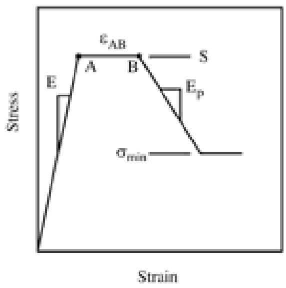

5.2.2.2 *Boundary conditions and contact definition*

The FE simulations were divided into three distinct phases. First, the femoral component was virtually implanted using the node-to-segment contact algorithm of the FE software. The femur was fixed 5.5 cm from the proximal end (corresponding to the height of the cylindrical cement pot) in all directions in all phases. In the implantation phase, the surface nodes of the bone that initially penetrated the implant (Figure 5-4) were incrementally pulled towards the implant surface by simulating a negative interference fit in MSC.Marc 2024.2, which was gradually reduced to zero. During this process, the bone was progressively compressed until it made contact with the implant surface, resulting in the buildup of contact pressure at the interface. For each reconstruction, the simulation was performed three times with different virtual levels of bone abrasion, in addition to a scenario where no virtual abrasion was simulated (with the interference fit set to zero at the end of the implantation). The interference fit values at the end of the implantation were set to -0.50 mm and -0.75 mm, derived from the implant's nominal interference fit of 1.5 mm as specified by the manufacturer. Since previous studies have shown that the effective interference fit can range from 2% to 59% of the nominal interference fit, we modeled virtual bone abrasion levels of 0.50 mm and 0.75 mm on both the anterior and posterior sides of the implant [21, 22]. Notably, 0.50 mm of virtual abrasion on both sides leads to a 1 mm reduction in the nominal interference fit, which is within the reported effective interference fit range. When the interference fit was gradually reduced to -0.50 mm, it meant that, by the end of the implantation phase, the bone was allowed to penetrate the implant by 0.50 mm, effectively simulating 0.50 mm of virtual bone abrasion (Figure 5-4). A frictional contact algorithm based on a Coulomb bilinear friction model (with a coefficient of friction (CoF) of 0.95) was applied to the implant-bone interface. The CoF value, determined through testing with Sawbones® bone analogues, was provided by the implant manufacturer. For convergence purposes, the implant was fixed distally in all directions during this phase (Figure 5-5A). The implantation phase was followed by a second phase in which the trabecular bone elements were subjected to stress relaxation.

In the final phase, a pull-off test was simulated. During this phase, the implant was pulled from the bone at the slots on the femoral component on the medial and lateral side, which is similar to the experiments (Figure 5-5B). The implant was displaced 3 mm in 0.1 mm increments to ensure complete release of the implant-bone interface. The maximum sum of the nodal reaction forces on the medial and lateral slots was recorded as the pull-off force.

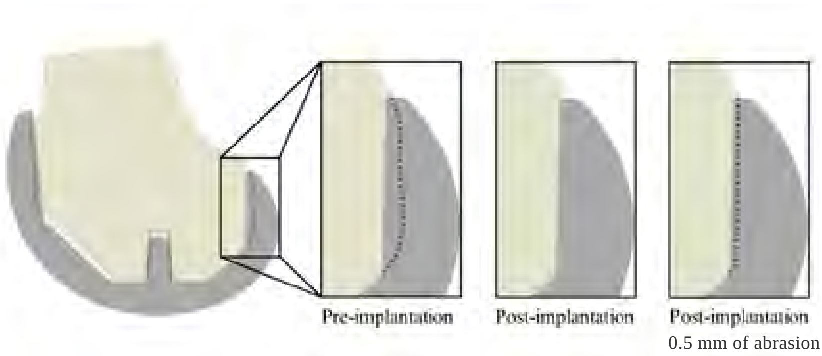

Figure 5-4: A cross-section of the femur, obtained by cutting through the lateral condyle in the coronal plane, provides a view toward the femoral center. The bone elements that penetrate the implant are visible on the anterior and posterior sides, as well as around the peg. During the implantation phase, these elements are progressively compressed until the bone nodes that initially penetrate the implant surface come into contact with it. After the virtual implantation, the surface nodes are in direct contact with the implant surface if no abrasion is simulated. In models incorporating virtual abrasion, the bone nodes that initially penetrated the implant surface are retracted to align with the bone surface, leaving a uniform layer of 0.5 mm or 0.75 mm of bone penetration to simulate abraded bone.

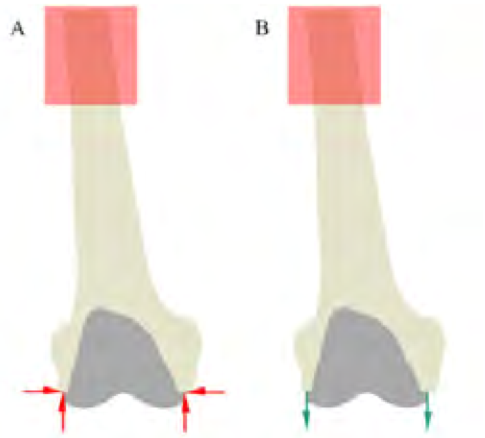

Figure 5-5: A) The boundary condition used to fix the femur proximally in all directions throughout all simulation stages is represented by the red bar, mimicking the bone cement potting in the experiments. During the implantation phase, the implant was also secured distally at the femoral component slots on the medial and lateral sides. The red arrows represent the constraints applied to the femoral component, restricting movement in all directions. **B)** The pull-off experiment was simulated by separating the implant from the bone at the medial and lateral slots, replicating the experimental setup. This separation occurred along the axial axis of the femoral component, with the proximal femur remaining constrained. The green arrows represent the downward displacement (3 mm) of the implant to simulate pull-off from the bone.

5.2.3 Data analysis

In the schematic graph of Figure 5-6, the outer surface strain on the implant is shown with the different experimental phases: implantation, 24-hours stress relaxation, and pull-off. The following sections will discuss the data analysis in these phases.

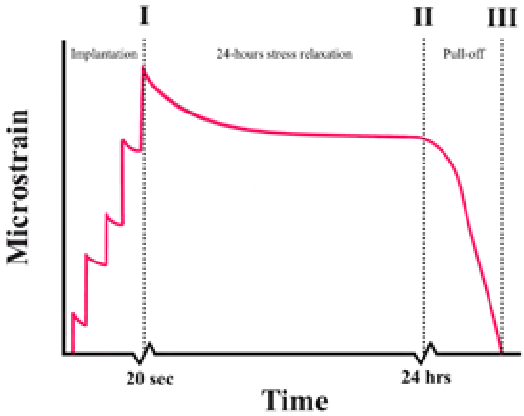

Figure 5-6: Schematic overview of the strain response on the implant's outer surface over time. The implantation phase showed increases in strain after each impaction. This phase ends with the implant firmly secured to the bone, with the final strain observed at point I being discussed in Section 5.3.1. After the 24-hours stress relaxation period (II), the reduction in implant strain is calculated and compared to computational values, as detailed in Section 5.3.2. At point III, the implant is pulled from the bone, and the experimental pull-off results are compared to the simulated pull-off, as described in Section 5.3.3.

5.2.3.1 Bone density

To investigate the influence of bone mineral density (BMD), the mean BMD was calculated by averaging the values from three regions of interest (ROIs): the anterior flange, and the medial and lateral posterior condyles. These regions were chosen because they correspond to areas where press-fit forces are primarily applied to the bone, predominantly in the anteroposterior direction. The ROIs were defined from the contact interface to a depth of 5 mm, with the width aligned to the implant size.

5.2.3.2 Implant outer surface strain

Experimental strain data were used from the moment the surgeon delivered the final mallet strike up to 24 hours afterward. The reduction of the implant outer surface strain was calculated for each strain gauge by comparing the strain at the last strike to the strain 24 hours later.

To compare the experimental strain with the computational strain, the measurement locations and orientations were replicated in the models using a model of the 3D-printed mold that was used for placement of the gauges. The average computational strain tensor was based on the elements within each strain gauge location. The reduction in implant outer surface strain was determined by comparing the strain at the end of the implantation phase and at the end of the stress relaxation phase for each strain gauge.

Initial experimental strains were compared to initial computational strains under different levels of virtual bone abrasion. Moreover, the experimentally measured strain reductions were compared to computational strain reductions.

5.2.3.3 Pull-off data

The maximal applied force during the pull-off test was compared to the computational pull-off force for the six reconstructions with different levels of virtual bone abrasion.

5.2.3.4 Elastic strain energy

To investigate the influence of elastic energy in the bone on the pull-off force, the elastic strain energy was calculated over all bone elements between the anterior flange and the posterior condyles. Elastic strain energy was calculated as a measure for fixation energy accumulated in the bone due to the press-fit condition.

5.2.4 Statistical analysis

Statistical analyses were conducted using GraphPad Prism 10.1.2 (GraphPad Software, USA), with the significance level set to 0.05. The outer surface strain of the implant after implantation, as well as the strain reduction at each strain gauge location, were tested for normality using the Shapiro-Wilk test to enable comparisons between strain gauge location. All data were normally distributed, except for the strain reduction in one strain gauge location during the 0.75 mm abrasion simulation. To compare strain gauge locations in the experiments and across the three simulations, a one-way ANOVA was used when standard deviations were not significantly different, as assessed by Bartlett's test. If standard deviations differed significantly, a Welch's ANOVA was performed. For the strain reduction during the 0.75 mm abrasion simulation, comparisons between strain gauge locations were made using a Kruskal-Wallis test. In this case, Dunn's post-hoc test was applied to determine which groups differed significantly. Moreover, linear regression analysis was applied to assess relationships between experimental and computational data for the implant's outer surface strain post-implantation, the reduction in implant outer surface strain (defined as the bone stress relaxation proxy), and the pull-off force. Additionally, linear regression was used to evaluate the relationship between the BMD and the pull-off forces and between the elastic strain energy and computational pull-off forces.

5.3 Results

The BMD of the six specimens ranged from 134 to 254 mg cm^{-3}, with an average bone density of 198 mg cm^{-3}.

5.3.1 Implant strain after implantation

Large variations in experimental strain were observed between the specimens, with one specimen averaging 187 microstrain and another reaching 656 microstrain. Experimental strains were generally higher in the lateral posterior region (Figure 5-7A), however, this was not statistically significant. Similar trends were observed in the computational simulations. The computational model without abrasion resulted in a 350% higher implant strain than measured experimentally. Incorporating virtual bone abrasion brought the computational strains closer to the experimental measurements. At 0.75 mm of virtual abrasion, the computational strain after implantation most closely matched the experimental values, although it remained 150% higher. Significant linear correlations were identified between implant strain calculated by the FE model and experimental strains. Figure 5-7B illustrates the overestimation by the FE model and highlights the improved predictive accuracy achieved with 0.75 mm of simulated bone abrasion.

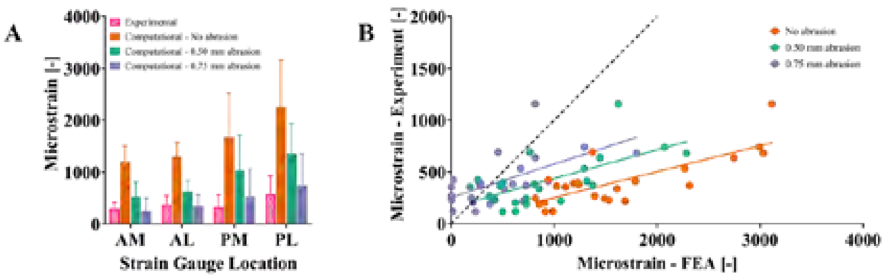

Figure 5-7: A) The average implant outer surface strain (with standard deviation) after implantation is shown for the different strain gauge locations: AM (anterior-medial), AL (anterior-lateral), PM (posterior-medial), and PL (posterior-lateral). **B)** The correlation between the strain calculated by the FE model and the experimental strain measurements is presented. The dotted line indicates where the strains from both measurements are equal.

5.3.2 Implant strain reduction

The average reduction in implant surface strain, serving as a proxy for bone stress relaxation, varied substantially between specimens 24-hour post-implantation (17%-37%). Variation within specimens was observed across different strain gauge locations, with a 49% reduction noted at the anterior medial flange and only a 16% reduction at the posterior lateral condyles for one specimen. However, no significant differences were found between strain gauge locations, except in the simulations with 0.75 mm of virtual abrasion, where the anterior lateral region showed lower strain reductions compared to other regions. The prediction from the computational models without simulated bone abrasion exhibited varying accuracy, with the computational reduction being 21% to 53% lower than experimentally measured (Figure 5-8A). Moreover, the computational models had less variability in implant strain reduction in comparison to the experimental measurements. Simulating bone abrasion led to an increase in relaxation, with results observed for both 0.5 mm and 0.75 mm showing comparable stress relaxation levels. Simulations with 0.75 mm of virtual abrasion caused convergence issues for specimens 5 and 6, and these results were excluded from the analysis. The FE model without bone abrasion reasonably predicted lower levels (<25%) of implant strain reduction, but overpredicted these values when bone abrasion was simulated (Figure 5-8B). Particularly higher levels of strain reduction (>30%) were underpredicted by all three models (0.0, 0.50 and 0.75mm virtual abrasion).

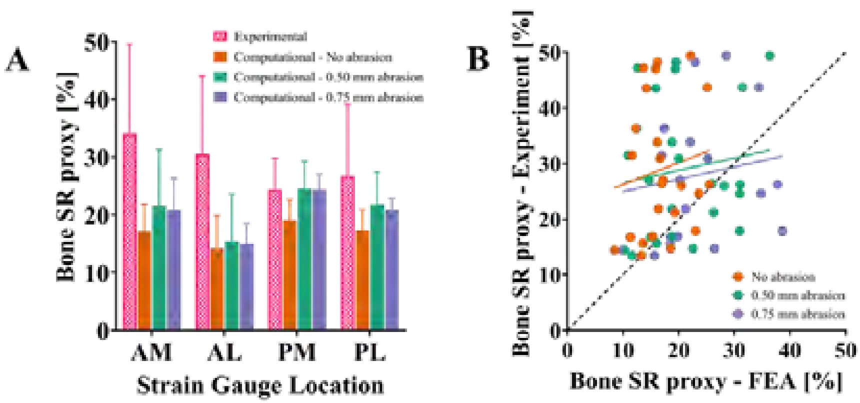

Figure 5-8: A) The average reduction in implant outer surface strain (with standard deviation), which serves as a proxy for bone stress relaxation (SR) 24-hours post implantation is shown for the different strain gauge locations: AM (anterior-medial), AL (anterior-lateral), PM (posterior-medial), and PL (posterior-lateral). **B)** This figure illustrates the correlation between this bone stress relaxation proxy, calculated by the FE model, and the experimental measurements. The dotted line indicates where the strains from both measurements are equal.

5.3.3 Bone strain

In the FE simulations, elastic strain in the bone after implantation decreased with higher levels of simulated abrasion. Similarly, plastic strain in the bone following implantation also showed a reduction as the simulated abrasion levels increased (Figure 5-9). When 0.75 mm of abrasion was simulated almost no plasticity was observed.

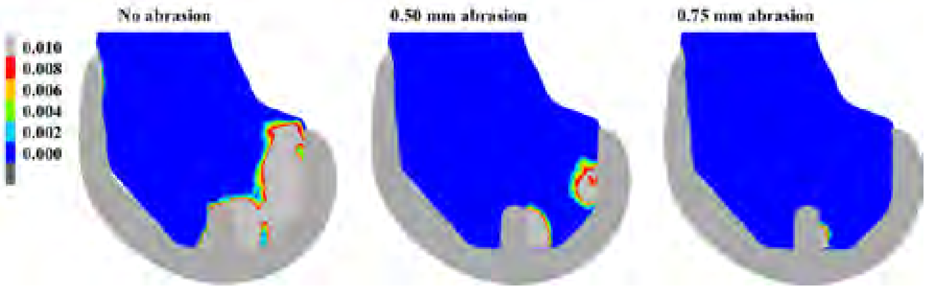

Figure 5-9: The equivalent plastic strain is shown for a simulation without abrasion and for cases with 0.50 mm and 0.75 mm of simulated abrasion after implantation, with areas where the plastic strain exceeds 1% highlighted in light gray.

5.3.4 Pull-off

A typical pull-off graph for one specimen is shown in Figure 5-10A. As the level of simulated bone abrasion increased, the pull-off force decreased, bringing the results closer to the experimental curve. There was a considerable variation in the experimental pull-off forces between specimens, with specimen 1 exhibiting more than three times the pull-off force of specimen 6 (Figure 5-10B). In models without simulated abrasion, the computational pull-off forces were 180% to 360% higher than the experimental pull-off forces. By including 0.5 mm of virtual bone abrasion, the pull-off values in the simulations were lowered and closer to the experimental values. Three specimens showed an underestimation of the pull-off force with 0.75 mm of simulated abrasion compared to the experimental results. For two models (5 and 6), the pull-off simulations failed to convergence at the virtual abrasion level of 0.75 mm, resulting in an assumed pull-off force of 0 N, as the implant was essentially loose on the bone. These two specimens also exhibited the lowest experimental pull-off values among the six specimens. Linear regression analysis revealed significant positive correlations ($p = 0.03$, $R^2 = 0.72$) between BMD and the experimental and computational (without bone abrasion) pull-off forces, as shown in Figure 5-10C. However, when bone abrasion was considered, no significant correlations were observed ($R^2 = 0.35$ and $R^2 = 0.04$ for 0.50 and 0.75 mm abrasion, respectively). Overall, the computational models were capable to distinguish between specimens, as demonstrated by the correlations in

Figure 5-11A. This indicates that specimens with low experimental pull-off forces also had lower pull-off forces in the simulations. Pull-off force was positively correlated with elastic strain energy, meaning higher strain energy led to higher pull-off forces (Figure 5-11B). Higher levels of virtual bone abrasion resulted in lower strain energy and, consequently, lower pull-off forces.

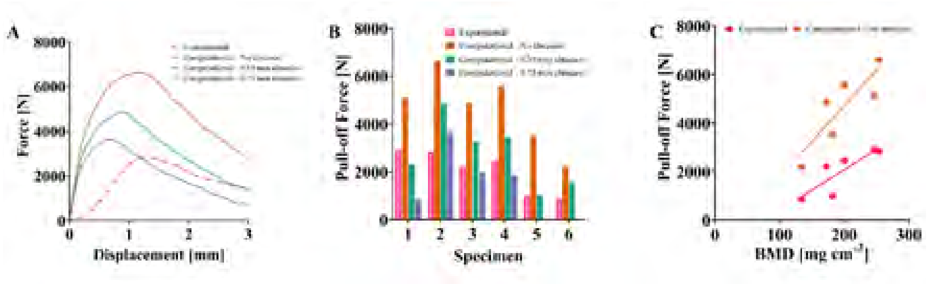

Figure 5-10: A) A typical example of the experimental and computational force-displacement relationship for one specimen. The pull-off force is determined as the maximal value of each curve. **B)** The average pull-off force for every specimen is shown for the experimental and simulated pull-off test. Since, the simulations with 0.75 mm virtual abrasion did not convergence for specimen 5 and 6, no pull-off force was calculated. **C)** The relationship between experimental and computational pull-off forces (without abrasion), with trendlines indicated. An increase in BMD results in higher pull-off forces in both the experiments and simulations.

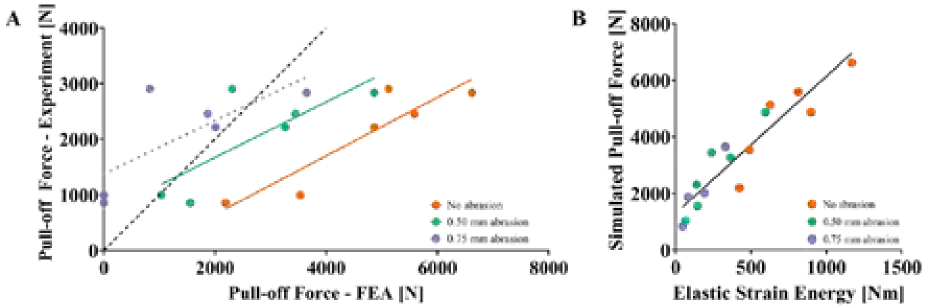

Figure 5-11: A) The correlation between the pull-off force calculated by the FE model, with different levels of virtual bone abrasion, and the experimental pull-off force is shown. Since two models did not convergence in the 0.75 mm virtual abrasion group, their pull-off force was assumed to be 0 N, and the trendline for this group is shown as dotted to reflect this assumption. The black dashed line indicates where the strains from both measurements are equal. **B)** The pull-off force versus the elastic strain energy for the different simulations is presented. The black line, representing linear regression analysis, highlights the positive relation between the two.

5.4 Discussion

This study aimed to incorporate bone relaxation and bone abrasion into simulations of cementless femoral component implantation and pull-off, using a newly developed plastic-viscoelastic bone material model. The results were compared to experimental measurements to assess the model's accuracy. Simulations without bone abrasion overestimated the outer surface strain on the flange and condyles of the femoral component when compared to experimental strain gauge measurements. Additionally, the simulated reduction in strain due to bone relaxation was less pronounced than what was observed experimentally during the 24-hour stress relaxation period. This combination of higher surface strains and less bone relaxation likely led to an overprediction of fixation, resulting in higher pull-off forces than measured experimentally. When bone abrasion was included in the simulations, implant strains decreased, reductions over time became more pronounced, and pull-off forces were lower, all of which brought the simulation results closer to the experimental values. These results highlight the importance of incorporating both bone stress relaxation and abrasion effects to improve the alignment of simulation outcomes with experimental data.

The experimental outer surface strains of the implant ranged from 115 to 1156 microstrain, consistent with findings from previous studies that evaluated a different implant, but with similar coating and strain gauge locations [1, 4]. Notably, the highest strain was observed at the lateral posterior condyle. Our simulations indicated that implant outer surface strain was 3.5 times higher at the end of implantation when virtual bone abrasion was not accounted for. Several factors may explain this finding. The Young's modulus – apparent density relationship used in this study may not fully account for the variability observed in different studies. To demonstrate this variability, consider the following example: in this study, bone apparent density ranging from 0.1 to 1.3 g cm^{-3} corresponds to elastic moduli between 206 MPa and 24 GPa [19]. When recalculated using the lower and upper bounds of elastic-density relationships reported in the literature, the same apparent density would result in elastic moduli between 39 MPa and 4 GPa, and 213 MPa and 60 GPa, respectively [23]. Due to the considerable variation in these relationships, employing a model more specific to our specimens could yield different results. Furthermore, the interference fit in our simulations was influenced by implant deformation, despite the implant being assumed completely rigid during the registration of the surface scan. Strain measurements confirm that the implant is not rigid, which could result in an overestimation of the interference fit.

The reduction in implant strain, serving as a proxy for bone stress relaxation, has been previously studied in two types of femoral implants: one over a 2-hour period and the other over 25 minutes (and extrapolated to 24 hours). The first study reported an average strain reduction of 27%, which closely aligns with the 25% reduction observed in our study [24]. Even with differences in experimental duration, the reduction in implant strain remains minimal, as our prior research shows that only a small portion of stress relaxation occurs between 2 and 24 hours [25]. Burgers et al. reported a strain reduction of 5% to 40% when extrapolated to 24 hours, a range comparable to 11% to 49% observed in our study [26]. This wide variation is evident not only between specimens, but also within individual specimens at different strain gauge locations. While we adhered to a standardized protocol for implanting the knee components, the inherent variability of the surgical procedure and the complexity of the bone-implant interface likely contributed to the observed differences.

In our previous work, stress relaxation experiments on femoral and tibial bone cores revealed a 24-hour relaxation range of 38 and 82%, with similar variability observed both between specimens and across anatomical locations within the tibia and femur [16]. The computational bone relaxation proxy (without simulated bone abrasion) ranged from 8% to 25% across all specimens and strain gauge locations, showing lower values and less variability compared to the experimental measurements. The discrepancy in strain reduction levels may stem from the computational models using an average stress relaxation value of 54%, derived from bone core experiments [16]. Especially locations with high strain reduction were underestimated with the uniform level of relaxation. The use of an average stress relaxation value also contributed to the reduced variability in implant strain reduction observed in the computational models. The stress relaxation levels measured in bone cores were higher than the experimentally measured implant strain reduction. This difference may be explained by the experimental setup: in bone core tests, a constant strain was applied using an MTS machine, while the implant is free to deform during the relaxation phase. This deformation likely results in different stress relaxation dynamics in the underlying bone. In the simulations, this effect appeared slightly exaggerated, further reducing the implant strain reduction. Including virtual bone abrasion in the models increased implant strain reduction, aligning it more closely with experimental observations.

As far as we are aware of, this is the first published paper to experimentally determine the pull-off force of a cementless femoral component. Since no previous studies have performed this specific test, there is no direct comparison available.

The closest comparison would be high-flexion pull-off tests (also known as roll-off tests), but due to the differences in experimental setup, even these cannot be directly compared to our results [24]. In our study, the computational model overestimated the experimental pull-off forces, with computational pull-off force being 180% to 360% higher than experimental pull-off force when bone abrasion was not simulated. The previously mentioned higher implant strains observed after implantation, as predicted by the computational models, also highlight the overestimated fixation of the implant in the FE models. Despite inaccuracies in absolute pull-off forces, the model effectively differentiated between specimens with low or high experimental pull-off forces. Incorporating virtual abrasion reduced the overestimation the overestimation, with 0.75 mm of abrasion even resulting in underestimations for three out of six specimens. It was revealed that reduced pull-off forces corresponded to lower elastic strain energy, consistent with the positive correlation observed in our previous computational study [15]. The decrease in pull-off forces with increasing abrasion levels can be attributed to the reduction in elastic strain and, consequently, the elastic strain energy with higher levels of simulated abrasion. Additionally, it was observed that plastic strain decreased with increasing levels of bone abrasion. At 0.75 mm of simulated abrasion, plastic deformation was almost negligible, resulting in an almost entirely elastic response. This finding contrasts with our previous study, where an elastic bone material model resulted in pull-off forces that were five times higher than when plasticity was included [15]. However, in this study, the significant reduction in elastic strain due to higher levels of abrasion overshadowed the decrease in plastic strain, ultimately leading to the observed reduction in pull-off forces with increased bone abrasion. Additionally, our previous research demonstrated that bone stress relaxation had minimal impact on pull-off forces when compared to plastic models, likely due to the significant shearing deformation observed at the bone-implant interface in both plastic and viscoelastic models. As a result, it was suggested that the CoF used in both this and the previous study, set at 0.95, may be too high, as it was based on tests using Sawbones® bone analogues rather than cadaveric bones. However, the CoF was measured for the POROCOAT® coating against femoral bone cubes in another study and was on average 0.86 [22]. That study also found that the CoF increases with higher interference fits. Since our study employed higher levels of interference fit than theirs, the choice of 0.95 seems realistic. Investigating the effects of varying the CoF could provide insights into its impact on pull-off forces and the extent of bone abrasion, given its demonstrated sensitivity to these parameters [13, 27].

A notable finding of this study is the considerable variance observed in both the experimental and computational pull-off forces. Experimental measurements showed a wide range of pull-off forces, from 855 N to 2903 N, reflecting variations in patient characteristics as well as differences in surgical techniques, which are factors commonly encountered in biomechanical studies involving biological tissues and the inherent variability of surgical procedures. To account for the effects of gender and age, the study included both male and female patients, with an age range of 53 to 79 years. BMD was calculated from the calibrated CT-scans for each specimen and correlated with the pull-off force. A significant positive correlation was found between BMD and the pull-off forces in both the experimental and computational (no abrasion) conditions. These findings are consistent with previous studies, which have shown that higher BMD is associated with increased pull-off and roll-off forces [13, 24].

While a pull-off test offers an indirect measure of femoral component fixation quality, it does not reflect a clinical failure scenario. Primary fixation is typically assessed by measuring or simulating micromotions at the implant-bone interface, which serves as an indicator of osseointegration and bone ingrowth. It is currently unclear how the reduction in bone stresses, due to the bone stress relaxation, affect interface micromotions. Further research is needed to explore this, potentially using a model like the one presented by Berahmani et al. [12]. Moreover, an alternative approach was used to simulate the insertion procedure. Simulating an actual implantation procedure would significantly increase the complexity, leading to considerably longer simulation times and most likely non-convergence of the models. Instead, we focused on a more controllable scenario in which we applied the interference fit in the virtual implantation. While this does not fully replicate the experimental conditions, it provides a well-defined, manageable situation that minimizes variability, leading to more consistent results.

The simulation of bone abrasion in this study was simplified by applying uniform abrasion across the bone-implant interface, specifically at regions where the bone initially penetrated the implant. In reality, the extent and distribution of bone abrasion are likely influenced by factors such as surgical cuts, local variations in bone density, and the implant insertion angle. We hypothesize that the implant strain predictions from our computational models, which were significantly overestimated compared to the strain gauge measurements, correspond to regions with greater abrasive activity in the experiments. Consequently, locally a higher level of bone abrasion may have been required in the simulations to reflect these experimental conditions more accurately. However, the extent of bone abrasion was not quantitively analyzed using micro-CT, as was previously done with bone blocks and titanium platens featuring various surface coatings [27]. In this study, the concept of effective interference fit, which accounts for the elastic deformation of the bone, was used to simulate virtual levels of bone abrasion. Effective interference fit has been reported to range between 2% and 59% of the nominal interference fit [21, 22]. For the implants used here, the manufacturer specified a nominal bilateral interference fit of 1.5 mm. Based on this, virtual abrasion levels of 0.5 mm and 0.75 mm on both the anterior and posterior sides were modeled. Determining the exact levels of bone abrasion experimentally through micro-CT analysis would allow us to test the hypothesis proposed earlier and to refine our simulations accordingly. Moreover, this study did not differentiate between the various types of bone abrasion that occur during the implantation of a femoral component. Bone abrasion generates particles at three distinct locations [21]: (1) On the implant's surface coating, (2) within the porosity of the bone, and (3) bone particles being scraped out. In our simulations, all bone abrasion was modeled as scraped particles removed from the interface, neglecting the other two modes of abrasion. These modes may influence both the short- and long-term fixation of the implantation. Previous research has demonstrated that bone debris at the bone-implant interface can alter pull-out forces by filling the rough surface of a simplified implant, thereby affecting the effective CoF [27]. Furthermore, the penetration of bone particles into inter-trabecular spaces was not simulated, and its potential effect on short-term fixation remains unclear. While it is known that such particles can promote bone ingrowth and improve fixation over the long term, these biological effects fall outside the scope of this study, which focuses exclusively on primary fixation [28].

This study, in addition to the previously mentioned limitations, has several shortcomings. For instance, only one type of implant was investigated with a limited sample size (N=6), and all implantations were performed by a single surgeon. Furthermore, stress relaxation was not applied to the cortical bone in our simulations. Given that the implant primarily contacts trabecular bone at the interface, it is unlikely that including the viscoelastic behavior of cortical bone would significantly affect the fixation strength. Moreover, a softening von Mises yield criterion was used in this study, which tends to cause the yielding zone to extend deeply into the bone. However, in reality, damage is more localized near the bone-implant interface [29]. Alternative plastic models, such as an isotropic crushable foam model, may better capture the bone behavior in this context [30]. The level of bone stress relaxation used in our model was based on experiments with trabecular bone cores subjected to strains up to 0.8% [16], while plasticity in our simulations was modeled with strains well beyond this range. There is no consensus in the literature regarding stress relaxation beyond the yield strain [31, 32]. Therefore, further stress relaxation experiments beyond the yield strain could provide valuable insights into the material behavior of human trabecular bone. In our previous study, stress relaxation was also only measured in compression, and this aligns with the current study, where the strain field is predominantly compressive [16]. However, in other studies, the strain field may not be compression-dominated. Since no previous research has quantified stress relaxation in tension or shear, it would be beneficial to investigate these strain states, particularly when they are relevant to bone-implant interactions.

The findings of this study mark a significant step forward in understanding the mechanics of primary fixation in cementless femoral components. By incorporating both bone stress relaxation and virtual bone abrasion into FE simulations, this research provides valuable insight into how these factors influence fixation strength. This is the first study to explore the combined effect of bone plasticity, stress relaxation, and abrasion on bringing computational models closer to experimental observations of implant strains and pull-off forces. The results demonstrate progress, with trends in fixation behavior aligning more closely with experimental data. By incorporating virtual abrasion, the FE results clearly approached the experimental findings more closely than without taking abrasion into account. This was particularly evident at 0.75 mm of virtual abrasion, where the computational strain predictions were closer to the experimental values, though still slightly overestimated. While the computational models successfully captured the general trends in implant strain reduction and pull-off force, some discrepancies persist. For instance, the pull-off force was overestimated when no or only 0.5 mm of bone abrasion was simulated, whereas it was underestimated with 0.75 mm of virtual abrasion. Additionally, the models consistently underpredicted strain reduction at locations where higher bone stress relaxation was observed in the experimental data. These findings highlight the need for further refinement of computational models to enhance their predictive accuracy and clinical relevance. The implications of this study extend beyond these findings, providing a robust foundation for future research. By systematically varying critical parameters, ranging from interference fit and CoF to surgical cutting errors, and the extend and type of bone abrasion, future studies can assess their individual and interactive effects on implant fixation. This iterative process of refining and comparison to experimental data will enable more tailored simulations for specific implant designs, surgical techniques, and patient conditions, which will be beneficial for advancing implant design and optimizing surgical outcomes.

References

1. Bellemans, J., Ries, M.D., Victor, J.M.K., Total Knee Arthroplasty: A Guide to Get Better Performance. 2005, Springer S.
2. Aggarwal, V.K., et al., Revision total knee arthroplasty in the young patient: is there trouble on the horizon? J Bone Joint Surg Am, 2014. 96(7): p. 536-42.
3. Australian Orthopaedic Association National Joint Replacement Registry (AOANJRR) Hip, Knee & Shoulder Arthroplasty: 2023 Annual Report. AOA, Adelaide, 2023.
4. National Joint Registry for England, W., Northern Ireland and the and Isle of Man, 20th Annual Report 2023. 1821, Hertfordshire, 2023.
5. Abdul-Kadir, M.R., et al., Finite element modelling of primary hip stem stability: the effect of interference fit. J Biomech, 2008. 41(3): p. 587-94.
6. Chong, D.Y., U.N. Hansen, and A.A. Amis, Analysis of bone-prosthesis interface micromotion for cementless tibial prosthesis fixation and the influence of loading conditions. J Biomech, 2010. 43(6): p. 1074-80.
7. Conlisk, N., et al., The influence of stem length and fixation on initial femoral component stability in revision total knee replacement. Bone Joint Res, 2012. 1(11): p. 281-8.
8. Tarala, M., et al., Experimental versus computational analysis of micromotions at the implant-bone interface. Proc Inst Mech Eng H, 2011. 225(1): p. 8-15.
9. Taylor, M., D.S. Barrett, and D. Deffenbaugh, Influence of loading and activity on the primary stability of cementless tibial trays. J Orthop Res, 2012. 30(9): p. 1362-8.
10. van der Ploeg, B., et al., Toward a more realistic prediction of peri-prosthetic micromotions. J Orthop Res, 2012. 30(7): p. 1147-54.
11. Viceconti, M., et al., Large-sliding contact elements accurately predict levels of bone-implant micromotion relevant to osseointegration. J Biomech, 2000. 33(12): p. 1611-8.
12. Berahmani, S., D. Janssen, and N. Verdonschot, Experimental and computational analysis of micromotions of an uncemented femoral knee implant using elastic and plastic bone material models. J Biomech, 2017. 61: p. 137-143.
13. Berahmani, S., et al., An experimental study to investigate biomechanical aspects of the initial stability of press-fit implants. J Mech Behav Biomed Mater, 2015. 42: p. 177-85.
14. Norman, T.L., et al., Cortical bone viscoelasticity and fixation strength of press-fit femoral stems: an in-vitro model. J Biomech Eng, 2006. 128(1): p. 13-7.
15. Gersie, T., et al., The effect of bone relaxation on the simulated pull-off force of a cementless femoral knee implant. J Biomech, 2025. 181: p. 112528 DOI: 10.1016/j.jbiomech.2025.112528.
16. Gersie, T., et al., Characterization of nonlinear stress relaxation of the femoral and tibial trabecular bone for computational modeling. Med Eng Phys, 2025. 138: p. 104324 DOI: 10.1016/j.medengphy.2025.104324.
17. Caravaggi, P., et al., CoCr porous scaffolds manufactured via selective laser melting in orthopedics: Topographical, mechanical, and biological characterization. J Biomed Mater Res B Appl Biomater, 2019. 107(7): p. 2343-2353.
18. Derikx, L.C., et al., Implementation of asymmetric yielding in case-specific finite element models improves the prediction of femoral fractures. Comput Methods Biomech Biomed Engin, 2011. 14(2): p. 183-93.

19. Keyak, J.H., et al., Predicting proximal femoral strength using structural engineering models. Clin Orthop Relat Res, 2005(437): p. 219-28.
20. Keyak, J.H., et al., Prediction of femoral fracture load using automated finite element modeling. J Biomech, 1998. 31(2): p. 125-33.
21. Berahmani, S., et al., Evaluation of interference fit and bone damage of an uncemented femoral knee implant. Clin Biomech (Bristol), 2018. 51: p. 1-9.
22. Damm, N.B., M.M. Morlock, and N.E. Bishop, Friction coefficient and effective interference at the implant-bone interface. J Biomech, 2015. 48(12): p. 3517-21.
23. Helgason, B., et al., Mathematical relationships between bone density and mechanical properties: a literature review. Clinical biomechanics, 2008. 23(2): p. 135-146.
24. Berahmani, S., et al., The effect of surface morphology on the primary fixation strength of uncemented femoral knee prosthesis: a cadaveric study. J Arthroplasty, 2015. 30(2): p. 300-7.
25. Gersie, T., et al., Quantification of long-term nonlinear stress relaxation of bovine trabecular bone. J Mech Behav Biomed Mater, 2024. 152: p. 106434.
26. Burgers, T., et al., Time-dependent fixation and implantation forces for a femoral knee component--an in vitro study. Med Eng Phys, 2010. 32(9): p. 968-73.
27. Bishop, N.E., et al., The influence of bone damage on press-fit mechanics. J Biomech, 2014. 47(6): p. 1472-8.
28. Franchi, M., et al., Biological fixation of endosseous implants. Micron, 2005. 36(7-8): p. 665-71.
29. Rapagna, S., et al., Quantification of human bone microarchitecture damage in press-fit femoral knee implantation using HR-pQCT and digital volume correlation. J Mech Behav Biomed Mater, 2019. 97: p. 278-287.
30. Soltanihafshejani, N., et al., The application of an isotropic crushable foam model to predict the femoral fracture risk. PLoS One, 2023. 18(7): p. e0288776.
31. Burgers, T.A., et al., Post-yield relaxation behavior of bovine cancellous bone. J Biomech, 2009. 42(16): p. 2728-33.
32. Leng, H., X.N. Dong, and X. Wang, Progressive post-yield behavior of human cortical bone in compression for middle-aged and elderly groups. J Biomech, 2009. 42(4): p. 491-7.

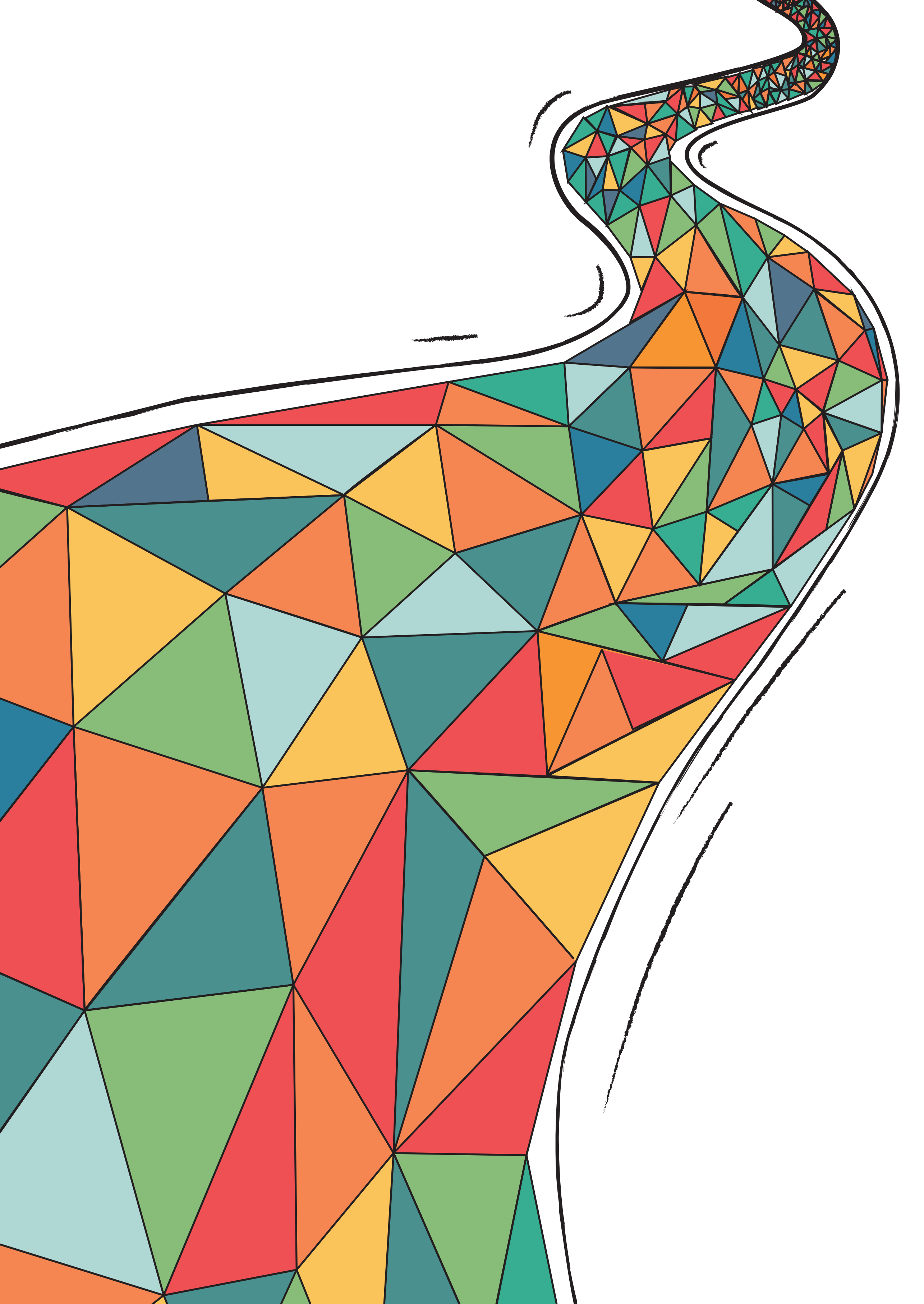

Chapter 6

Influence of bone stress relaxation and abrasion on micromotions in uncemented femoral knee implants: A finite element study

Thomas Gersie, Thom Bitter, Robert Freeman, Nico Verdonschot, Dennis Janssen

Submitted to PLOS ONE

Abstract

Aseptic loosening is the primary cause of revision in cementless total knee arthroplasty, highlighting the importance of reliable primary fixation. Pre-clinical evaluations are crucial for understanding implant fixation mechanics. Finite element (FE) models commonly use linear elastic bone properties, which inadequately represent bone behavior. While incorporating bone plasticity increases the realism of primary fixation simulations, it tends to underestimate micromotions at the bone-implant interface compared to experimental data. This discrepancy is potentially due to the exclusion of bone viscoelasticity and abrasion.

This study aimed to assess whether including bone relaxation and abrasion enhances micromotion predictions at the bone-implant interface of an uncemented femoral knee implant, in comparison to experimental measurements. Micromotion data from five prosthetic components implanted in cadaveric femora were compared with cadaver-specific FE models, assigned either elastic, plastic, or plastic-viscoelastic bone properties with varying degrees of virtual abrasion.

Stress relaxation had minimal impact on micromotions, which remained significantly lower than experimental values. Introducing virtual bone abrasion resulted in increased micromotions across all models. For the plastic-viscoelastic model with 0.75 mm of abrasion, the predicted micromotions were 53.0 ± 43.0 µm, closely matching the experimental micromotions (53.1 ± 42.3 µm). However, the simulation failed to converge for two specimens at 0.75 mm abrasion due to minimal implant-bone contact.

These findings emphasize the need to incorporate bone abrasion into FE models and suggest that future research should focus on refining simulations by addressing limitations associated with bone plasticity, friction, and the simplifications of the abrasion model used.

6.1 Introduction

Total knee arthroplasty (TKA) is a widely performed orthopedic procedure that alleviates pain and restores function in patients with knee osteoarthritis [1]. As the number of TKA surgeries rises, so does the incidence of revision surgeries, particularly among younger, more active patients who are at greater risk [2]. Aseptic loosening is the leading cause of revision in cementless TKA, making reliable primary stability essential for long-term fixation [3, 4].

Primary stability in cementless TKA relies on several factors, including bone quality, the friction coefficient of the bone-implant interface, the compressive forces generated by the press-fit, and the overall prosthetic design. This stability can be assessed by measuring relative motion between the implant and the bone. To this end, various experimental and numerical testing techniques have been developed to evaluate micromotions at the bone-implant interface [5-7]. Among these, finite element (FE) analysis offers the unique advantage of simulating complex loading conditions and quantifying interfacial micromotions that are otherwise unmeasurable experimentally, such as those occurring in between measurement locations or in occluded regions [8].

Although FE models are widely used, many still rely on a linear elastic representation of bone's mechanical properties, which inaccurately predicts stresses and deformations within the bone [9-12]. This simplification leads to unrealistic primary stability predictions, with bone stresses surpassing the yield limit. While one study has incorporated a von Mises yield criterion to simulate bone's plastic behavior, it still tends to underestimate micromotions and overestimate fixation strength compared to experimental data [13]. This discrepancy is potentially due to the exclusion of bone viscoelasticity and abrasion.

The viscoelastic behavior leads to a reduction of the stresses in the bone over time, and may therefore play a crucial role in implant stability, as it can reduce press-fit forces through stress relaxation [14-17]. An experimental study on cementless femoral components reported a 17 to 37% reduction in implant surface strains within 24 hours post-implantation, indirectly indicating bone relaxation in the femur [17]. Similarly, a cadaveric study with human femurs showed a significant decrease in pull-out force of press-fit pegs within 30 minutes of implantation [14], and another study observed a substantial reduction in fixation strength of press-fit hip stems after 24-hours [16]. FE analyses incorporating bone stress relaxation combined with a plastic bone material model revealed a 79% reduction in pull-off force compared to an elastic model, although the isolated effect of bone relaxation was minimal [18]. However, the impact of reduced bone stresses due to bone relaxation on interface micromotions remains unclear.

Bone abrasion, as considered in this study, refers to the damage and removal of bone tissue caused by mechanical friction between the implant and bone during implantation, which may compromise implant stability. In experimental studies on cementless TKA fixation, bone debris was observed along the edges of the implant-bone interface at the posterior condyles post-implantation [13]. In addition, residual particles were found on the inner surface of the implant after its removal from the bone. The effect of virtual abrasion, a simplified simulation of abrasion during implantation, was examined in a combined experimental and computational study of femoral component pull-off [17]. Incorporating virtual bone abrasion in the model brought the computational pull-off force closer to the experimental results, highlighting the importance of including bone abrasion in simulations for more accurate predictions of implant stability. However, the effect of virtual bone abrasion on bone-implant micromotions has not yet been investigated.

Therefore, this study aimed to determine if incorporating bone relaxation and abrasion improves the accuracy of micromotion predictions at the bone-implant interface of an uncemented femoral knee implant, compared to previously acquired experimental measurements. To achieve this, experimental micromotion data from prosthetic components implanted in cadaveric femora were compared with cadaver-specific finite element models, which were assigned either elastic, plastic, or plastic-viscoelastic bone material properties with varying levels of virtual bone abrasion.

6.2 Methods

In a previous experimental study, five cadaveric femurs (two pairs, average age 85± 4 years old (mean ± standard deviation (SD)) were implanted with uncemented SIGMA® cruciate retaining femoral knee implants (DePuy Synthes Joint Reconstructions, UK) [13]. No history of musculoskeletal or metabolic disease was known, but CT scans revealed no abnormalities. Based on clinical pre-planning, four size 5 implants and one size 3 implant were used. The femur specimens were CT- and micro-CT scanned after being cut, but before implantation, allowing for the extraction of material properties and detailed bone cut geometries. Following implantation, the implant position relative to the bone was determined using optical scans, enabling the use of cut-dependent interference fit in subsequent simulations, rather than assuming an ideal fit. Digital Image Correlation (DIC) was then used to measure micromotion as close as possible to the bone-implant interface. Seven regions of interest (ROIs) were chosen: the anterior flange (from the coronal plane view) and the anterior, distal, and posterior regions (from the sagittal plane view) on both the medial and lateral sides of the femur (Figure 6-1). Micromotion measurements were taken under four static loading conditions derived from physical loading profiles for gait and deep knee bend (DKB) activities [19, 20] (Table 6-1). The loading profiles at angles of 14° and 90° represented the peak tibiofemoral (TF) forces during gait and DKB, respectively. Peak forces were selected, as it has been demonstrated that using a simplified peak force is effective in assessing the stability of cementless femoral implants [19]. To prevent bone fracture at the distal fixation, only 60% of the maximum load was applied for the 90° flexion condition. Prior to measurements, the specimens were pre-conditioned for 15 minutes at 1 Hz under the position-dependent loading profile to allow for the initial settling of the implant. All loads were applied using a servo-hydraulic testing machine with a force-control system that applied compressive loads at a rate of 100 N/sec. Micromotions at the ROIs were calculated by subtracting the bone displacements from the implant displacements. These displacements were then composed into normal and shear components based on the orientation of the bone-implant interface. A matched size tibial implant was used during loading.

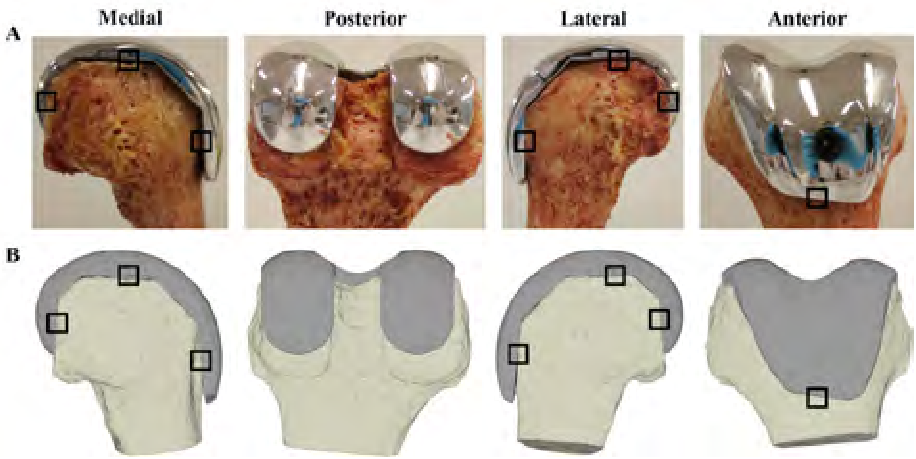

Figure 6-1: A) Medial, posterior, lateral, and anterior views of an experimental specimen, with schematic ROIs for the micromotions marked by rectangles [13]. **B)** The corresponding finite element model.

6.2.1 Finite element model

For the FE analysis, CAD files were provided by the manufacturer (DePuy Synthes Joint Reconstruction, USA) to replicate the experimental setup. All simulations were carried out using Marc/Mentat 2024.2 (MSC Software, USA), with a mesh of linear four-noded tetrahedral elements for both the bone and implants. An average edge length of 1 mm was selected based on a previous mesh convergence study [19]. Further details on the DIC procedure and the model reconstruction are available in Berahmani et al. [13].

Table 6-1: Preconditioning and static loading profiles for both the experiments and simulations, derived from physical loading profiles [19, 20].

Activity	Flexion angle [°]	Load [N]	Applied percentage of load [%]		Medial - lateral ratio [%]
			Pre-conditioning	Static	
Gait	14	2.387	100	100	50-50
	30	1.782	100	100	40-60
DKB	60	1.974	100	100	64-36
	90	2.250	60	60	63-37

6.2.1.1 Material behavior

The implants were assigned isotropic elastic material properties with a Young's modulus of 210 GPa and a Poisson's ratio of 0.3. Bone material properties were determined using in-house software that converted Hounsfield units to pQCT values based on calibrated CT scans [21]. The ash density for each element was then calculated using the relationship: $\rho_{ash} = 0.0633 + 0.887\rho_{QCT}$ [22]. Elements with a ρ_{ash} below 250 mg cm^{-3} were categorized as trabecular bone, following previous studies [23]. The calcium content of each element was linked to Young's modulus using established bone density-stiffness relationships [22]. Three different bone material models were applied: elastic, plastic, and plastic-viscoelastic. An isotropic elastic material model was initially applied. For the plastic model, a non-linear isotropic post-yield material model was used, based on the von Mises yield criterion, with the yield stress determined by the ash density for both the trabecular and cortical bone [22]. In addition, viscoelastic behavior was incorporated based on our prior research on femoral and tibial trabecular bone, applying a stress relaxation level of 54% [24]. Stress relaxation was simulated through a subroutine that incrementally introduced creep strain, based on the elastic strain after implantation and the target relaxation level. As creep strain increased, the elastic strain decreased, leading to a corresponding reduction in stress. The viscoelastic response was applied only to trabecular bone elements. For elements with a ρ_{ash} below 600 mg cm^{-3}, stress relaxation was simulated, as this threshold marked a distinction between trabecular bone characteristics observed in the CT scans and the cortical bone mechanical properties based on their ρ_{ash} values. The stress relaxation was applied during a specific stress relaxation phase (see section 6.2.1.2). Table 6-2 outlines the mechanical property relationships used for each material model.

Table 6-2: The mechanical property relationships per bone material model for the trabecular and cortical bone [22]. The plastic behavior for each model was represented by an initial perfectly plastic phase at stress S until the plastic strain was ε_{AB}, followed by a strain softening phase with plastic modulus E_p until the stress was σ_{min} and then an indefinite perfectly plastic phase. In the plastic-viscoelastic model, the stress at the end of the stress relaxation phase (Phase 2) is calculated as the stress at the end of the virtual implantation (Phase 1) after 54% of stress relaxation [24].

Relationship	Type of Bone	Bone material model
$E = 14900\rho_{ash}^{1.86}$	Trabecular and cortical	Elastic, Plastic, Plastic-Viscoelastic
$S = 102\rho_{ash}^{1.86}$	Trabecular and cortical	Plastic, Plastic-Viscoelastic
$\varepsilon_{AB} = 0.00189 + 0.0241\rho_{ash}$	Trabecular	Plastic, Plastic-Viscoelastic
$\varepsilon_{AB} = 0.00184 - 0.0100\rho_{ash}$	Cortical	Plastic, Plastic-Viscoelastic
$\varepsilon_{AB} = 0.00189 + 0.0241\rho_{ash}$	Trabecular	Plastic, Plastic-Viscoelastic
$E_p = -2080\rho_{ash}^{1.45}$	Trabecular	Plastic, Plastic-Viscoelastic
$E_p = -1000$	Cortical	Plastic, Plastic-Viscoelastic
$\sigma_{min} = 43.1\rho_{ash}^{1.81}$	Trabecular and cortical	Plastic, Plastic-Viscoelastic
$\sigma_{Phase\ 2} = \sigma_{Phase\ 1} - 0.54\sigma_{Phase\ 1}$	Trabecular	Plastic-Viscoelastic

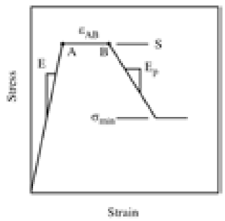

6.2.1.2 *Boundary conditions, contact definition, and micromotion*

The simulations were conducted in distinct phases, as illustrated in Figure 6-2. In the initial phase, the femoral component was virtually implanted using the node-to-segment contact algorithm of the FE software. A negative interference fit was applied to allow penetration of the contacting surfaces without generating contact stresses. The interference fit was then reduced to zero, allowing the bone surface nodes that initially penetrated the implant to compress until the surfaces were in contact (Figure 6-3). For simulations in which the bone was modeled as plastic-viscoelastic, different levels of bone abrasion were considered, in addition to a scenario without virtual abrasion. Virtual bone abrasion levels of 0.50 mm and 0.75 mm were chosen based on the implant's nominal interference fit of 1.5 mm, as specified by the manufacturer. Since previous studies have reported that the effective interference fit can range from 2% to 59% of the nominal value, we modeled these abrasion levels on both the anterior and posterior sides of the implant [25, 26]. Notably, 0.50 mm of abrasion on both sides resulted in a total reduction of 1 mm in the nominal interference fit, which falls within the reported effective interference range. In our previous study, we found that incorporating virtual bone abrasion levels of 0.50 mm and 0.75 mm resulted in promising outcomes, as these levels of abrasion improved the accuracy of pull-off force predictions, bringing them closer to the experimental findings [17]. Importantly, while the nominal interference fit is based on manufacturer specifications, the actual interference fit used in the simulations was determined by the optical scans, reflecting a cut-dependent and variable fit. In the simulations, reducing the interference fit to 0.50 mm effectively allowed the bone to penetrate 0.50 mm into the implant by the end of the implantation phase, thereby simulating 0.50 mm of virtual bone abrasion (Figure 6-3). A frictional touching contact algorithm, based on a Coulomb bilinear (displacement) friction model, was applied to the implant-bone interface, with a coefficient of friction (CoF) of 0.95 specified by the manufacturer for the POROCOAT® surface coating (DePuy Synthes Joint Reconstruction, UK). During the implantation phase, the implant was fixated distally in all directions, while the femur was fixated proximally in all directions throughout all phases. For simulations incorporating plastic-viscoelastic bone behavior, the implantation phase was followed by a stress relaxation phase where trabecular bone elements were subjected to relaxation. In the final phase, experimental loading conditions were applied to the implant to replicate the experimental tests. Each of the four loading conditions was applied incrementally, with the first condition repeated twice to allow for initial settling of the implant (Table 6-1) [19]. Consistent with the experimental protocol, micromotions at seven ROIs were calculated by subtracting the nodal displacements of the bone and the implant (Figure 6-1).

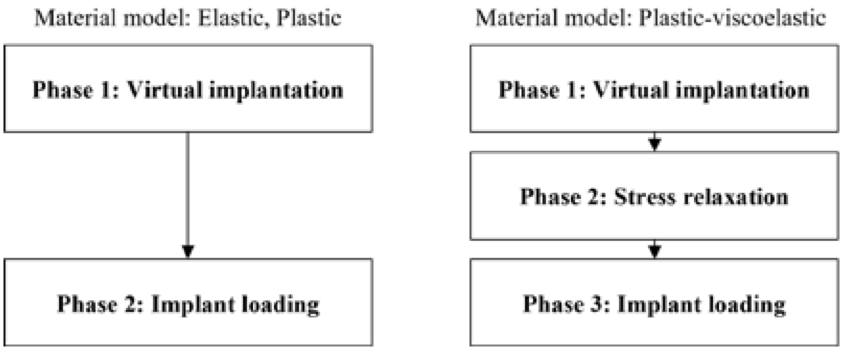

Figure 6-2: Flowchart of different simulation phases for the models with elastic or plastic bone material models and the models with plastic-viscoelastic bone mechanical properties.

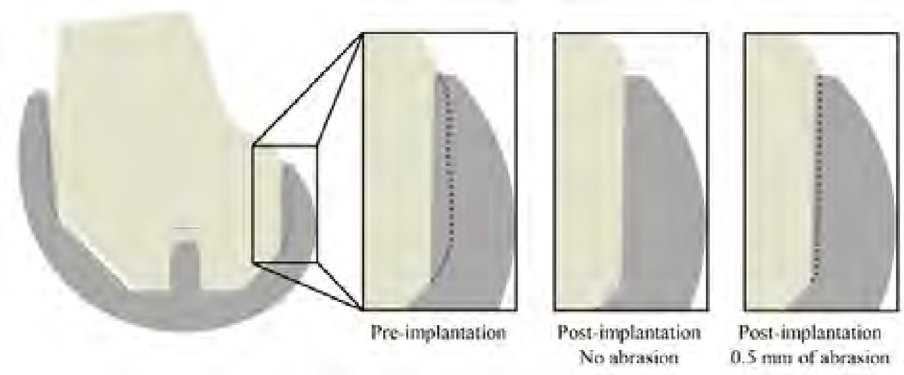

Figure 6-3: A cross-sectional view of the femur, taken through the lateral condyle in the coronal plane. Bone elements that initially penetrate the implant are visible on both the anterior and posterior sides. During the implantation phase, these elements are gradually compressed until the bone nodes that were penetrating the implant surface make contact with it. After the virtual implantation, the surface nodes are in direct contact with the implant surface in the absence of simulated abrasion. In models that include virtual abrasion, the bone nodes that initially penetrated the implant surface are retracted to match the bone surface, leaving a consistent layer of 0.5 mm or 0.75 mm of bone penetration to represent abraded bone.

6.2.2 Data analysis

Statistical analyses were conducted using GraphPad Prism 10.1.2 (GraphPad Software, USA), with a significance level set at 0.05. The micromotions of all ROIs under the four loading conditions were compared between experimental and FE-predicted micromotions for each material model using a Kruskal-Wallis test, with Dunn's test for post-hoc comparisons, following a Kolmogorov-Smirnov normality test. Linear regression analysis was performed to examine the correlation between experimental and FE-predicted micromotions for each material model, focusing on the overall trend by comparing the average micromotion across all ROIs per specimen for each loading condition. The strength of the correlation was assessed using the R-squared (R^2) value, with thresholds for categorizing the strength of the association as follows: very weak (R^2 = 0-0.19), weak (R^2 = 0.2-0.39), moderate (R^2 = 0.4-0.59), strong (R^2 = 0.6-0.79), and very strong (R^2 = 0.8-1).

6

6.3 Results

Figure 6-4 shows the distribution of micromotions predicted by different computational models for a single specimen. The elastic, plastic, and plastic-viscoelastic (without abrasion) models exhibit relatively low micromotion magnitudes, with localized areas of higher micromotion on the anterior-lateral side. Incorporating virtual bone abrasion led to increased micromotions across all regions of the implant, with the 0.75 mm abrasion model displaying the most extensive increase.

Quantitatively, considering all five specimens, the micromotions predicted by the computational models without bone abrasion were 25.0 ± 26.1 µm for the elastic model, 21.9 ± 24.0 µm for the plastic model, and 21.1 ± 22.9 µm for the plastic-viscoelastic model (Figure 6-5). No significant differences were observed between these three models. However, all predictions were significantly lower than the average experimental micromotion of 53.1 ± 42.3 µm ($p < 0.001$ for all comparisons).

When virtual bone abrasion was introduced in the plastic-viscoelastic model, predicted micromotions increased significantly ($p < 0.0001$). With 0.5 mm of abrasion, the average predicted micromotion was 41.9 ± 31.3 μm, which was still significantly lower than the experimental values ($p = 0.0485$). At 0.75 mm of abrasion, the predicted micromotions increased to 53.0 ± 43.0 μm, aligning closely with the experimental values (no significant difference) (Figure 6-5). However, for specimens 2 and 3, the simulation failed to converge at 0.75 mm abrasion due to minimal implant-bone contact.

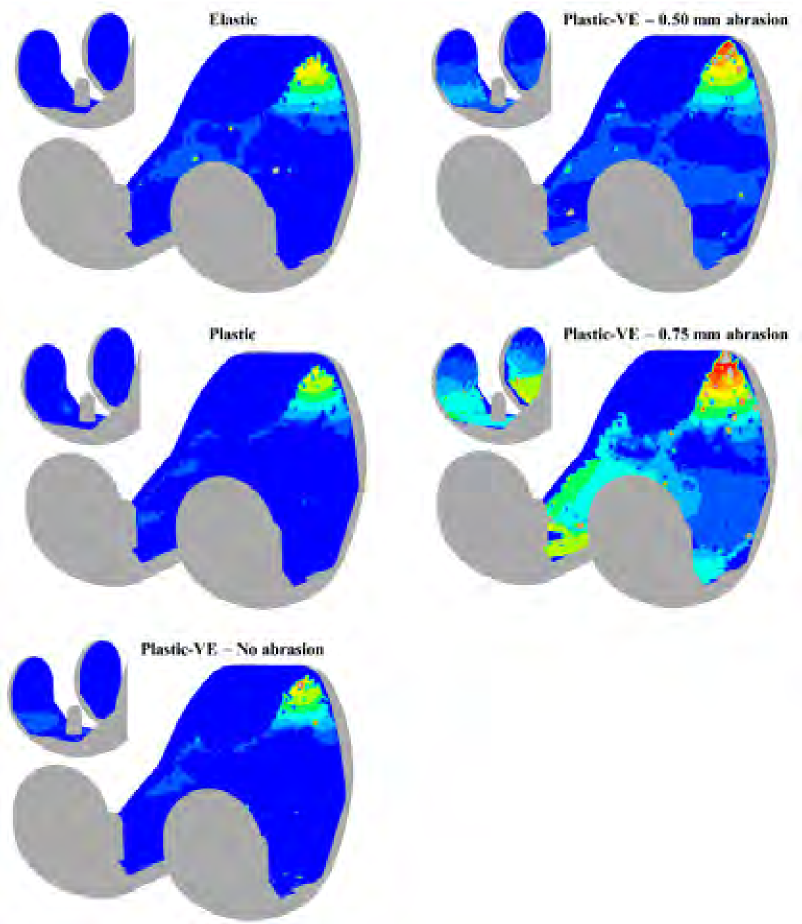

Figure 6-4: Predicted micromotion distributions for a single specimen across different computational models. The elastic, plastic, and plastic-viscoelastic models (without abrasion) exhibit limited micromotion, with localized peaks on the anterior-lateral side. In contrast, introducing virtual bone abrasion results in a broader increase in micromotion, particularly in the 0.75 mm abrasion model, where the effect is more pronounced across the entire contact area.

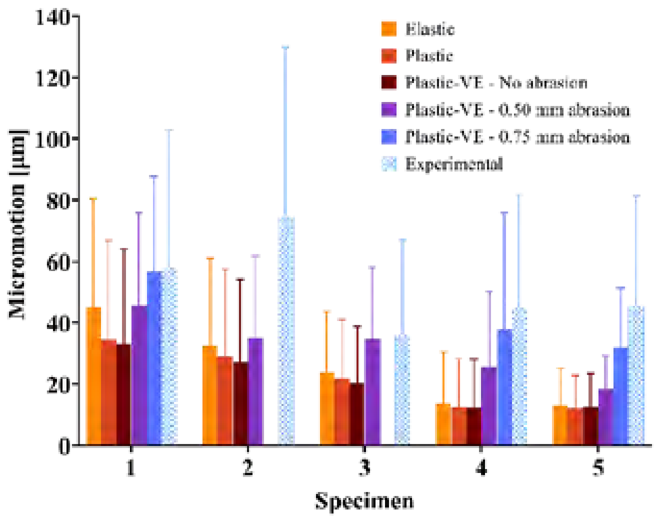

Figure 6-5: Average micromotion measurements, both experimental and computational, for each material model. The plastic-viscoelastic model is referred to as plastic-VE. The specimens are arranged in order of increasing bone quality. Significant variations are observed both between specimens and within individual specimens, for both the experimental and computational results. Simulations without abrasion show considerable deviation from experimental data, whereas incorporating 0.75 mm of virtual abrasion brings the computational results closer to the experimental findings. For specimens 2 and 3, the simulation failed to converge at 0.75 mm abrasion due to minimal implant-bone contact; consequently, no data is available for these cases.

The correlation between the average micromotions (from the seven ROIs) per specimen for the four loading conditions showed a moderate correlation ($p = 0.0008$) between the experimental and predicted micromotions using the elastic model (Figure 6-5 - Elastic). In contrast, the plastic and plastic-viscoelastic (no abrasion) models exhibited a high degree of correlation ($p = 0.0002$ and $p < 0.0001$, respectively) (Figures 6-5 - Plastic and 6-5 - Plastic-VE – No abrasion). When 0.5 mm of virtual abrasion was included, a weak correlation was observed between the experimental and predicted micromotions ($p = 0.0282$) (Figure 6-5 - Plastic-VE – 0.5 mm abrasion). However, for 0.75 mm of virtual abrasion, no significant correlation was found (Figure 6-5 - Plastic-VE – 0.75 mm abrasion). It is worth noting that this last result missed eight data points due to non-converging simulations.

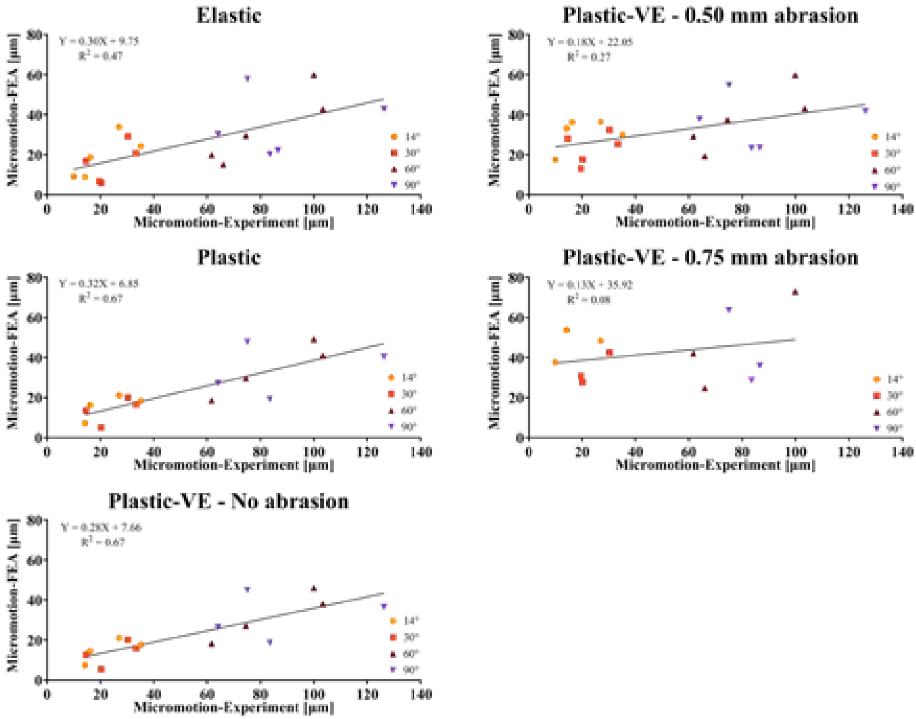

Figure 6-6: Correlation between average experimental micromotions (from the seven ROIs) per specimen and predicted micromotions by the finite element analysis (FEA) for each material model under four loading conditions. Elastic: A moderate correlation ($p = 0.0008$) was observed between experimental and predicted micromotions using the elastic model. Plastic: The plastic material model exhibited a strong correlation ($p = 0.0002$) between experimental measurements and computational predictions. Plastic-VE (plastic-viscoelastic) – No abrasion: The plastic-viscoelastic model also demonstrated a good correlation ($p < 0.0001$) between experimental and simulated micromotions. Plastic-VE – 0.5 mm abrasion: Including 0.5 mm of virtual abrasion in the plastic-viscoelastic model resulted in a weak correlation ($p = 0.0282$). Plastic-VE – 0.75 mm abrasion: With 0.75 mm of virtual abrasion, no significant correlation was found. Data from two femoral reconstructions were not included due to simulation non-convergence.

6.4 Discussion

This study examined whether incorporating bone stress relaxation and bone abrasion into FE simulations of the primary fixation of cementless femoral knee components would yield more realistic predictions of bone-implant micromotions. Our results showed that including stress relaxation in a plastic bone material model did not significantly affect micromotion, as micromotions remained underestimated compared to experimental measurements. In contrast, bone abrasion led to increased micromotions, bringing predictions closer to experimental values. Notably, a virtual abrasion of 0.75 mm resulted in average micromotions comparable to experimental data; however, for two out of five specimens, this scenario could not be simulated due to non-convergence.

The effect of bone stress relaxation on interface micromotions using FE simulations has not been investigated until now, making this the first study to explore this aspect. Our results showed virtually no difference in micromotions between the plastic and plastic-viscoelastic bone material models, suggesting that viscoelasticity alone does not significantly influence implant stability under the tested conditions. While previous experimental research explored the role of viscoelastic behavior in implant fixation, such studies have been limited to press-fit hip stems and press-fit pegs [14, 16]. Observations of reduced strain on the surface of femoral knee implants after implantation suggests that bone stress relaxation may also occur in these implant, with this reduction in strain serving as an indirect indicator of this process [15, 17]. This suggest that bone viscoelasticity also plays a role in the fixation of femoral components. Notably, both the hip stem and peg study suggest that rough surfaces are less sensitive to stress relaxation. For example, a CoF of 1.0 in the press-fit hip implant study showed almost no relaxation, while the peg study demonstrated only a 13% reduction in pull-off force with a CoF of 1.4 [14, 16]. Similarly, our previous computational study, which used a CoF of 0.95, found that incorporating bone viscoelasticity into a plastic material model had little impact on the pull-off force, despite a 50% reduction in strain energy [17]. This aligns with the present study, where micromotions were also unaffected by stress relaxation. The CoF of 0.95 used in our study was determined based on testing against Sawbones® bone analogues. However, real bone, being a fatty tissue, likely has a lower frictional capacity than the Sawbones® material, which may affect the accuracy of the frictional interactions in our simulations. When bone stress relaxation occurs, the grip of the implant on the bone weakens over time. If the CoF between the implant and bone is low, this loss of grip happens more quickly, causing the implant to slip sooner. As a result, the effect of stress relaxation on implant stability becomes more pronounced for lower-friction implants, while higher-friction implants maintain their grip longer, reducing the impact of relaxation. Therefore, a CoF value based on experiments with actual bone may lead to more pronounced effects of stress relaxation, resulting in lower pull-off forces and higher micromotions that better align with experimental observations.

It was surprising that the simulated micromotions did not differ significantly between the elastic and plastic material models. In a previous computational study using the same femoral reconstructions as in the current study, we observed a 79% reduction in pull-off force when bone plasticity was included [18]. This reduction was linked to a decrease in elastic strain energy, which consequently led to lower pull-off forces. The results of the current study align with those of Rothstock et al., who also found no significant difference in micromotions between elastic and plastic bone models [27]. However, in that study, an interference fit of about one-fifth the size of ours was used. Given the much larger interference fit in our study, we had expected greater plastic deformation and higher micromotions compared to the elastic material model. Despite the lack of effect on interface micromotions shown here, we still advocate for including bone plasticity in FE simulations of cementless primary fixation, as it offers a more realistic representation of bone behavior. The elastic bone model led to unrealistically high contact forces and bone stresses beyond the yield point, distributed over a limited number of nodes, which is why most computational studies tend to use much smaller interference fits than those clinically applied. For example, studies by Schultz et al. and Rothstock et al. utilized interference fits ranging from 0.01 to 0.50 mm and 0.08 to 0.32 mm, respectively, while typical implant systems have designed press-fits of 1.00 to 2.00 mm [27, 28]. In contrast, the plastic bone model produced a more uniform distribution of contact forces across the bone-implant interface, making it possible to accurately simulate a nominal interference fit of 1.5 mm, as provided by the implant manufacturer (DePuy Synthes Joint Reconstruction, USA). It is well-established that bone undergoes plastic deformation and damage during implantation, which underscores the importance of incorporating this aspect into FE simulations [29]. Additionally, when using the elastic bone material model, the femoral reconstruction behaved like a spring, with the implant returning to its initial position at the end of the loading cycle. In contrast, the plastic bone model allowed for movement of the implant throughout the cycles, capturing not only micromotions but also implant migration. These effects are critical factors that influence the primary fixation and long-term stability of the implant [30].

The inclusion of bone abrasion in the FE simulations of femoral component pull-off improved the accuracy of predictions, aligning more closely with experimental results [17]. This was also observed in this study, when simulating bone-implant micromotions. However, there is still considerable potential for improvement in simulating virtual abrasion. While the average micromotions predicted by the plastic-viscoelastic model with 0.75 mm of abrasion were not statistically different from the experimental results, no significant correlation was found when comparing micromotions per specimen and per loading angle. This lack of correlation could be attributed to the low sample size, with two specimens excluded due to simulation non-convergence. It may also highlight limitations in the current abrasion simulation procedure. Without the inclusion of abrasion, the

FE model was quite accurate in predicting micromotions for loading profiles at 14° and 30°, where experimental micromotions were relatively low. However, the model tended to underpredict micromotions at higher loading angles. When abrasion was included, the predictions for high micromotions improved, though they were still underestimated. On the other hand, the inclusion of 0.75 mm abrasion led to an overprediction of micromotions by the model at 14° and 30°, balancing out the predictions to match average experimental values. The smaller experimental micromotions, which were observed at lower loading angles, appeared to be more influenced by the inclusion of bone abrasion. This could be because these loading profiles result in less micromotion overall, making the effect of bone abrasion more pronounced. In the virtual abrasion model, a uniform level of abrasion was applied across the bone-implant interface. However, this approach oversimplified the situation, as areas with lower interference fit are likely to experience decreased abrasion compared to areas with higher interference fit. This led to non-convergence in two out of five specimens, where the 0.75 mm abrasion models failed due to minimal implant-bone contact. The uniform abrasion model caused excessive loss of contact between the implant and bone. While the current model represents a first step toward realistically including abrasion in simulations, it does not account for the variable nature of abrasion across the bone-implant interface. In reality, the distribution and extent of bone abrasion depend on factors such as the applied load, interference fit, and implant insertion angle. To improve accuracy, experimental validation, such as micro-CT analysis, as performed in previous studies with bone blocks and titanium platens featuring various surface coatings, is necessary to refine the abrasion model [31].

Moreover, this study did not distinguish between the different types of bone abrasion that occur during the implantation of a femoral component. Bone abrasion produces particles at three primary locations [25]: (1) on the implant's surface coating, (2) within the intertrabecular spaces of the bone, and (3) bone particles that are scraped out. In our simulations, we modeled all bone abrasion as the removal of particles from the interface, overlooking the other two types of abrasion. These unmodeled abrasion modes could have implications for both short- and long-term fixation of the implant. Previous studies have shown that bone debris at the bone-implant interface can influence pull-out forces by filling in the rough surface of the implant, thus affecting the effective CoF [31]. Additionally, the penetration of bone particles into inter-trabecular spaces was not considered in our simulations, leaving the potential impact on short-term fixation uncertain. While it is understood that such particles may promote bone ingrowth and enhance long-term fixation, these biological effects fall outside the scope of our study, which focuses on primary fixation [32].

There are several limitations to this research. First, only one type of implant was analyzed, and the sample size was small (N=5), with all implantations performed by a single surgeon. Additionally, the average age of patients receiving a cementless prosthesis is typically around 68 years old [3, 4], but in this study, the average age at death of the cadaveric specimens was 85, reflecting the limited availability of younger cadaveric material at our hospital. Another limitation is the use of a von Mises yield criterion, which tends to cause the yielding zone to extend deeply into the bone. However, in reality, bone damage is more localized near the bone-implant interface [29]. Therefore, alternative plasticity models, such as an isotropic crushable foam model, may be more appropriate [33]. The bone stress relaxation was based on experiments with trabecular bone cores subjected to strains up to 0.8% [24], but in this study, plasticity was modeled with strains exceeding this range. There is a lack of consensus in the literature regarding stress relaxation beyond the yield strain; some studies report increased relaxation in bovine cancellous bone, while others show constant relaxation in human cortical bone after yielding [34, 35]. Further research into stress relaxation beyond the yield strain in human trabecular bone would provide valuable insights into its material behavior. Moreover, stress relaxation has only been measured in compression in our previous work, and this study also primarily involved compressive strain fields [24]. However, other studies may encounter different strain states, such as tension or shear, which have not yet been studied in relation to stress relaxation. Investigating stress relaxation in these strain states could be beneficial. Despite these limitations, the study offers valuable insights into the simulation of orthopedic implant fixation, highlighting the importance of incorporating bone stress relaxation and abrasion into the modeling process.

In conclusion, this study provides new insights into the role of bone stress relaxation and bone abrasion in simulating the primary fixation of cementless femoral knee components. While stress relaxation did not significantly influence micromotions, bone abrasion was shown to improve the accuracy of the simulations, bringing predicted average micromotions closer to experimental values. The implications of this study extend beyond these findings, providing a robust foundation for future research. By systematically varying critical parameters, such as interference fit, CoF, surgical cutting errors, and the extent, type, and local variability of bone abrasion, future studies can assess their individual and interactive effects on implant fixation. This iterative process of refining simulations and comparing them to experimental data will enable more tailored models for specific implant designs, surgical techniques, and patient conditions, advancing implant design and optimizing surgical outcomes. However, the findings also highlight several limitations, including the need for more realistic models of bone behavior, particularly with respect to frictional interactions and the complexity of bone abrasion mechanisms. Despite these limitations, the study contributes to the growing body of knowledge on implant fixation, emphasizing the importance of incorporating both stress relaxation and abrasion into finite element simulations to better reflect the complexities of the bone-implant interface. Future work should address these limitations, particularly by incorporating more advanced frictional and plasticity models. Furthermore, further research into the effects of stress relaxation in different strain states and its impact on bone-implant interactions could provide more comprehensive insights into the long-term stability and performance of cementless implants.

References

1. Bellemans, J., Ries, M.D., Victor, J.M.K., Total Knee Arthroplasty: A Guide to Get Better Performance. 2005, Springer S.
2. Aggarwal, V.K., et al., Revision total knee arthroplasty in the young patient: is there trouble on the horizon? J Bone Joint Surg Am, 2014. 96(7): p. 536-42 DOI: 10.2106/JBJS.M.00131.
3. Australian Orthopaedic Association National Joint Replacement Registry (AOANJRR) Hip, Knee & Shoulder Arthroplasty: 2023 Annual Report. AOA, Adelaide, 2023.
4. National Joint Registry for England, W., Northern Ireland and the Isle of Man, 20th Annual Report 2023. 1821, Hertfordshire, 2023.
5. Abdul-Kadir, M.R., et al., Finite element modelling of primary hip stem stability: the effect of interference fit. J Biomech, 2008. 41(3): p. 587-94 DOI: 10.1016/j.jbiomech.2007.10.009.
6. Chong, D.Y., U.N. Hansen, and A.A. Amis, Analysis of bone-prosthesis interface micromotion for cementless tibial prosthesis fixation and the influence of loading conditions. J Biomech, 2010. 43(6): p. 1074-80 DOI: 10.1016/j.jbiomech.2009.12.006.
7. Conlisk, N., et al., The influence of stem length and fixation on initial femoral component stability in revision total knee replacement. Bone Joint Res, 2012. 1(11): p. 281-8 DOI: 10.1302/2046-3758.111.2000107.
8. Yang, H., et al., Validation and sensitivity of model-predicted proximal tibial displacement and tray micromotion in cementless total knee arthroplasty under physiological loading conditions. J Mech Behav Biomed Mater, 2020. 109: p. 103793 DOI: 10.1016/j.jmbbm.2020.103793.
9. Tarala, M., et al., Experimental versus computational analysis of micromotions at the implant-bone interface. Proc Inst Mech Eng H, 2011. 225(1): p. 8-15 DOI: 10.1243/09544119JEIM825.
10. Taylor, M., D.S. Barrett, and D. Deffenbaugh, Influence of loading and activity on the primary stability of cementless tibial trays. J Orthop Res, 2012. 30(9): p. 1362-8 DOI: 10.1002/jor.22056.
11. van der Ploeg, B., et al., Toward a more realistic prediction of peri-prosthetic micromotions. J Orthop Res, 2012. 30(7): p. 1147-54 DOI: 10.1002/jor.22041.
12. Viceconti, M., et al., Large-sliding contact elements accurately predict levels of bone-implant micromotion relevant to osseointegration. J Biomech, 2000. 33(12): p. 1611-8 DOI: 10.1016/s0021-9290(00)00140-8.
13. Berahmani, S., D. Janssen, and N. Verdonschot, Experimental and computational analysis of micromotions of an uncemented femoral knee implant using elastic and plastic bone material models. J Biomech, 2017. 61: p. 137-143 DOI: 10.1016/j.jbiomech.2017.07.023.
14. Berahmani, S., et al., An experimental study to investigate biomechanical aspects of the initial stability of press-fit implants. J Mech Behav Biomed Mater, 2015. 42: p. 177-85 DOI: 10.1016/j.jmbbm.2014.11.014.
15. Burgers, T., et al., Time-dependent fixation and implantation forces for a femoral knee component--an in vitro study. Med Eng Phys, 2010. 32(9): p. 968-73 DOI: 10.1016/j.medengphy.2010.06.011.
16. Norman, T.L., et al., Cortical bone viscoelasticity and fixation strength of press-fit femoral stems: an in-vitro model. J Biomech Eng, 2006. 128(1): p. 13-7 DOI: 10.1115/1.2133766.
17. Gersie, T., et al., Bone stress relaxation in press-fit femoral knee implant fixation: A combined experimental and computational analysis. SSRN, 2025. DOI: 10.2139/ssrn.5071979.
18. Gersie, T., et al., The effect of bone relaxation on the simulated pull-off force of a cementless femoral knee implant. J Biomech, 2025. 181: p. 112528 DOI: 10.1016/j.jbiomech.2025.112528.

19. Berahmani, S., et al., FE analysis of the effects of simplifications in experimental testing on micromotions of uncemented femoral knee implants. J Orthop Res, 2016. 34(5): p. 812-9 DOI: 10.1002/jor.23074.

20. Fitzpatrick, C.K., et al., Evaluating knee replacement mechanics during ADL with PID-controlled dynamic finite element analysis. Comput Methods Biomech Biomed Engin, 2014. 17(4): p. 360-9 DOI: 10.1080/10255842.2012.684242.

21. Derikx, L.C., et al., Implementation of asymmetric yielding in case-specific finite element models improves the prediction of femoral fractures. Comput Methods Biomech Biomed Engin, 2011. 14(2): p. 183-93 DOI: 10.1080/10255842.2010.542463.

22. Keyak, J.H., et al., Predicting proximal femoral strength using structural engineering models. Clin Orthop Relat Res, 2005(437): p. 219-28 DOI: 10.1097/01.blo.0000164400.37905.22.

23. Keyak, J.H., et al., Prediction of femoral fracture load using automated finite element modeling. J Biomech, 1998. 31(2): p. 125-33 DOI: 10.1016/s0021-9290(97)00123-1.

24. Gersie, T., et al., Characterization of nonlinear stress relaxation of the femoral and tibial trabecular bone for computational modeling. Med Eng Phys, 2025. 138: p. 104324 DOI: 10.1016/j.medengphy.2025.104324.

25. Berahmani, S., et al., Evaluation of interference fit and bone damage of an uncemented femoral knee implant. Clin Biomech (Bristol), 2018. 51: p. 1-9 DOI: 10.1016/j.clinbiomech.2017.10.022.

26. Damm, N.B., M.M. Morlock, and N.E. Bishop, Friction coefficient and effective interference at the implant-bone interface. J Biomech, 2015. 48(12): p. 3517-21 DOI: 10.1016/j.jbiomech.2015.07.012.

27. Rothstock, S., et al., Primary stability of uncemented femoral resurfacing implants for varying interface parameters and material formulations during walking and stair climbing. J Biomech, 2010. 43(3): p. 521-6 DOI: 10.1016/j.jbiomech.2009.09.052.

28. Shultz, T.R., et al., Cortical bone viscoelasticity and fixation strength of press-fit femoral stems: finite element model. J Biomech Eng, 2006. 128(1): p. 7-12 DOI: 10.1115/1.2133765.

29. Rapagna, S., et al., Quantification of human bone microarchitecture damage in press-fit femoral knee implantation using HR-pQCT and digital volume correlation. J Mech Behav Biomed Mater, 2019. 97: p. 278-287 DOI: 10.1016/j.jmbbm.2019.04.054.

30. Zinno, R., et al., Migration of the femoral component and clinical outcomes after total knee replacement: a narrative review. Musculoskelet Surg, 2021. 105(3): p. 235-246 DOI: 10.1007/s12306-020-00690-8.

31. Bishop, N.E., et al., The influence of bone damage on press-fit mechanics. J Biomech, 2014. 47(6): p. 1472-8 DOI: 10.1016/j.jbiomech.2014.01.029.

32. Franchi, M., et al., Biological fixation of endosseous implants. Micron, 2005. 36(7-8): p. 665-71 DOI: 10.1016/j.micron.2005.05.010.

33. Soltanihafshejani, N., et al., The application of an isotropic crushable foam model to predict the femoral fracture risk. PLoS One, 2023. 18(7): p. e0288776 DOI: 10.1371/journal.pone.0288776.

34. Burgers, T.A., et al., Post-yield relaxation behavior of bovine cancellous bone. J Biomech, 2009. 42(16): p. 2728-33 DOI: 10.1016/j.jbiomech.2009.08.005.

35. Leng, H., X.N. Dong, and X. Wang, Progressive post-yield behavior of human cortical bone in compression for middle-aged and elderly groups. J Biomech, 2009. 42(4): p. 491-7 DOI: 10.1016/j.jbiomech.2008.11.016.

Chapter 7

Summary and general discussion

7.1 Summary

This thesis aimed to enhance the accuracy of finite element (FE) models of cementless total knee arthroplasty (TKA) by incorporating bone viscoelasticity and abrasion. By including these aspects, computational simulations should provide more accurate predictions of primary stability and fixation strength. To achieve this, experimental stress relaxation tests were first conducted on bovine trabecular bone to establish a testing protocol, which was then applied to human trabecular bone specimens to develop a constitutive material model describing their viscoelastic behavior. This model was subsequently validated using femoral TKA reconstructions, in which virtual abrasion was implemented to simulate the effect of bone abrasion on implant fixation. This virtual abrasion approach provides a simplified, yet effective way to model bone abrasion in FE simulations and has not been applied previously. Finally, the impact of bone stress relaxation and abrasion on the primary fixation of femoral TKA components was investigated, with micromotions at the bone-implant interface serving as a key outcome measure.

The first step was to develop a material model for capturing the stress relaxation of trabecular bone. In **Chapter 2**, stress relaxation experiments were conducted on bovine trabecular bone to characterize its nonlinear viscoelastic behavior and assess the influence of bone mineral density (BMD). Uniaxial compressive stress relaxation tests were performed on cylindrical trabecular bone samples, with strain held constant for 24 hours. Additional experiments were conducted using multiple (repeated) strain levels with shorter holding times to evaluate whether shorter tests could reliably predict long-term relaxation. The results showed that while most stress relaxation occurred within the first 10 minutes after loading (up to 53% of relaxation), it continued over 24 hours, reaching up to 69% stress relaxation. Extrapolating 30-minute data to 24 hours provided accurate predictions, allowing to significantly reduce the time required for experimental testing to predict longer term stress relaxation. The results furthermore indicated that BMD actually did not influence the time-dependent response. Two modeling approaches, Schapery and superposition models, were used to describe the nonlinear viscoelastic response. While both models effectively captured the stress relaxation behavior on a sample-by-sample basis, only the superposition model proved to be suitable for a generalized, group-based fit. These findings established a foundation for incorporating viscoelasticity into computational models of bone mechanics as used in this thesis.

The developed method was used in **Chapter 3** to construct a material model for the viscoelastic behavior of human trabecular bone and implement it in FE

simulations. Stress relaxation experiments were performed on femoral and tibial bone specimens, and the data were extrapolated to 24 hours. On average, 54% stress relaxation was observed, with a maximum of 82%. A modified superposition model successfully captured the nonlinear viscoelastic response on a specimen-specific level. However, when all samples were considered collectively, no correlation between BMD and stress relaxation was found. Similarly, no correlation was observed between BMD and stiffness, which was not in agreement with relationships reported in the literature. As a result, previously published BMD-stiffness relationships were implemented in the FE simulations, leading to an average overestimation of overall stiffness by 64%. Despite this, the FE models were able to adequately capture the stress relaxation response.

In **Chapter 4**, the developed viscoelastic material model was implemented in FE simulations of femoral TKA reconstructions to assess its impact on implant fixation. Simulated pull-off tests were performed using three different bone material models: elastic, plastic, and plastic-viscoelastic. Incorporating plasticity significantly reduced the predicted pull-off force, from an average of 31 kN with an elastic model to 6.3 kN. However, adding viscoelasticity had only a minor effect, further reducing pull-off forces by only 0.8%. A strong correlation was observed between bone mineral density and pull-off force across all models. Furthermore, elastic strain energy in the femur was also found to be a good predictor of fixation strength.

Building on the integration of bone viscoelasticity in Chapter 4, **Chapter 5** further enhanced the credibility of FE simulations by incorporating both bone viscoelasticity and bone abrasion into the modeling of the initial fixation of cementless femoral TKA. While Chapter 3 established the stress relaxation behavior of trabecular bone in controlled experiments, its effect on primary fixation had not yet been experimentally validated in TKA reconstructions. Therefore, experimental data from cadaveric femurs were used to assess the impact of bone relaxation and virtual abrasion. The experiments investigated the strain reduction over 24 hours on the outer surface of the implant, serving as a proxy for stress relaxation in the bone. In addition, pull-off tests were performed as a measure of overall fixation strength. The simulations initially overestimated implant strains and fixation strength but including bone abrasion significantly improved agreement with experimental results. A level of 0.75 mm of virtual abrasion reduced the strain overestimation from 350% to 150%, while more realistic pull-off forces were simulated with 0.5 mm of abrasion. Experimental strain reductions due to bone relaxation ranged from 17% to 37%, whereas the computational model predicted strain values that were, on average, 41% lower than the experimental measurements, significantly underestimating the strain reduction. These results highlight the necessity of incorporating both time-dependent bone behavior and bone abrasion into FE models to refine implant fixation predictions and optimize surgical strategies.

In **Chapter 6**, the focus shifted from implant pull-off to predicting micromotions at the bone-implant interface in cementless femoral TKA, as micromotions are the more commonly used measure of primary stability, serving as an indicator of osseointegration and bone ingrowth. This chapter aimed to assess whether including bone relaxation and abrasion improves micromotion predictions compared to experimental measurements. Micromotion data from five prosthetic components, implanted in cadaveric femora were compared with cadaver-specific FE models, which were assigned either elastic, plastic, or plastic-viscoelastic bone properties with varying levels of virtual abrasion. Similarly to the findings in Chapter 5, stress relaxation had minimal effect on the predicted micromotions, just as it had little influence on pull-off forces, whereas incorporating bone abrasion significantly improved agreement with experimental data. The most accurate micromotion predictions were obtained using the plastic-viscoelastic model with 0.75 mm of virtual abrasion, yielding micromotions of 53.0 ± 43.0 µm, closely matching the experimental values of 53.1 ± 42.3 µm. However, for two specimens, simulations with 0.75 mm of abrasion failed to converge, likely due to reduced implant-bone contact. These findings further highlight the crucial role of bone abrasion in improving FE model accuracy for primary fixation predictions. They also underscore the need for continued refinement of bone plasticity models, as well as friction and abrasion modeling, to improve simulation realism and strengthen the reliability of FE-based predictions of the initial stability of cementless TKA components.

7.2 General discussion

7.2.1 Key findings and limitations

In contrast with initial expectations, incorporating bone stress relaxation in simulations had a limited effect on the primary fixation of cementless femoral components compared to models incorporating plasticity only. While the inclusion of viscoelasticity did reduce bone stresses and thereby bone-implant contact stresses, it did not significantly affect initial stability. When combining plasticity and viscoelastic behavior, the pull-off force was still overestimated, while micromotions were underestimated relative to experimental findings. This is likely due to an underestimation of stress relaxation and the high friction coefficient assumed at the bone-implant interface. While bone stress relaxation has been shown to affect implant fixation strength in cadaveric peg and press-fit hip stem studies, our results failed to show a significant effect on simulated primary fixation in TKA [1, 2]. The reduction in elastic strain energy due to relaxation observed in the FE simulations did not lead to a meaningful improvement in the prediction of fixation, particularly in the prediction of micromotions.

Several factors may explain these differences. First, the level of stress relaxation measured in human trabecular bone cores, which was incorporated into our TKA simulations, did not lead to the same reduction in implant surface strains as observed experimentally. Since our experimental strain reduction values were consistent with those reported in previous studies, the simulations likely underestimated bone relaxation [3, 4]. In addition, prior research on cadaveric pegs and press-fit stems indicates that high-friction surfaces, such as those in our femoral components, may mitigate the effect of stress relaxation on pull-off forces compared to low-friction implants [1, 2, 5]. This likely reduced the impact of stress relaxation on fixation strength in our model.

Determining whether the discrepancy between experimental and computational findings is caused by an underestimation of stress relaxation would require additional experimental validation, although this may be challenging due to inherent experimental limitations. Ideally, pull-off tests should be conducted on the same bone specimen both at t=0 and after 24 hours, but this obviously is practically unfeasible. Similarly, measuring micromotions at these same timepoints is not possible due to the extensive preparation time required. Given that approximately 72% of total stress relaxation occurs within the first 10 minutes, conducting tests only after ~2-3 hours is not quite representative for the initial status at t=0, and therefore influences the evaluation of the effect of time-dependent bone behavior.

To further assess whether stress relaxation was underestimated in our simulations, it is important to consider the extent of bone relaxation incorporated in our model. The relaxation behavior was based on trabecular bone core experiments with strains up to 0.8% (the yield strain of trabecular bone), whereas strains in our simulations extended well beyond this range [6]. There is no consensus in the literature regarding stress relaxation beyond the yield strain, highlighting the need for further experiments in this domain [7, 8]. Additionally, our studies only examined stress relaxation under compressive loading. While this aligns with our simulation conditions (where strains were predominantly compressive), it does not account for potential effects under tension or shear, which may be relevant in different bone-implant interactions. Investigating stress relaxation in these loading modes could provide further insight into the mechanical behavior of trabecular bone.

Next to stress relaxation, this thesis is the first to integrate bone abrasion into simulations of primary fixation in cementless TKA. Our findings demonstrate that modeling bone abrasion may lead to more realistic predictions, improving agreement with experimental data for both pull-off forces and micromotions. However, our approach relied on a simplified, uniform abrasion model, which does not fully capture the complexity of bone wear at the implant-bone interface during implantation. In reality, bone abrasion is influenced by several factors, including surgical technique and instrumentation, local bone density variations, and implant position. Moreover, bone abrasion does not occur uniformly across the interface and abraded bone particles can migrate on and into the implant's surface coating, within the intertrabecular spaces in the bone, or they can be scraped out of the interface [9]. Our model effectively simulated this last type, assuming that all abraded bone was removed from the interface. However, previous studies have shown that bone debris in the inter-trabecular spaces or at the implant coating may influence frictional properties and may potentially alter fixation strength [10]. While such effects may impact both the short-and long-term stability of stability of cementless implants, their role in primary fixation remains unclear. Future research should focus on experimentally quantifying bone abrasion through micro-CT and incorporating more detailed abrasion mechanics into computational models to lead to a more localized and adaptive abrasion model [10]. Additionally, investigating how different types of bone abrasion interact with implant stability experimentally could provide deeper insights into optimizing press-fit designs for improved fixation.

Another aspect that may influence the outcome of computational modeling is the choice of plasticity model. In this thesis we employed a softening von Mises yield criterion, which resulted in a plastic zone that typically extended deep into the bone. However, in reality, bone damage is often more localized near the bone-implant interface [11], as demonstrated by µCT analyses of TKA reconstructions. Alternative plastic models, such as an isotropic crushable foam model, have shown to produce a plasticity zone that is more localized around the implant-bone interface, and therefore may better capture the actual mechanical response of trabecular bone under press-fit conditions [12, 13].

As mentioned earlier, the coefficient of friction between the bone and implant also strongly influences micromotions predictions [14]. A sensitivity analysis could help determine how variations in friction affect micromotions and overall fixation strength. While we assumed a fixed coefficient of friction, true in vivo conditions remain unknown, introducing uncertainty in our simulations. Efforts have been made to investigate in vivo frictional conditions, demonstrating a complex non-linear mechanical response with elastic and plastic deformation and slip at the interface [15]. However, these characteristics likely vary across different types of implants and surface coatings, making it challenging to define a single friction value for use in models like ours.

In this thesis, we used computational methods to evaluate pull-off forces and micromotions as indicators of implant fixation. While micromotions are known to influence osseointegration, the exact relationship between pull-off strength and in vivo implant stability remains uncertain [16]. In this work, pull-off forces were treated solely as a measure of fixation strength. However, future studies should explore their correlation with long-term osseointegration. Alternatively, one approach could be first to measure micromotions experimentally and then perform pull-off tests on the same specimens, which would offer a clearer understanding of how pull-off force relates to interface micromotions and primary stability.

In summary, our simulations provided valuable insights into primary fixation mechanics, but also highlighted the complexity of bone-implant interactions. The inclusion of viscoelasticity reduced bone stresses significantly, though its effect on initial stability was minimal, suggesting that viscoelastic behavior influences stress distribution without greatly affecting primary fixation strength. Additionally, incorporating bone abrasion improved the predictions of pull-off forces and micromotions, enhancing simulated primary stability. However, the simplified abrasion model used here does not fully capture the complexities of bone wear during implantation. Future improvements in both experimental testing and computational modeling are necessary to better capture bone-implant interactions and enhance the accuracy of implant performance predictions.

7.2.2 Challenges in biomechanical experimental and computational testing

Throughout this thesis the challenges of experimentally testing of human bone have become evident. Large variability in cadaveric material arising from differences in age, bone quality, and morphology, makes it difficult to compare specimens and establish correlations. For instance, we did not find a correlation between BMD with the level of stress relaxation, while previous studies did suggest such a relation [17, 18]. Obtaining cadaveric bone from individuals matching the typical TKA patient demographic (mean age: 68 years) is challenging [19, 20]. While including bones from younger donors would have increased the number of high-density specimens, leading to a wider BMD range and potentially improving statistical power, practical constraints prevented the inclusion of more high-density specimens. This limitation may have contributed to the lack of correlation observed between viscoelastic response and bone density.

Variability was also evident in experimental strain reductions measured on the implant surface, which could not be fully replicated in our FE simulations. This discrepancy stems not only from inherent variability in the bone specimens, but also from inconsistencies in the TKA procedure itself. Although we attempted to minimize variations by following the standard surgical technique performed by an experienced orthopedic surgeon, complete standardization is difficult to obtain. Cutting errors, which have been shown to be significant in previous studies, along with variations in interference fit and minor differences in implant positioning, all may have contributed to the variability observed in bone abrasion and fixation [9]. Consequently, exactly replicating individual specimens in computational models remains challenging.

Moreover, the conditions in cadaveric testing differ from in vivo environments, raising concerns about clinical relevance. While implementing in vivo loading conditions could enhance realism, peak forces have shown potential as a useful metric for micromotion assessment [21]. Experimental challenges also extended to maintaining sterile and controlled testing environments. Prolonged testing (e.g., 24-hour experiments) was hindered by issues such as fungal growth, temperature fluctuations affecting small strain measurements, and material wear from repeated water bath exposure. These factors made long-term testing of biological specimens particularly difficult.

Beyond experimental challenges, this thesis also highlights the complexities of FE modeling of biological materials. While FE analysis is widely used in engineering applications such as bridge and aircraft design, where materials have well-defined mechanical properties, biological tissues introduce an additional layer of complexity and uncertainty. Unlike engineered materials, bone exhibits substantial variability (between and within specimens), making its mechanical behavior less predictable. This was evident in our findings, where counterintuitive results emerged, such as the absence of increased micromotions despite incorporating plastic deformation in the bone model. Our pull-off force simulations indicated that the pull-off force was nearly 80% lower with the plastic material model compared to the elastic one, suggesting that plasticity would lead to a looser implant fit. This looser fit could allow for more movement between the implant and bone during loading. However, this anticipated increase in micromotions was not observed in our simulations.

A major challenge in FE modeling is selecting appropriate material properties. For example, the apparent density – elastic modulus relationship used in this study may not fully capture the variability reported literature [22]. To illustrate: in this study, bone apparent density values between 0.1 and 1.3 g cm^{-3} corresponded to elastic moduli ranging from 206 MPa to 24 GPa. However, when recalculated using literature-reported upper and lower bounds, these same density values could yield elastic moduli anywhere between 39 MPa and 4 GPa or between 213 MPa and 60 GPa. This variability highlights the significant impact of material model selection on FE outcomes. In Chapter 3, for example, the use of the BMD-stiffness relationship may have led to a 63.9% overestimation of specimen stiffness, suggesting that the material model chosen might not have been the most appropriate for our specific specimens. To improve simulation accuracy, a model more specifically tailored to the unique properties of our specimens would be necessary. However, this would require tuning of each individual specimen to a specific input set of experimental results (e.g. stiffness evaluation based on deflection measurements).

Validating FE models presents additional difficulties. In mechanical testing, inconsistencies such as slip in the MTS machine introduce variations that do not exist in the simulated environment. In this study, we used micromotions as the primary validation metric, yet discrepancies remained between simulations and experimental results suggest that our models may still require refinement. It may be beneficial to validate intermediary steps, such as bone strain distributions, which can experimentally be quantified using digital image correlation (DIC) techniques, before focusing on micromotions [23]. This could help pinpoint sources of error.

As George Box famously stated: "All models are wrong, but some are useful". This also applies to FE modeling of cementless fixation. Due to time and resource constraints, we were unable to validate each individual aspect of the model, nor can we claim absolute accuracy. However, despite its limitations, this work represents an important step forward in integrating bone stress relaxation and bone abrasion into FE simulations of cementless TKA fixation. With further advancements, such as those presented in this thesis, these models can become more reliable tools to assess primary stability of cementless implants which can be used to optimize prosthetic design and assess surgical techniques and ultimately enhancing patient outcomes.

7.2.3 Implications for implant design and clinical practice

In this thesis, we aimed to advance FE simulations to the next level, enabling the prediction of primary implant stability. While our findings indicate that we are not yet there, it is important to reflect on the broader implications for these types of simulations in the field of arthroplasty.

FE models on initial stability have the potential to play an important role in implant design, accelerating the development of next-generation implants. In particular, there is a growing interest in smaller implants for localized defects and designs that better replicate the mechanical properties of bone and degraded cartilage. In knee arthroplasty, unicondylar knee implants are gaining popularity, yet their primary fixation remains poorly understood in comparison to total knee components [19]. Our models provide a (relatively) fast and cost-effective approach to evaluate and optimize the fixation of these implants. Given that unicondylar implants exhibit lower survival rates than total knee components, largely due to inadequate fixation, there is significant room for improvement [24]. Their smaller fixation features may make them even more critical to implant stability, emphasizing the importance of optimized design.

Beyond unicondylar implants, FE models can be used to test a wide range of geometries and assess their impact on micromotion and fixation. This enables innovative implant designs to be evaluated without the need for costly and time-consuming prototyping and experimental testing [25]. Additionally, there is a growing trend toward implants with mechanical properties closer to those of bone. Emerging materials such as PEEK and advanced (porous) titanium alloys will inevitably influence primary fixation, and their behavior can be investigated using FE simulations [14]. Similarly, new porous coatings produced through additive manufacturing can also be analyzed to determine their effect on implant stability [26].

While this thesis has focused on TKA, the same modeling approach can be applied to other cementless joint replacements, such as total hip, shoulder, or ankle arthroplasties. This broad applicability enhances the value of these models across the entire field of arthroplasty.

FE simulations are not only valuable for implant design but also for preclinical validation of surgical techniques. A current debate in the field concerns alignment strategies, whether mechanical, kinematic, or functional alignment provides the best outcomes, and whether these approaches should be tailored to individual patients [27]. FE models offer an efficient way to investigate how different alignment strategies influence primary fixation. Additionally, variations in surgical technique, such as bone preperation methods, level of press-fit, and other intraoperative factors, can be systemically evaluated without the need for testing in patients.

To translate these findings into clinical practice, large-scale simulations on diverse populations, including variations in anatomy, surgical technique, and implant design, will be necessary [28]. This will help identify key clinical, implant-related, and patient-specific factors that influence long-term implant survival. By integrating these insights, FE models can significantly contribute to the optimization of both implant design and surgical decision-making, ultimately improving patient outcomes in arthroplasty.

Finally, it is important to recognize that while this thesis focuses on the mechanical aspects of primary fixation, implant failure in vivo is often a complex process involving both mechanical and biological factors. Although many cementless implants achieve long-term success, some fail prematurely, and our findings are most relevant to these early failures rather than cases of aseptic loosening occurring after more than five years. Biological processes such as bone remodeling and osseointegration play a significant role in implant longevity, but these factors develop over extended periods and were not explicitly modeled in our study [29].

7.2.4 Future perspectives

Over the past decades, FE simulations of implant fixation have advanced tremendously. Early models were relatively coarse and computationally demanding, whereas modern simulations have become highly detailed, allowing us to refine numerous parameters at a granular level. With these advancements, we have gained new insights, as increased model fidelity has made previously overlooked details more critical than ever. In contrast, when using rough approximations, fine details played a less significant role.

This thesis has identified several key areas where improvements are needed to enhance the accuracy of FE simulations to predict initial stability of cementless implants. Specifically, incorporating more sophisticated bone abrasion effects, refining the coefficient of friction, and implementing advanced plasticity models will be essential. These advancements will help bring simulation micromotions between the implant and bone in closer agreement with experimental data.

However, a major limitation of the experimental validation methods used in this thesis is that DIC can only measure surface micromotions, whereas FE simulations also provide insights into the micromotions occurring within the bone-implant interface. Since all micromotions, both at the outer and internal surface, play a role in the primary fixation, new techniques are required for a more comprehensive validation. Digital volume correlation (DVC) has emerged as a promising candidate for this purpose, demonstrating the ability to accurately measure strain within bone beneath the tibial tray [30]. By leveraging this technique, it will become possible to assess interface micromotions in greater detail, beyond what can be captured with DIC, including subsurface measurements.

While this thesis has primarily focused on TKA, it has specifically examined only the femoral component. The tibial tray, however, has a fundamentally different fixation mechanism, making it valuable to investigate the differences in micromotion and stress distribution between these components. Additionally, exploring the role of stress relaxation could yield important insights. A deeper understanding of interface properties and fixation features (such as peg shapes) will be particularly beneficial for implant manufacturers seeking to optimize early fixation strategies [25].

Despite advancements in simulation-experiment agreement, a crucial question remains: what is the threshold between stable and unstable micromotions in terms of osseointegration and long-term stability? The existing literature provides limited clarity on this matter. For example, the mean micromotion value for implants that successfully integrated was 32% of the value for those that did not (112 ± 176 µm versus 349 ± 231 µm) [31]. However, the large variability and substantial overlap in the data ranges highlight the absence of a universal threshold, making it difficult to define a clear boundary between stable and unstable micromotions. To address this gap, improved experimental validation is essential, ideally through in vivo animal models or retrieval studies. However, due to increasing regulatory constraints and ethical considerations, animal models are becoming less common. As an alternative, ex vivo models using biological tissues obtained from surgical resections, such as the femoral head during total hip replacement, may provide a viable solution. These specimens, which still contain living cells, can be maintained in a laboratory environment and subjected to controlled loading conditions to simulate micromotions in vivo. Recent advancements include techniques to affix implants to these biological samples and apply mechanical loading to determine the critical micromotion threshold for stable fixation. However, this approach is still in very early stages, and as of now, there is no available literature on this specific methodology or its outcomes.

Finally, even with the significant progress in FE modeling, computational efficiency remains to be a major hurdle. The FE models used in this study required runtimes ranging from 1 to 6 hours, far too long for practical clinical application. If patient-specific FE simulations are to be integrated into clinical workflows for preoperative planning, results must be available almost instantaneously after acquiring a CT scan. One promising avenue to achieve this is through artificial intelligence (AI), particularly machine learning. By training AI algorithms on large datasets of precomputed FE simulations, the model could learn to predict implant stability and optimal surgical strategies based on a patient's CT scan data, without the need to run new simulations for each patient. This approach would enable real-time, patient-specific treatment planning, significantly improving clinical decision-making. However, to develop such AI models, extensive datasets of credible FE simulations across diverse patients must first be generated. Looking ahead, the integration of AI-driven models into clinical practice could revolutionize orthopedic surgery, providing surgeons with rapid, data-driven insights to optimize implant selection and surgical techniques.

7.3 General conclusion

This thesis has advanced FE models for cementless TKA by incorporating bone viscoelasticity and abrasion, providing more realistic predictions of bone stress distribution and improving the overall understanding of bone-implant interactions. While bone stress relaxation had a significant impact on bone stresses, it did not significantly affect primary fixation strength, pull-off forces, or micromotions. However, the inclusion of bone abrasion led to more realistic predictions of implant stability. The importance of validation in computational models was highlighted, with experimental measurements of pull-off strength and bone-implant micromotions. These findings can aid to improve the development of next generation cementless implants for the knee and for other joints as well, optimize surgical techniques and ultimately enhance patient outcomes.

References

1. Berahmani, S., et al., An experimental study to investigate biomechanical aspects of the initial stability of press-fit implants. J Mech Behav Biomed Mater, 2015. 42: p. 177-85 DOI: 10.1016/j.jmbbm.2014.11.014.
2. Norman, T.L., et al., Cortical bone viscoelasticity and fixation strength of press-fit femoral stems: an in-vitro model. J Biomech Eng, 2006. 128(1): p. 13-7 DOI: 10.1115/1.2133766.
3. Berahmani, S., et al., The effect of surface morphology on the primary fixation strength of uncemented femoral knee prosthesis: a cadaveric study. J Arthroplasty, 2015. 30(2): p. 300-7 DOI: 10.1016/j.arth.2014.09.030.
4. Burgers, T., et al., Time-dependent fixation and implantation forces for a femoral knee component--an in vitro study. Med Eng Phys, 2010. 32(9): p. 968-73 DOI: 10.1016/j.medengphy.2010.06.011.
5. Shultz, T.R., et al., Cortical bone viscoelasticity and fixation strength of press-fit femoral stems: finite element model. J Biomech Eng, 2006. 128(1): p. 7-12 DOI: 10.1115/1.2133765.
6. Kopperdahl, D.L. and T.M. Keaveny, Yield strain behavior of trabecular bone. J Biomech, 1998. 31(7): p. 601-8 DOI: 10.1016/s0021-9290(98)00057-8.
7. Burgers, T.A., et al., Post-yield relaxation behavior of bovine cancellous bone. J Biomech, 2009. 42(16): p. 2728-33 DOI: 10.1016/j.jbiomech.2009.08.005.
8. Leng, H., X.N. Dong, and X. Wang, Progressive post-yield behavior of human cortical bone in compression for middle-aged and elderly groups. J Biomech, 2009. 42(4): p. 491-7 DOI: 10.1016/j.jbiomech.2008.11.016.
9. Berahmani, S., et al., Evaluation of interference fit and bone damage of an uncemented femoral knee implant. Clin Biomech (Bristol), 2018. 51: p. 1-9 DOI: 10.1016/j.clinbiomech.2017.10.022.
10. Bishop, N.E., et al., The influence of bone damage on press-fit mechanics. J Biomech, 2014. 47(6): p. 1472-8 DOI: 10.1016/j.jbiomech.2014.01.029.
11. Rapagna, S., et al., Quantification of human bone microarchitecture damage in press-fit femoral knee implantation using HR-pQCT and digital volume correlation. J Mech Behav Biomed Mater, 2019. 97: p. 278-287 DOI: 10.1016/j.jmbbm.2019.04.054.
12. Kelly, N., et al., An investigation of the inelastic behaviour of trabecular bone during the press-fit implantation of a tibial component in total knee arthroplasty. Med Eng Phys, 2013. 35(11): p. 1599-606 DOI: 10.1016/j.medengphy.2013.05.007.
13. Soltanihafshejani, N., et al., The application of an isotropic crushable foam model to predict the femoral fracture risk. PLoS One, 2023. 18(7): p. e0288776 DOI: 10.1371/journal.pone.0288776.
14. Post, C.E., et al., A FE study on the effect of interference fit and coefficient of friction on the micromotions and interface gaps of a cementless PEEK femoral component. J Biomech, 2022. 137: p. 111057 DOI: 10.1016/j.jbiomech.2022.111057.
15. Sanchez, E., et al., The effect of coating characteristics on implant-bone interface mechanics. J Biomech, 2024. 163: p. 111949 DOI: 10.1016/j.jbiomech.2024.111949.
16. Jasty, M., et al., In vivo skeletal responses to porous-surfaced implants subjected to small induced motions. J Bone Joint Surg Am, 1997. 79(5): p. 707-14 DOI: 10.2106/00004623-199705000-00010.
17. Manda, K., et al., Nonlinear viscoelastic characterization of bovine trabecular bone (vol 16, pg 173, 2017). Biomechanics and Modeling in Mechanobiology, 2017. 16(1): p. 191-195 DOI: 10.1007/s10237-016-0819-9.

18. Manda, K., et al., Linear viscoelasticity - bone volume fraction relationships of bovine trabecular bone. Biomechanics and Modeling in Mechanobiology, 2016. 15(6): p. 1631-1640 DOI: 10.1007/s10237-016-0787-0.
19. Australian Orthopaedic Association National Joint Replacement Registry (AOANJRR) Hip, Knee & Shoulder Arthroplasty: 2023 Annual Report. AOA, Adelaide, 2023.
20. National Joint Registry for England, W., Northern Ireland and the and Isle of Man, 20th Annual Report 2023. 1821, Hertfordshire, 2023.
21. Berahmani, S., et al., FE analysis of the effects of simplifications in experimental testing on micromotions of uncemented femoral knee implants. J Orthop Res, 2016. 34(5): p. 812-9 DOI: 10.1002/jor.23074.
22. Helgason, B., et al., Mathematical relationships between bone density and mechanical properties: a literature review. Clinical biomechanics, 2008. 23(2): p. 135-146.
23. Mann, K.A., et al., Peri-implant bone strains and micro-motion following in vivo service: a postmortem retrieval study of 22 tibial components from total knee replacements. J Orthop Res, 2014. 32(3): p. 355-61 DOI: 10.1002/jor.22534.
24. Di Martino, A., et al., Unicompartmental knee arthroplasty has higher revisions than total knee arthroplasty at long term follow-up: a registry study on 6453 prostheses. Knee Surgery Sports Traumatology Arthroscopy, 2021. 29(10): p. 3323-3329 DOI: 10.1007/s00167-020-06184-1.
25. Quevedo Gonzalez, F.J., et al., An Anterior Spike Decreases Bone-Implant Micromotion in Cementless Tibial Baseplates for Total Knee Arthroplasty: A Biomechanical Study. J Arthroplasty, 2024. 39(5): p. 1323-1327 DOI: 10.1016/j.arth.2023.11.020.
26. England, T., et al., Additive manufacturing of porous titanium metaphyseal components: Early osseointegration and implant stability in revision knee arthroplasty. J Clin Orthop Trauma, 2021. 15: p. 60-64 DOI: 10.1016/j.jcot.2020.10.042.
27. Minoda, Y., Alignment techniques in total knee arthroplasty. Journal of Joint Surgery and Research, 2023. 1(1): p. 108-116 DOI: https://doi.org/10.1016/j.jjoisr.2023.02.003.
28. Post, C.E., et al., The primary stability of a cementless PEEK femoral component is sensitive to BMI: A population-based FE study. Journal of Biomechanics, 2024. 168: p. 112061 DOI: https://doi.org/10.1016/j.jbiomech.2024.112061.
29. Anijs, T., et al., Computational tibial bone remodeling over a population after total knee arthroplasty: A comparative study. J Biomed Mater Res B Appl Biomater, 2022. 110(4): p. 776-786 DOI: 10.1002/jbm.b.34957.
30. Wearne, L.S., et al., Quantifying the immediate post-implantation strain field of cadaveric tibiae implanted with cementless tibial trays: A time-elapsed micro-CT and digital volume correlation analysis during stair descent. J Mech Behav Biomed Mater, 2024. 151: p. 106347 DOI: 10.1016/j.jmbbm.2023.106347.
31. Kohli, N., J.C. Stoddart, and R.J. van Arkel, The limit of tolerable micromotion for implant osseointegration: a systematic review. Sci Rep, 2021. 11(1): p. 10797 DOI: 10.1038/s41598-021-90142-5.

Chapter 8

Nederlandse samenvatting

Het doel van dit proefschrift was om de nauwkeurigheid van eindige-elementen (EE) modellen van ongecementeerde totale knie arthroplastiek (TKA) te verbeteren door de viscoelasticiteit en abrasie van het bot te integreren in de EE simulaties. Door deze aspecten mee te nemen, zouden computersimulaties een betere voorspelling moeten geven van de primaire fixatiestabiliteit, uitgedrukt in de microbewegingen tussen het bot en het implantaat. Om dit te bereiken werden eerst spanningsrelaxatie-experimenten uitgevoerd op trabeculair bot afkomstig van runderen om een testprotocol vast te stellen, dat vervolgens werd toegepast op menselijke trabeculaire botspecimens voor de ontwikkeling van een constitutief materiaalmodel dat het viscoelastische gedrag van bot beschrijft. Dit model werd vervolgens gevalideerd met femorale TKA-reconstructies, waarbij virtuele abrasie werd geïmplementeerd om het effect van botabrasie op de implantaatfixatie te simuleren. Deze virtuele abrasiebenadering biedt een vereenvoudigde maar effectieve manier om botabrasie in EE-simulaties te modelleren en was nog niet eerder toegepast. Ten slotte werd het effect van spanningsrelaxatie van het bot en abrasie op de primaire fixatie van femorale TKA-componenten onderzocht, waarbij de microbewegingen tussen het bot en het implantaat als uitkomstmaat werden gebruikt.

De eerste stap was het ontwikkelen van een materiaalmodel dat de spanningsrelaxatie van trabeculair bot beschrijft. In **Hoofdstuk 2** werden spanningsrelaxatie-experimenten uitgevoerd op trabeculair bot van runderen om het niet-lineaire viscoelastische gedrag te karakteriseren en het eventuele effect van de botmineraaldichteid (BMD) op het viscoelastistische gedrag te bepalen. Uniaxiale drukproeven met constante rek werden uitgevoerd gedurende 24 uur, aangevuld met kortere experimenten om te evalueren of spanningsrelaxatie met kortdurende testen over langere tijd kon worden voorspeld. De resultaten toonden aan dat de meeste spanningsrelaxatie plaatsvond binnen de eerste 10 minuten na belasting (tot 53%), maar dat de daling in spanning doorzette tot 69% na 24 uur. Het extrapoleren van 30-minuten data naar 24 uur gaf nauwkeurige voorspellingen, wat de benodigde tijd voor experimenten aanzienlijk verkleinde. Opvallend was dat BMD geen invloed had op de tijdsafhankelijke respons. Twee modelleringsbenaderingen, het Schapery-model en het superpositie-model, werden gebruikt om de niet-lineaire viscoelastische respons te beschrijven. Hoewel beide modellen effectief waren op individuele specimens, was alleen het superpositie model geschikt voor een gegeneraliseerd model. Deze bevindingen legden de basis voor de integratie van viscoelasticiteit in computermodellen van botbiomechanica die verder in het proefschrift werden gebruikt.

In **Hoofdstuk 3** werd de ontwikkelde methode uit het vorige hoofdstuk gebruikt om een materiaalmodel te construeren voor de viscoelastische eigenschappen van menselijk trabeculair bot en dit te implementeren in EE-simulaties. Spanningsrelaxatie-experimenten werden uitgevoerd op femorale en tibiale botmonsters en de data werd geëxtrapoleerd naar 24 uur. Gemiddeld werd 54% spanningsrelaxatie waargenomen, met een maximum van 82%. Een aangepast superpositie-model legde de niet-lineaire viscoelastische respons nauwkeurig vast op een specimen-specifiek niveau. Echter, wanneer alle specimens gezamenlijk werden beschouwd, werd er geen correlatie gevonden tussen BMD en spanningsrelaxatie. Evenmin werd een correlatie waargenomen tussen BMD en botstijfheid wat niet in overeenstemming is met de literatuur. Als gevolg hiervan werden eerder vastgestelde en gepubliceerde BMD-stijfheidsrelaties toegepast in de EE-simulaties, wat resulteerde in een gemiddelde overschatting van de algehele stijfheid met 64%. Desondanks lieten de EE-modellen de correcte spanningsrelaxatie van het bot zien.

In **Hoofdstuk 4** werd het ontwikkelde viscoelastische materiaalmodel geïmplementeerd in EE-simulaties van cementloze femorale TKA-reconstructies om de invloed op de primaire implantaatfixatie te onderzoeken. Fixatietesten onder een trekbelasting (pull-off) werden gesimuleerd met drie verschillende botmodellen: elastisch, plastisch en plastisch-viscoelastisch. Het integreren van plasticiteit verlaagde de voorspelde uittrekkracht aanzienlijk, van gemiddeld 31 kN met een elastisch model naar 6,3 kN. Het toevoegen van viscoelasticiteit had slechts een gering effect, waarbij de fixatiekrachten slechts met 0,8% afnamen. Er werd een sterke correlatie waargenomen tussen botmineraaldichtheid en fixatiekracht, terwijl elastische vervormingsenergie in het femur eveneens een goede voorspeller was van fixatiesterkte.

In **Hoofdstuk 5** werd de realiteit van de EE-simulaties verder verbeterd door zowel botviscoelasticiteit als botabrasie (wat optreedt tijdens het aanbrengen van de cementloze femorale component) te integreren in de modellering van de fixatie van femorale TKA. Terwijl Hoofdstuk 3 het spanningsrelaxatiegedrag van trabeculair bot in gecontroleerde experimenten onderzocht, was het effect ervan op de primaire fixatie nog niet experimenteel gevalideerd. Daarom werd experimentele data van femora afkomstig van kadavers gebruikt om het effect van botspanningsrelaxatie en virtuele abrasie te beoordelen. De experimenten onderzochten de vermindering van de rekken op het buitenoppervlak van het implantaat over 24 uur als een proxy voor spanningsrelaxatie in het bot. Daarnaast werden faaltesten onder een trekbelasting uitgevoerd om de algehele fixatiesterkte te meten. In eerste instantie overschatten de simulaties zowel de implantaatrekken als de fixatiesterkte, maar door botabrasie toe te voegen, verbeterde de overeenkomst met de experimentele resultaten aanzienlijk. Een abrasieniveau van 0,75 mm verminderde de overschatting van de rek met 350% tot 150%, terwijl realistischere fixatiekrachten werden voorspeld met 0,5 mm abrasie. De experimentele rekreductie als gevolg van botrelaxatie varieerde van 17% tot 37%, terwijl het computermodel gemiddeld 41% lagere reducties voorspelde dan experimentele metingen. Deze resultaten onderstrepen de noodzaak om zowel tijdsafhankelijk botgedrag als botabrasie op te nemen in EE-modellen om implantaatfixatie beter te voorspellen en implantaatdesigns en chirurgische strategieën te optimaliseren.

In **Hoofdstuk 6** verschoof de focus van faaltesten naar het voorspellen van microbewegingen tussen het bot en het implantaat in ongecementeerde TKA, omdat microbewegingen een gangbare maat zijn voor primaire stabiliteit en een indicatie geven van botingroei. Dit hoofdstuk onderzocht of het opnemen van botspanningsrelaxatie en abrasie de voorspellingen van microbewegingen verbeterde in vergelijking met experimentele metingen. Microbeweging data van vijf prothesen, geïmplanteerd op kadaver femora, werden vergeleken met kadaver-specifieke EE-modellen met elastische, plastische of plastich-viscoelastische botmateriaaleigenschappen en verschillende niveaus van virtuele abrasie. Net als in Hoofdstuk 5 had spanningsrelaxatie een minimale invloed op de voorspellingen van de simulaties, terwijl botabrasie de overeenstemming met experimentele data aanzienlijk verbeterde. De meest accurate voorspellingen werden verkregen met het plastisch-viscoelastische model en 0,75 mm abrasie, met een gemiddelde voorspelde microbeweging van 53,0 ± 43,0 μm, wat nauw overeenkwam met de experimentele waarde van 53,1 ± 42,3 μm. Voor twee specimens convergeerden de simulaties met 0,75 mm abrasie echter niet, waarschijnlijk door het verminderde implantaat-botcontact.

Samenvattend heeft dit proefschrift de EE-modellering van ongecementeerde TKA verbeterd door botviscoelasticiteit en botabrasie te integreren. Hoewel botspanningsrelaxatie een aanzienlijke invloed had op de botspanningen, had het geen significante invloed op de primaire fixatiesterkte. Het meenemen van botabrasie in de simulaties leidde echter tot realistischere voorspellingen van de implantaatstabiliteit. Het belang van validatie in computermodellen werd benadrukt, met experimentele metingen van uittrekkracht en bot-implantaat microbewegingen. Klinisch gezien kunnen deze bevindingen de ontwikkeling van nieuwe implantaten versnellen en chirurgische technieken optimaliseren, met toepassingen die niet alleen voor het kniegewricht gelden, maar ook voor andere gewrichten. Toekomstig onderzoek zou zich moeten richten op het nog nauwkeuriger simuleren van de complexe mechanische interacties die een rol spelen tijdens en kort na de implantatie van cementloze gewrichtsprothesen, waarbij nieuwe experimentele validatietechnieken kunnen worden ingezet om de betrouwbaarheid van simulaties te verbeteren. Daarnaast moet er gewerkt worden aan het integreren van AI om de rekensnelheid van EE-modellen te verhogen, zodat deze modellen uiteindelijk toepasbaar zijn in de klinische praktijk.

Chapter 9

Data management

Since this research did not involve animals or human participants, ethical approval from a commission was not required. No identifiable information regarding cadaveric material was provided by the Anatomy Department of Radboudumc.

Data for Chapters 2 and 3 were obtained through laboratory experiments involving animal cadaveric material and anonymous human cadaveric material. Chapter 4 was based on both experimental and computational data from Berahmani et al. (2017) (DOI: 10.1016/j.jbiomech.2017.07.023), which were stored on the department's server, accessible only to project members at Radboudumc. The data for Chapter 5 was acquired through laboratory experiments with anonymous human cadaveric material, along with simulations based on this data. Finally, the models referenced in Chapter 4 were also used in Chapter 6.

All study documentation, including research protocols, experimental setups, software versions, and a readme file, is archived in the Research Documentation Collection (RDC) in the Radboud Data Repository (RDR). The processed data is stored in the Data Acquisition Collection (DAC) within the same repository. Detailed information on the storage locations within the RDR is provided in Table 9.1. All studies are published open access in alignment with institutional policies.

Table 9-1: Digital Object Identifiers (DOIs) for Data Acquisition Collection (DAC), Radboud Documentation Collection (RDC), and Data Sharing Collection (DSC) are provided for each chapter, along with the corresponding DSC license type (CC-BY-NC or RUMC-RA-DUA-1.0).

Chapter	DAC	RDC	DSC	DSC License
2	ru.rumc.p1phdtg_ r0005620_dac_479	ru.rumc.p1phdtg_ r0005620_rdc_986	ru.rumc.p1phdtg_ r0005620_dsc_963	CC-BY-NC
3	ru.rumc.p2phdtg_ r0005620_dac_531	ru.rumc.p2phdtg_ r0005620_rdc_087	ru.rumc.p2phdtg_ r0005620_dsc_255	CC-BY-NC
4	ru.rumc.p3phdtg_ r0005620_dac_409	ru.rumc.p3phdtg_ r0005620_rdc_923	ru.rumc.p3phdtg_ r0005620_dsc_415	RUMC-RA-DUA-1.0
5	ru.rumc.p4phdtg_ r0005620_dac_118	ru.rumc.p4phdtg_ r0005620_rdc_135	ru.rumc.p4phdtg_ r0005620_dsc_729	RUMC-RA-DUA-1.0
6	ru.rumc.lshdepuy_ r005620a_dac_555	ru.rumc.lshdepuy_ r0005620_rdc_809	ru.rumc.lshdepuy_ r0005620a_dsc_553	RUMC-RA-DUA-1.0

9

Chapter 10

Academic contributions

Publications in international (peer-reviewed) journals

T. Gersie, T. Bitter, D. Wolfson, R. Freeman, N. Verdonschot, D. Janssen. Quantification of long-term nonlinear stress relaxation of bovine trabecular bone. Journal of the Mechanical Behavior of Biomedical Materials, 152, 106434 (2024). 10.1016/j.jmbbm.2024.106434

T. Gersie, T. Bitter, D. Wolfson, R. Freeman, N. Verdonschot, D. Janssen. Characterization of Nonlinear Stress Relaxation of the Femoral and Tibial Bone for Computational Modeling. Medical Engineering & Physics, 138, 104324 (2025). 10.1016/j.medengphy.2025.104324

T. Gersie, T. Bitter, R. Freeman, N. Verdonschot, D. Janssen. The effect of bone relaxation on the simulated pull-off force of a cementless femoral knee implant. Journal of Biomechanics, 112528 (2025). 10.1016/j.jbiomech.2025.112528

T. Gersie, T. Bitter, R. Freeman, N. Verdonschot, D. Janssen. Bone Stress Relaxation in Press-Fit Femoral Knee Implant Fixation: A Combined Experimental and Computational Analysis. Journal of the Mechanical Behavior of Biomedical Materials, 169, 107067 (2025). 10.1016/j.jmbbm.2025.107067

T. Gersie, T. Bitter, R. Freeman, N. Verdonschot, D. Janssen. Influence of Bone Stress Relaxation and Abrasion on Micromotions in Uncemented Femoral Knee Implants: A Finite Element Study. SSRN pre-print (submitted to PLOS ONE), Rheumatology & Orthopedics eJournal (2025) 10.2139/ssrn.5181419

Scientific presentations at (inter)national conferences

T. Gersie, T. Bitter, D. Wolfson, R. Freeman, N. Verdonschot, D. Janssen. Determining stress relaxation of trabecular bone to simulate realistic press-fit conditions of cementless implants. 33rd Congress of the International Society for Technology in Arthroplasty – Maui, USA, Sept 2022), Oral presentation.

T. Gersie, T. Bitter, D. Wolfson, R. Freeman, N. Verdonschot, D. Janssen. Determining stress relaxation of trabecular bone to simulate realistic press-fit conditions of cementless orthopaedic implants. 9th Dutch Bio-medical Engineering Conference, Egmond aan Zee, Netherlands, Jan 2023, Oral presentation.

T. Gersie, T. Bitter, D. Wolfson, R. Freeman, N. Verdonschot, D. Janssen. Determining stress relaxation of trabecular bone to simulate realistic press-fit conditions of cementless implants. Orthopaedic Research Society 2023 Annual Meeting, Dallas, USA, Feb 2023, Poster presentation.

T. Gersie, T. Bitter, D. Wolfson, R. Freeman, N. Verdonschot, D. Janssen. Determining stress relaxation of trabecular bone to simulate realistic press-fit conditions of cementless implants. 28th Congress of the European Society of Biomechanics, Maastricht, Netherlands, Jul 2023, Oral presentation.

T. Gersie, T. Bitter, D. Wolfson, R. Freeman, N. Verdonschot, D. Janssen. Up to 69% stress relaxation in bovine trabecular bone in 24 hours: the potential to improve models of primary fixation of press-fit implants. 34th Congress of the International Society for Technology in Arthroplasty, New York, USA, Sept 2023, Oral presentation.

T. Gersie, T. Bitter, D. Wolfson, R. Freeman, N. Verdonschot, D. Janssen. Femoral and tibial trabecular bone shows up to 82% stress relaxation which could affect the simulated initial stability of cementless implants. 34th Congress of the International Society for Technology in Arthroplasty, New York, USA, Sept 2023, Oral presentation.

T. Gersie, T. Bitter, D. Wolfson, R. Freeman, N. Verdonschot, D. Janssen. Trabecular bone shows more viscoelasticity than earlier reported: An experimental and finite element study. Orthopaedic Research Society 2024 Annual Meeting, Long Beach, USA, Feb 2024, Poster presentation.

T. Gersie, T. Bitter, R. Freeman, N. Verdonschot, D. Janssen. The effect of bone relaxation on the simulated pull-out force of a cementless femoral implant. 29th Congress of the European Society of Biomechanics, Edinburgh, Scotland, Jun 2024, Oral presentation.

T. Gersie, T. Bitter, R. Freeman, N. Verdonschot, D. Janssen. The effect of bone relaxation on the simulated pull-out force of a cementless femoral knee implant. 35th Congress of the International Society for Technology in Arthroplasty, Nashville, USA, Aug 2025, Oral presentation.

T. Gersie, T. Bitter, R. Freeman, N. Verdonschot, D. Janssen. The effect of bone relaxation on the simulated pull-out force of a cementless femoral knee implant. Orthopaedic Research Society 2025 Annual Meeting, Phoenix, USA, Feb 2025, Poster presentation.

T. Gersie, T. Bitter, R. Freeman, N. Verdonschot, D. Janssen. Bone stress relaxation in press-fit femoral knee implant fixation: experimental and computational analysis. 29th Congress of the European Society of Biomechanics, Zurich, Switzerland, Jul 2025, Oral presentation.

Chapter 11

Curriculum vitae

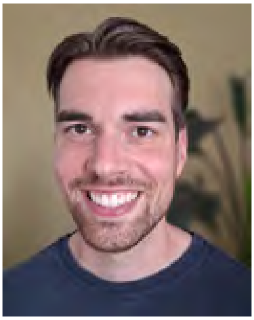

Thomas Gersie was born on October 12, 1996, in Nijmegen, the Netherlands. He completed his gymnasium education at NSG Groenewoud in Nijmegen before pursuing a Bachelor's degree in Biomedical Engineering at Eindhoven University of Technology. In 2019, he obtained his Master's degree in Medical Engineering, with a specialization in orthopedic biomechanics.

During his Master's program, Thomas gained diverse clinical and research experience through two clinical internships at Maastricht University Medical Center, a research internship at the University of Auckland in New Zealand, and a graduation internship at DSM-Firmenich. At DSM-Firmenich, he explored innovative osteoconductive coatings for polymer implants designed to treat focal cartilage defects in the knee.

After graduating, Thomas spent a year working in industry as an R&D Engineer at Summox Dental. On March 1, 2021, he returned to Nijmegen to begin his PhD at the Orthopaedic Research Lab of Radboudumc. His doctoral research focused on advanced computational modeling of the primary fixation of cementless total knee implants, with a particular emphasis on the role of bone viscoelasticity. This project was carried out in collaboration with implant manufacturer DePuy Synthes and supervised by Nico Verdonschot, Dennis Janssen, Thom Bitter, David Wolfson (DePuy Synthes), and Robert Freeman (DePuy Synthes).

During his PhD, Thomas earned his university teaching qualification and served on the organizing committee for the 2022 PhD Day of the Dutch Society for Movement Sciences (VvBN). He is currently looking to advance his academic career through a postdoctoral position in orthopedic biomechanics.

Chapter 12

Radboudumc PhD portfolio

Department: Orthopedics
PhD period: 01/03/2021 – 28/02/2025
PhD Supervisors: Prof. dr. N.J.J. Verdonschot, dr. D.W. Janssen
PhD Co-supervisor: Dr. T. Bitter

Training activities	Hours
Courses	
• Radboudumc - Introduction day (2021)	6.00
• RIHS - Introduction course for PhD candidates (2021)	15.00
• RU - Achieving your Goals and performing more successfully in your PhD (2021)	42.00
• RU - Presenting and Poster Pitching (2021)	42.00
• RU - Project management for PhD students (2022)	45.00
• Radboudumc - Scientific integrity (2022)	20.00
• RU - Education in a Nutshell (2022)	28.00
• RU - Effective Writing Strategies (2022)	75.00
• RU - Academic English Conversation and Pronunciation (2024)	43.00
• Radboudumc - Career development for PhD candidates & postdocs (2025)	20.00
Seminars	
• Research Integrity Round - The Dark Side of Science: Misconduct in Biomedical Research (2021)	1.50
• Radboud Research Rounds - Innovation in personalized care for orthopaedic patients (2021)	1.00
• RIHS PhD Council Workshop - How to Write a Rebuttal (2021)	1.00
• RIHS Workshop - Work is fun... isn't it? (2021)	1.50
• Donders PhD Council Workshop - Spice up your thesis with LaTeX (2021)	2.00
• RIMLS Meet the Expert - Managing Your Interns; blessing or curse (2022)	2.00
• ICMS lecture 2022 (2022)	1.00
• ICMS lecture 2023 (2023)	1.50
• Meet the Expert session - How to prepare for your PhD defence (2025)	1.50
Conferences	
• Radboudumc PhD retreat 2022, Nijmegen (2022)	16.00
• 27th Congress of the ESB, Porto, Portugal (2022)	24.00
• Podium presentation at 33rd Congress of the ISTA, Maui, USA (2022)	36.00
• VvBN PhD Day 2022, Nijmegen (2022)	8.00
• Podium presentation at 9th Dutch BME Conference, Egmond aan Zee (2023)	24.00
• Poster presentation at ORS 2023 Annual Meeting, Dallas, USA (2023)	36.00
• Two podium presentations at 34th Congress of the ISTA, New York, USA (2023)	42.00
• Radboudumc PhD retreat 2023, Nijmegen (2023)	8.00
• Podium presentation at 28th Congress of the ESB, Maastricht (2023)	32.00
• Poster presentation at ORS 2024 Annual Meeting, Long Beach, USA (2024)	36.00
• Radboudumc PhD retreat 2024, ‘s-Hertogenbosch (2024)	17.00
• Podium presentation at 29th Congress of the ESB, Edinburgh, Scotland (2024)	32.00
• Podium presentation at 35th Congress of the ISTA, Nashville, USA (2024)	36.00
• Poster presentation at ORS 2025 Annual Meeting, Phoenix, USA (2025)	8.00
Other	
• Co-organizing VvBN PhD Day 2022 (2022)	28.00
• University Teaching Qualification traject (2024)	72.00

Teaching activities	
Lecturing	
• MSc course BMS53 – Orthopaedic biomechanics in motion (2021)	56.00
• BSc course 6MBB – Loading and load-bearing capacity of tissues (2022)	28.00
• MSc course BMS53 – Orthopaedic biomechanics in motion (2022)	56.00
• BSc course 6MBB – Loading and load-bearing capacity of tissues (2023)	28.00
• MSc course BMS82 – Applied Matlab for biomedical problems (2023)	76.00
• MSc course BMS53 – Orthopaedic biomechanics in motion (2023)	56.00
• BSc course 6MBB – Loading and load-bearing capacity of tissues (2024)	28.00
• MSc course BMS82 – Applied Matlab for biomedical problems (2024)	76.00
• MSc course BMS53 – Orthopaedic biomechanics in motion (2024)	56.00
• BSc course BMS – Research project (2024)	45.00
Supervision of internships	
• MSc internship – Sainivedhitha Arunajatesan, University of Twente (2022)	30.00
• MSc internship – Mart Verhoeven, University of Technology Eindhoven (2023)	30.00
Total	**1369.00**

Chapter 13

Dankwoord

Het meest gelezen deel van mijn proefschrift is hier, het dankwoord, en dit is dan ook het laatste wat ik schrijf voor dit boekje. Na vier jaar met veel plezier bij het ORL te hebben gewerkt en ontzettend veel geleerd te hebben, is mijn promotie (op de verdediging na natuurlijk) officieel klaar. Ik had dit niet kunnen doen zonder de directe en/of indirecte hulp van alle mensen hieronder.

Nico, jouw enthousiasme voor alles wat met orthopedische biomechanica te maken heeft, werkte heel aanstekelijk. Als ik weer eens met (in mijn ogen) teleurstellende resultaten bij jou aanklopte, wist jij altijd wel te zeggen dat er vast ergens op de wereld iemand was die dit fantastisch zou vinden. Mooi om te zien hoeveel je geeft om de community, bij zowel de ISTA als bij 'onze vrienden' bij de ESB. Je bent echt een voorbeeld van een betrokken begeleider en een sterke vertegenwoordiger van de MedTech in Nederland. Jouw kritische blik heeft mijn papers echt naar een hoger niveau getild, ook al dacht ik soms wel eens: 'had ik maar eerder bij Nico aangeklopt, dan had ik niet dat halve artikel geschreven dat uiteindelijk de prullenbak in kon'. Het was super hoe jij mijn enthousiasme voor een academische carrière deelde, en mede dankzij jouw steun en contacten heb ik een mooie eerste stap kunnen zetten!

Beste **Dennis,** na een nogal bijzondere sollicitatieprocedure kwam ik vier jaar geleden bij het ORL terecht, en vanaf het begin voelde het als een fijne plek om te werken. Echt knap hoe jij, samen met Nico en Sebastiaan, een omgeving hebt neergezet waar alle typische problemen van de academische wereld niet lijken te bestaan. Gewoon een plek waar je als jonge onderzoeker de ruimte krijgt om te groeien en waar je je gewaardeerd voelt. Ik heb veel bewondering voor hoe jij met al onze (soms nogal uiteenlopende) karakters weet om te gaan. Gedurende dit traject heb ik echt ontzettend veel aan jou gehad. Vooral jouw vermogen om, juist op de momenten dat ik er zelf even niet meer uitkwam, snel met een scherpe, praktische oplossing te komen, vind ik echt indrukwekkend. Wat ik ook enorm waardeer, is dat je altijd oog had voor de persoon achter de PhD'er. Samen met Nico heb jij ook veel tijd in mijn vervolg carrière gestopt, wat ik niet snel zal vergeten. Eerlijk gezegd denk ik dat de prijs voor 'Supervisor of the year' al jaren omgekocht is, want jij had hem allang moeten krijgen. Ik moet ook nog vaak terugdenken aan onze allereerste meeting over dit project, toen ik jou vroeg of je 'nog even tijd had' om de laatste dingen door te spreken. Je antwoordde in één seconde: 'Nu?', en dat typeert precies hoe laagdrempelig het altijd was om bij jou binnen te lopen met vragen. Daar heb ik dan ook graag (en veel) gebruik van gemaakt. Soms twijfelde ik wel eens of je het nog leuk vond om samen te werken, of dat nou aan het project of aan mij lag, weet ik nog steeds niet, maar gelukkig hebben we ook ontzettend veel gelachen. Over straattaal, slechte woordgrappen (waar jij harder om lachte dan ik), en alles daartussenin. Bedankt voor alles!

Thom, ik denk dat jij ook opgelucht was toen we na de eerste serie experimenten eindelijk mochten gaan simuleren. Al bracht dat ook weer zijn eigen verrassingen met zich mee. We hebben heel wat uren samen achter mijn computer gezeten om van alles en nog wat op te lossen, meestal terwijl Dennis op vakantie was. Soms vroeg ik mij wel eens af wat we aan het doen waren als ik een presentatie had van wel twintig grafieken over elastic, creep, plastic en total strain van verschillende nodes. Maar zelfs de vele uren die we naar Fortran staarden, waren een stuk leuker omdat we het samen deden. Bij het schrijven van de micromotion-subroutine was jouw hulp ontzettend waardevol en daar ben ik je heel dankbaar voor. En eerlijk is eerlijk: zonder jouw talent om overbodige woorden te schrappen, was dit proefschrift waarschijnlijk twee keer zo dik geweest. De afgelopen vier jaar heb ik mijzelf enorm zien groeien als onderzoeker, maar ik heb ook jou zien groeien als begeleider. Ik heb onze samenwerking als heel prettig en leerzaam ervaren. Hopelijk kun je jouw enthousiasme en scherpe oog voor detail nog aan veel andere PhD'ers overbrengen!

Dear **Dave** and **Rob**, I truly believe that, no matter how fundamental a PhD project may be, it greatly benefits from close collaboration with industry. Our biweekly meetings, even when brief, consistently helped me stay focused on the clinical relevance of the work and aligned with DePuy's vision for the project. The encouraging feedback from within DePuy was also very motivating and reinforced the value of continuing this line of research. I sincerely hope that similar collaborations can continue in the future. Thank you both for your time, support, and commitment throughout the project!

Beste **Richard**, ik had makkelijk tien pagina's kunnen schrijven over hoe groot jouw hulp voor mij is geweest. Ik weet nog goed dat ik aan begin van mijn PhD vroeg of we niet binnen één week wat experimenten gedaan konden hebben, en jij meteen zei dat er alleen al weken voorbereiding voor nodig was. Nou, dat bleek inderdaad zo te zijn, want ik weet niet hoeveel uren wij samen beneden in het lab hebben doorgebracht. Wat ik echt ongelooflijk vond, is dat jij altijd vrolijk bleef en mij letterlijk op elk moment van de dag hebt geholpen. Als er weer iets misging (en dat ging er weleens), had ik vaak het gevoel van 'gedeelde smart is halve smart', en samen zijn we er gelukkig altijd weer bovenop gekomen. Jouw technische en praktische kijk op alles wat we hebben gedaan is echt een enorme meerwaarde geweest. Ik hoop dan ook dat ik anderen niet heb afgeschrikt om experimenten te doen, want met jou werken is niet alleen heel leerzaam, maar ook nog eens heel leuk!

Florieke, ik had mij geen betere onderwijs- en BKO-mentor kunnen wensen. Vanaf het allereerste moment heb jij mij begeleid bij het verbeteren van mijn onderwijsvaardigheden. Mede dankzij jouw nuchtere en praktische instelling heb ik mijn BKO-traject met succes kunnen afronden. Bedankt voor het vertrouwen en de vrijheid die ik kreeg in het onderwijs van het ORL. De hele dag in een te warm lokaal doorbrengen, terwijl Marleen weer ziek was, en ondertussen sinussen en cosinussen uitleggen, waren altijd het onderwijshoogtepunt van het jaar! Ik vraag mij soms nog wel eens af wat jij dacht van mijn gesprekken met Dennis en Thom, wanneer ik weer jullie kamer binnenstapte om (vaak iets minder positief) nieuws te brengen. Ik hoop dat je er om hebt kunnen lachen!

Max, in mijn eerste jaar had ik geen idee dat je bestond, maar daarna heb jij mij enorm geholpen met Matlab, wat jou dan ook de welverdiende titel 'Matlab Max' opleverde. Fijn dat je zo goed om kon gaan met mijn eigenwijze manier van werken en mij de ruimte gaf om zelf tot de conclusie te komen dat jij vanaf het begin al gelijk had, en mijn input, zoals zo vaak, toch niet klopte. Ik denk dat wij allebei verrast zijn (jij iets minder dan ik, aangezien dit jouw vooropgezette plan was) hoe veel beter ik ben geworden in Matlab én in onderzoek doen in het algemeen. Hoewel we uren samen naar code gekeken hebben, was het altijd gezellig door jouw prachtige lift- en wachtmuziek (ik denk dat Max en liften bij sommigen van ons voor altijd aan elkaar verbonden zijn), je gefluit en eindeloze smoofies, brony-series en DICPIX-grappen. Als je ooit wilt weten welke psychische stoornis het beste bij je past, of gewoon zin hebt in een psychologische analyse, spreek dan Max aan in de kroeg of bij de Aesculaaf! Ik moet je ook nog specifiek bedanken voor de DJ Blyatman Ultimate mix, dat was echt een gamechanger tijdens de laatste fase van het schrijven van mijn proefschrift.

Sjors, we begonnen samen op dezelfde dag, terwijl iedereen vanwege corona nog thuis zat. Jij bent altijd nieuwsgierig en vriendelijk geweest, en hebt me enorm geholpen met het maken van 3D-geprinte malletjes voor van alles en nog wat. Daarnaast ben ik je heel dankbaar voor het corrigeren van de STLs van de femorale componenten, dat heeft me echt ontzettend geholpen.

Beste **Sebastiaan**, ik had het leuk gevonden om meer samen te werken, maar helaas is dat wat moeilijker met een fundamenteel project. Bedankt voor je vragen tijdens de research meetings en natuurlijk voor het plaatsen van de implantaten voor mijn studies. Ik hoop dat je een beetje leedvermaak hebt gehad toen ik er tijdens een sessie achter kwam dat we het verkeerde instrumentarium hadden. Op dat moment was ik niet zo blij, maar nu kan ik er gelukkig om lachen. Bedankt dat je ons later alsnog kwam helpen!

Sander, omdat mijn PhD redelijk soepel verliep, hebben wij niet heel vaak gesproken. Toch vind ik dat jij je rol als mentor uitstekend hebt ingevuld, vooral door mij te helpen relativeren tijdens het onderzoek en met jouw nuchtere kijk op het schrijven van artikelen. Daarnaast wil ik je ook heel erg bedanken voor het idee om een Rubicon-aanvraag te schrijven en de steun die jij mij in dat traject hebt gegeven.

Graag wil ik de leden van de manuscriptcommissie bedanken voor hun tijd en inzet bij het beoordelen van dit manuscript: Professor Loomans, Professor Laz en dr. Van Rietbergen. Dear **Peter**, I truly admire your enthusiasm. I believe many people don't fully realize how much a 'great job' from an (external) professor after a conference presentation can mean to a PhD student. Many thanks also for your support with the Rubicon application. Beste **Bert**, erg leuk dat jij lid wilde zijn van de manuscriptcommisie, nadat ik mijn master heb afgerond bij de Orthopaedics Biomechanics groep in Eindhoven. Bedankt voor de waardevolle sparmomenten over botviscoelasticiteit en mogelijke vervolgonderzoeken voor mijn postdoc. Ik heb genoten van jouw passie voor het vak en hoop dat we in de toekomst nog eens kunnen samenwerken.

Erim, het was eigenlijk al vrij snel duidelijk dat jij één van mijn paranimfen zou worden, een mooie voorbode van ons toekomstplan: een gedeeld kantoortje met op de deur Prof. dr. Özdemir & Prof. dr. ir. Gersie. Hopelijk volgt jouw promotie ook snel, zodra je zeventiende artikel erdoor is! Het was altijd gezellig bij het ORL, maar zeker ook daarbuiten. Ik waardeer het enorm dat we overal over kunnen praten. Ik moet altijd lachen als jij met volle overtuiging praat over dingen waar ik dan weer nét iets minder passie voor voel, zoals FIAT panda's. Ons jaarlijkse feestje was telkens weer een hoogtepunt. Ik denk dat ze in Oegstgeest nog steeds verhalen vertellen over die twee gasten uit Nijmegen. Ik ben erg dankbaar voor jouw betrokkenheid bij de ORL-activiteiten, zoals het legendarische ORL-zeilweekend en jouw bijdrage aan techn-ORL. Op nog vele leuke momenten!

Jasper, het was een eer om bijna vier jaar naast je te mogen zitten. Wat hebben we heerlijk samen Dumpert gekeken en over basketbal gepraat. Work hard, play hard, zoiets was het wel: veel ouwehoeren, maar ook serieus aan het werk en altijd bereid om elkaar te helpen als het nodig was. Het was daarom ook erg taai toen je klaar was met je PhD en ik het zonder je moest doen. Gelukkig gingen we nog wel af-en toe voor het biermenu, wat altijd erg mooi was. Ik verwacht dat we elkaar de komende jaren nog vaak gaan zien, zeker met onze double-dates. En dat is meteen een mooi bruggetje naar **Erin**. Jij had soms de ondankbare taak om ons na zo'n biermenu thuis te ontvangen, en jij dan couscous voorstelde en Jasper en ik stiekem naar Emmi's wilden. Ik moet nog steeds lachen om het moment dat jullie mij kwamen ophalen op het vliegveld van LA voor de ORS. We moesten iets minder hard lachen toen jij die stoeprand over het hoofd zag. En ook al zat jij 'aan de andere kant', na Jaspers vertrek werd jij mijn nieuwe wandelmaatje (als wij er op hetzelfde moment waren althans). Heel blij dat ik jullie beiden heb leren kennen!

Jurre, de laatste sterkhouder van onze kant! Waar je ooit begon als 'de squid', moet je het nu zonder ons doen. Onze dagelijkse fietstochten om stipt 17:00 uur naar Nijmegen-Oost waren altijd gezellig. Ik zal nooit vergeten hoe blij je reageerde toen Corine en ik met hangende pootjes de Underground binnenkwamen. Van dansbattles, wingmannen, en natuurlijk die gore broek van mij tijdens de PhD-retreat in den Bosch, het was altijd een feest als we op stap gingen! Carnaval in Roermond was ook prachtig, aangezien ik dan eindelijk mijn schminkkunsten aan de wereld kon tonen. Hopelijk gaat het schrijven van je boekje ook soepel, en laten we 'onze kant' in stijl achter!

Dear **Navid**, thanks for the help at the start of my PhD, your tips on how to approach the bone experiments were really valuable. **Ali**, I always found it amusing that during those odd moments when I happened to be at the ORL unexpectedly, you were there too. It definitely made working more enjoyable. Best of luck wrapping up the final stages of your PhD!

Dan de vrouwen van de andere kant: **Miriam**, wij hebben elkaar heel wat vragen gesteld over het werk, waarbij we elkaar zelden écht konden helpen. Toch vond ik onze 'samenwerking' altijd erg prettig. We hebben samen gezellige rondjes gelopen en ons goed vermaakt tijdens trips naar Egmond aan Zee, Maastricht, Edinburgh en Long Beach. Mooi ook dat je aansloot bij Techn-ORL, carnaval en natuurlijk een dikke SO naar Frank! **Mirthe**, qua inhoud hebben we elkaar niet veel gesproken, onze projecten lagen daarvoor gewoon te ver uit elkaar. Maar op het zeilweekend (mooi gesnorkeld in Friesland) en tijdens carnaval vonden we elkaar wél. En je weet het: cordon bleu is cordon bleu. **Dineke**, wij begonnen ook op dezelfde dag in 2021 en volgens mij waren wij lang de enige (samen met wat stagiaires) die in lockdown op het lab verschenen. Ik kan altijd lachen om je scherpe observaties en vond het leuk dat je telkens weer terugkwam!

I would like to thank my two master interns, **Sai** and **Mart**, for their contributions during my PhD. I hope you both enjoyed your time at the Radboudumc and that the experience may have sparked your interest in orthopedic biomechanics!

Daarnaast wil ik alle andere collega's van het ORL bedanken voor de gezelligheid, niet alleen op de werkvloer, maar ook tijdens alle leuke activiteiten zoals de barbecues, het curlen en het suppen!

Dan nog een speciaal bedankje voor de mannen van Atro: **Albert, Branco en Thijmen**. Tijdens de experimentele fases van mijn onderzoek zag ik jullie vaker dan mijn collega's boven. Albert, dank voor je enthousiasme en bereidheid om altijd te helpen, en natuurlijk ook voor de gezelligheid in Nashville! Thijmen, heel erg bedankt voor je hulp met de 3D-sacanner, dat bleek een echt een grote stap vooruit vergeleken met wat we eerder deden.

Dan zijn er nog de mensen die indirect (en soms ongewild) invloed hebben gehad op deze PhD.

Mark en **Teun**, het leven is zoveel leuker met jullie erbij. Heerlijk nuilen over de PhD terwijl jullie genoten van mijn ellende, altijd onder het genot van lekkere biertjes. Vroeger oneindige avonden op het bankje bij Trees, nu bij elke willekeurige kroeg, zolang er maar Guinness op de tap is. Het blijft de vraag wie van ons drieën de slechte invloed is, maar dat er één is, staat vast. Dankzij die invloed belanden we altijd in zeer apige situaties; denk aan Albufeira, Istanbul of het Nest. Mark, we zijn al vrienden sinds onze tijd bij de E-tjes van Orion, en het is mooi om te zien dat onze vriendschap altijd hetzelfde is gebleven. Hopelijk ga je nooit de Vierdaagse lopen. Teun, wat weet je eigenlijk van liften? Begonnen in de derde van de middelbare met elke dag naar de Sema of Tankie, en nu nog steeds smerig eten (ik iets meer dan jij) en drinken. Tegenwoordig vangen we nog steeds zwijntjes en: we pushen dat ding, met zijn allen rollen, tot heel die whip kapot is.

Dan Party 2.0; het is erg bijzonder dat vier van de zes van ons ooit samen in een introgroepje zaten en nog steeds vrienden zijn. **Nienke**, hoe voelt het om wél bij naam genoemd te worden? Jij bent echt een topvoorbeeld van hoe je je PhD rustig en zonder al te veel gedoe afrondt, iets waar ik volgens mij ook aardig in geslaagd ben. Sorry dat je vaak als laatste van de drie musketiers overbleef, omdat wij niet kunnen drinken. **Roy**, de problemen die Nienke en ik tijdens onze PhD niet hadden, heb jij helaas wél ervaren. Het is knap hoe jij je daar doorheen slaat, en ik vond het altijd fijn dat we zo open over onze PhD's (en alles eromheen) konden praten. En natuurlijk hebben we samen de beste Party-weekenden georganiseerd! **Janneke**, het was gezellig om af en toe samen op hetzelfde congres te zijn. Met jou in mijn leven, is mijn vliegschaamte ook ineens verdwenen. Erg nice dat we samen door Amerika hebben gereisd toen jij in Salt Lake City zat voor je PhD; heerlijk McDonalds-aanbiedingen gegeten en bevroren in Yellowstone in een tent! **Manouk**, helaas moet ik jou ook teleurstellen dat ik geen zwaard krijg na mijn verdediging. Ik ben blij om te zien hoe jij en Corine elkaar gevonden hebben. Dankjewel dat je ons altijd opvangt, en vooral voor mij op mijn slechtste momenten, met frikandellen en gebakken eieren voor feestjes, Koningsdag en festivals. En dan **Dieter,** de manager van de groep met altijd geweldige stapverhalen. Ik vind het altijd komisch dat we appen over de meest alledaagse dingen; verzekeringen, belastingen en noem maar op. Onze omgang is altijd chill en nooit ingewikkeld, behalve natuurlijk als we de vaatwasser moeten inruimen tijdens het kerstdiner of bij een potje Mexx. Hopelijk gaan we ook nog op onze 50ste naar een technofeest en besluiten we dan dat we er toch echt te oud voor zijn. Natuurlijk ook de aanhang, **Rens**, **Steffie**, **Aytunc**, **Teun** en **Evi**, bedankt voor alle leuke momenten samen met natuurlijk als grote hoogtepunt het 'naaktschilderen'!

Daan, wie had gedacht dat ons NAC2-project de basis zou worden voor mijn PhD? Ik zal nooit vergeten hoe wij samen in Gemini zaten, een paar dagen voor mijn masterverdediging (wie had kunnen weten dat je eerst al je vakken moest halen voordat je kon verdedigen?), en steeds afwisselend naar Rocky gingen om te vragen wat we eigenlijk moesten doen, terwijl wij hem telkens niet verstonden. Twee jaar in Geldrop wonen was ook genieten, ook al zagen we elkaar soms dagenlang niet door onze andere dag/nachtritmes. Ik waardeer onze directe communicatie, het feit dat je nooit te beroerd bent om mee te gaan naar een feestje, en dat je op Begijn lijkt. Op nog veel mooie avonden in Den Bosch en Skuimparty's in Schaijk!

Jesse, ik kan het mij niet herinneren, maar onze ontmoeting was toen jij nog een baby was. En wat is er sindsdien niet allemaal gebeurd: van Maplestory, de peanutman, auto's bouwen in de kelder bij mijn moeder, ontelbare cornies eten, en het is nog steeds gaande, ruim 20 jaar later. Heel erg bedankt voor het onvoorwaardelijke vertrouwen, vooral als je dacht dat ik zeven papers had geschreven, terwijl het er in werkelijkheid maar één was. Je bent altijd ontzettend geïnteresseerd en ook niet vies van een beetje smullen van de ellende! Hopelijk lukt het jou ook om een PhD-plek te bemachtigen, dan neem ik die rol graag van je over. En toen kwam **Sarah** erbij; eigenlijk de perfecte aanvulling, en vanaf dag één klikte het tussen ons. Het is prachtig om te zien hoe jij Jesse's sterke verhalen weet te relativeren wanneer hij weer buikpijn of een ander kwaaltje heeft. Fijn dat jij ook een cheapskate bent! Laten we vooral zo doorgaan, of dat nu in Eindhoven, Nijmegen of waar dan ook is. En als ik ook ooit nog een bankje in de prullenbak van de Sterkenburg wil gooien (of gewoon wil verhuizen), weet ik jullie te vinden!

Ellen, **Kees**, **Christiaan** en **Ingrid**, bedankt voor de gezellige (kerst)diners en jullie enthousiasme in mij en in mijn werk!

Jaap, papa, vroeger had ik nooit gedacht dat ik, net als jij, een wetenschappelijke carrière (waarbij ik onderwijs een van de leukste aspecten vind) zou nastreven. Daarom was het behalen van mijn BKO tijdens mijn PhD dan ook een hoogtepunt voor ons beiden. Jouw enthousiasme over mijn papers, ook al zei je er niets van te begrijpen, vond ik altijd heel leuk. Ik geniet ervan als je naar Eindhoven komt en we samen naar de ZabZab gaan, en van de koffie die we samen in het restaurant van het Radboud dronken terwijl ik eigenlijk moest werken.

Lieve **Isabelle**, ik had mij geen betere zus kunnen wensen, dus daar al mijn eeuwige dank voor. Daarnaast ben ik de tel kwijtgeraakt van hoeveel plaatjes en presentaties jij voor mij hebt gemaakt; ik denk dat je die masterscriptie inmiddels dubbel en dwars hebt terugverdiend. Ik waardeer het enorm dat je er altijd voor mij bent, en ik ben ontzettend trots dat jij mijn paranimf wilt zijn. Broeder en Sister, voor altijd! **Rick**, soms had ik met je te doen als jij 's avonds in je eentje op de bank zat en Isabelle en ik nog bezig waren met *-plaatjes. Of als wij samen aan het geiten zijn en jij er wat verloren bij zit. Toch hebben wij ook samen genoeg meegemaakt; ik kan mij nog iets vaag herinneren van een stapavond in Arnhem, en die keer dat we bijna opgesloten zaten in een carport in Niftrik. Nog heel veel geluk samen, en ik geniet altijd erg van ons samenzijn!

Xandra, mama, jij doet echt alles voor mij en daarvoor ben ik je altijd dankbaar. Je biedt mij onvoorwaardelijke steun en bent altijd trots op mij, en ik ben ook minstens zo trots op jou! Samen naar Duitsland, NEC of de vakanties, behoren tot mijn dierbaarste herinneringen. We kunnen over alles praten, en jouw scherpe blik heeft mij niet alleen persoonlijk, maar ook in dit PhD-traject enorm geholpen. Ik vind het heel erg knap hoe jij altijd alles begrijpt, van dingen op de middelbare school tot aan dit proefschrift. De koffietjes in de ochtend en het eten (en de bakken kwark) die na een Radboud-werkdag voor mij klaarstonden, maakten deze PhD niet alleen makkelijker, maar vooral ook veel gezelliger! Op nog heel veel leuke momenten samen!

Liefste **Corine**, jij hebt met gemak een plek in mijn promotieteam verdiend, gezien alle hulp tijdens het schrijven van artikelen en het FE-en. Dit was niet altijd even makkelijk, zeker niet als ik weer eens 'Marc-erig' deed. Ik vind het erg bijzonder hoe deze samenwerking heeft geleid tot de prachtige relatie die wij nu hebben. Ik dacht dat ik het ORL zou verlaten met een hoop nieuwe vaardigheden en een doctorstitel, maar nooit had ik verwacht dat ik er ook mijn levenspartner zou vinden. Samen zijn we naar de mooiste congressen geweest, met Hawaii natuurlijk als absoluut hoogtepunt. Mocht ik ooit een prestigieuze prijs winnen, dan word je uitvoerig bedankt in de stijl van Hennie. Ik houd van al onze avonturen samen, en hoe jij altijd overal voor in bent. Of het nu gaat om obscure restaurants in verre landen, heerlijke koffietjes, of fysieke uitdagingen zoals de Vierdaagse (die zonder jou écht ondraaglijk was geweest). We vullen elkaar perfect aan en mijn liefde voor jou is niet in woorden of gebaren (zelfs niet met het kleinste streepje licht tussen mijn duim en wijsvinger) te beschrijven. Op naar nog ontelbaar veel avonturen samen!

9 789465 152745 >

Radboudumc
university medical center

IN DEI NOMINE FELICITER

Radboud University